MICROCOPY RESOLUTION TEST CHART

NATIONAL BUREAU OF STANDARDS-1963-A

mechanical and aerospace engineering

mechanical engineering, aerospace engineering, energy systems engineering, engineering science, materials science

MATERIAL PROBLEMS FOR HIGH-TEMPERATURE,
HIGH-POWER SPACE ENERGY-CONVERSION SYSTEMS

(FIRST ANNUAL PROGRESS REPORT)

Produced for the

Authored by

Mysore L. Ramalingam, Dean L. Jacobson,
James F. Morris and Shlomo Snir

May 1984

Mark Elder, Director
Pre-Award Services
Research & Sponsored Programs Administration

College of Engineering & Applied Sciences
Arizona State University
Tempe, Arizona 85287

REPORT DOCUMENTATION PAGE		READ INSTRUCTIONS BEFORE COMPLETING FORM
1. REPORT NUMBER AFOSR-TR- 8	2. GOVT ACCESSION NO. AM5-940	3. RECIPIENT'S CATALOG NUMBER
4. TITLE (and Subtitle) MATERIAL PROBLEMS FOR HIGH-TEMPERATURE, HIGH-POWER SPACE ENERGY-CONVERSION SYSTEMS		5. TYPE OF REPORT & PERIOD COVERED First Annual Progress Report
		6. PERFORMING ORG. REPORT NUMBER CR-R-84032
7. AUTHOR(s) Mysore L. Ramalingam, Dean L. Jacobson, James F. Morris and Shlomo Snir		8. CONTRACT OR GRANT NUMBER(s) Grant AFOSR-83-0067C
9. PERFORMING ORGANIZATION NAME AND ADDRESS Mechanical and Aerospace Engineering Arizona State University, Tempe, AZ 85287		10. PROGRAM ELEMENT, PROJECT, TASK AREA & WORK UNIT NUMBERS 2306, A2 61102F
11. CONTROLLING OFFICE NAME AND ADDRESS Air Force Office of Scientific Research, AFOSR/NE, Bolling Air Force Base, DC 20332-6600		12. REPORT DATE May 1984
		13. NUMBER OF PAGES 120
14. MONITORING AGENCY NAME & ADDRESS(If different from Controlling Office)		15. SECURITY CLASS. (of this report) Unclassified
		15a. DECLASSIFICATION/DOWNGRADING SCHEDULE

16. DISTRIBUTION STATEMENT (of this Report)

Approved for public release;
distribution unlimited.

17. DISTRIBUTION STATEMENT (of the abstract entered in Block 20, If different from Report)

18. SUPPLEMENTARY NOTES

19. KEY WORDS (Continue on reverse side if necessary and identify by block number)

20. ABSTRACT (Continue on reverse side if necessary and identify by block number)

High-temperature, high-power space energy-conversion systems follow an evolutionary path through continually expanding materials frontiers. Exponential growth trends point to requirements for ultimate alloys comprising the most refractory metals and metallide additives. Therefore understanding properties, transport tendencies and interaction characteristics of these ultralloy components is a crucial essentiality. Studies of such thermophysicochemical phenonemena and their detailed parametric dependencies and influences for

DD FORM 1473 EDITION OF 1 NOV 65 IS OBSOLETE
1 JAN 73
S/N 0102-014-6601 |

refractory materials receive intensive and extensive support in the USSR and other iron-curtain countries. Obviously those nations recognize the critical importance of refractory materials to high-temperature, high-power space energy-conversion systems. But all potential users also recognize the generic ducti-lity, embrittlement enigmas of the highest-temperature alloys--and the related implications of recrystallization. This latter category is the research area of concentration for these studies. Thus theoretic and experimental verifica-tions require high-temperature purification (by zone refining) and determina-tion (of hardness, elongation, conductivity . . . as well as vaporization, emission...). In addition standard x-ray, metallographic, Auger and other room-temperature examinations provide supporting information. To this point the zone-refining and high-temperature, hard-vacuum test methods have received the bulk of attention in initial studies of additive and impurity effects on tung-sten.

BIBLIOGRAPHIES

SECTION	REFERENCES
1. An Introduction to Space Refractory-Material Problems	47
2. Zone Refining of Tungsten	25
3. Hardness Testing at Elevated Temperatures	16
4. Properties of Tungsten	15
5. Facilities	4

TABLE OF CONTENTS

MATERIAL PROBLEMS FOR HIGH-TEMPERATURE, HIGH-POWER SPACE ENERGY-CONVERSION SYSTEMS

Mysore L. Ramalingam, Dean L. Jacobson, James F. Morris and Shlomo Snir
Mechanical and Aerospace Engineering
Arizona State University, Tempe, AZ

ABSTRACT

High-temperature, high-power space energy-conversion systems follow an evolutionary path through continually expanding materials frontiers. Exponential growth trends point to requirements for ultimate alloys comprising the most refractory metals and metallide additives. Therefore understanding properties, transport tendencies and interaction characteristics of these ultralloy components is a crucial essentiality. Studies of such thermophysicochemical phenomena and their detailed parametric dependencies and influences for refractory materials receive intensive and extensive support in the USSR and other iron-curtain countries. Obviously those nations recognize the critical importance of refractory materials to high-temperature, high-power space energy-conversion systems. But all potential users also recognize the generic ductility, embrittlement enigmas of the highest-temperature alloys -- and the related implications of recrystallization. This latter category is the research area of concentration for these studies. Thus theoretic and experimental verifications require high-temperature purification (by zone refining) and determination (of hardness, elongation, conductivity . . . as well as vaporization, emission...). In addition standard x-ray, metallographic, Auger and other room temperature examinations provide supporting information. To this point the zone-refining[*] and high-temperature, hard-vacuum test methods[*] have received the bulk of attention in initial studies of additive and impurity effects on tungsten.

[*]Refer to Sections 2,3&4

1. AN INTRODUCTION TO SPACE REFRACTORY-MATERIALS PROBLEMS

A-1

1. AN INTRODUCTION TO SPACE REFRACTORY-MATERIALS PROBLEMS

1.1 GROWING NEEDS FOR HIGH-TEMPERATURE MATERIALS IN SPACE POWER

"By the year 2000, an increasingly large portion of our national defense will depend on space-based systems. Extrapolation of present trends indicates that prime-power sources operating at megawatt levels and beyond will be needed. These power levels must be achieved at significantly higher values of specific power (w/kg) and energy (w-hr/kg) than are presently available to satisfy defense needs for maneuverability and survivability" (ref. 1). Following this prefatorical dedication of the Proceedings of the AFOSR Special Conference on Prime Power for High Energy Space Systems reference 2 presents a tabulation exemplifying the assertions of reference 1:

DOD POTENTIAL HIGH-POWER REQUIREMENTS

APPLICATION	POWER LEVEL
SPACE-BASED RADARS	5 TO 400 Kw
SURVEILLANCE	30 TO 100 Kw
COMMUNICATIONS	100 Kw
OTV (NLP)	>100 Kw
JAMMERS	70 TO 200 Kw
LASERS	10 TO 100 Mw PULSED
PARTICLE BEAMS	10 TO 100'S Mw PULSED
ADVANCED CONCEPTS	1 TO 100's Mw PULSED

Integrating upper requirements for a few of these steady-state space-systemic prime-power necessities yields a megawatt order of magnitude while pulsed capabilities extend to hundreds of megawatts.

A 1981 IECEC paper by Mahefkey of the Air Force "reviews some of the potential requirements for future military space power systems and summarizes some of the potential advantages of nuclear power for these

missions" (ref. 3). In another 1981 IECEC publication Mullin, Randolph, Hudson and Ambrus indicate NASA needs (ref. 4):

> There are a variety of potential missions, such as space based manufacturing, high capacity communications, outer planetary orbiters and lunar and planetary bases that appear to demand compact, high power, very long-life power units which are independent of sunlight. Nuclear reactors are the obvious choice for such applications.

In still another 1981 IECEC presentation LANL's Buden representing DOE asserts, "Reactors are the key to our future expansion into space" (ref. 5). Obviously the USSR agrees with this viewpoint because it has designed and built space nuclear reactors (SNR's) for sometime and lost one called COSMOS 954 in Canada on January 24, 1978. In fact a 1976 IECEC reprint by Kuznetsov reports on "the tests of three 'Topaz' reactors" ("thermionic nuclear power plants") that "demonstrated... long-term stable and reliable operation with good reproducibility of parameters" (ref. 6).

Quite obviously the Soviet development of space nuclear reactors (SNR's, refs. 4 and 7 to 14) aims at military goals. Therefore, also quite obviously, while the 100-kW$_e$ level is acceptable, megawatts and more are desirable to the leaders of the USSR SNR program. Then, again quite obviously, the US SNR path must lead directly to expeditious demonstration and rapid growth (refs. 1, 2 and 15). Thus, still quite obviously, SP-100-Program Management contemplates the advantages of the demonstrated technology accumulation for in-core thermionic energy conversion (IC-TEC) in their selection of an appropriate SNR approach (refs. 15 to 23). Such developments involve critical considerations of "material problems for high-temperature, high-power space energy-conversion systems."

Ultimate alloys are mandatory for <u>Future Orbital Power systems</u> <u>Technology Requirements</u> (NASA CP-2058, ref. 24). This proclamation derives from a summary by the invited materials-workshop chairman, W. A. Ranken of LANL, in the proceedings of that NASA-convened conference (ref. 24):

> If there is a single general trend that applies to the
> various combinations of heat sources and conversion
> methods, it is the one toward higher source temperature
> and higher sink temperature--and consequently lighter
> weight systems. For this reason the workshop felt that
> high-temperature-materials data was (sic) of prime
> importance....

Again this emphasizes solving "material problems for high-temperature, high-power space energy-conversion systems."

1.2 SOME CONSIDERATIONS OF ULTIMATE SPACE MATERIALS

High-temperature, high-power space energy-conversion systems require conductors and insulators as well as structural materials. At very high temperatures ceramic materials generally become more electrically conductive. This transition precludes their effective use to transfer heat to energy converters while blocking electric transport. Then such service demands special provisions like vacuum-gap radiation or inert-gas conduction (refs. 25 and 26).

Even when solid insulators function adequately at high temperatures their comparative mechanical intransigence limits fabricability and service adaptability. Thus refractory alloys must in general accommodate ceramics as well as themselves to system fabrication and service requirements.

4

But ultimate refractory alloys, ultralloys for convenience, also experience difficulties in applications to high-temperature, high-power space energy-conversion systems: Problems often redound from recrystallization and ductility effects. Other complications result from intensified effects of high temperatures and hard vacuum on strength, creep, diffusion, segregation, chemical reaction, vaporization -- and other thermophysicochemical phenomena. Detailed theoretic and experimental studies of some of these processes, first in separate ultralloy constituents of highly controlled purities and then in simple combinations, will lead to better understanding of the complex interactions complicated by compounding.

Because ultimate refractory alloys generally comprise ultimate refractory components a promising approach begins with the examination of the highest-melting, least-vaporizing metals (Table 1). As Table 2 indicates the most refractory body-centered-cubic (BCC) metal is tungsten (W: 3650K melting point and 4×10^{-12} torr vapor pressure at 2000K). In fact W is the most refractory metal. Highest-melting, least-vaporizing members of the hexagonal close-packed (HCP) and face-centered-cubic (FCC) metals are respectively rhenium (Re: 3450K and 10^{-10} torr at 2000K) and iridium (Ir: 2720K and 2×10^{-7} torr). Ir and Re as well as osmium (Os) added to tungsten increase its ductility, strength and resistance to creep and recrystallization (refs. 18 to 23 and 27 to 45).

Tout au contraire general effects of interstitial impurities (hydrogen H, boron B, carbon C and nitrogen N), oxygen (O) and their compounds tend to diminish ductility -- often through intergranular segregation and concentration by recrystallization (Table 3; refs. 27, 28 and 41 to 43). But some of these impurities can produce beneficially dispersed refractory products through reactions with low-vapor-pressure getters such as thorium

5

TABLE 1

MATERIAL PROBLEMS FOR HIGH-TEMPERATURE, HIGH-POWER SPACE ENERGY-CONVERSION SYSTEMS

ULTIMATE REFRACTORY ALLOYS COMPRISE

ULTIMATE REFRACTORY COMPONENTS.

HIGHEST-MELTING, LEAST-VAPORIZING METALS

METAL	MELTING, K	2000K TORR
BODY-CENTERED-CUBIC (BCC)		
TUNGSTEN (W)	3650	4×10^{-12}
TANTALUM (T_A)	3270	5×10^{-11}
MOLYBDENUM (M_O)	2890	2×10^{-7}
NIOBIUM (N_B)	2750	5×10^{-9}
HEXAGONAL CLOSE-PACKED (HCP)		
RHENIUM (R_E)	3450	1×10^{-10}
OSMIUM (O_S)	~ 3300	~ 3×10^{-10}
RUTHENIUM (R_U)	~ 2700	1×10^{-6}
FACE-CENTERED-CUBIC (FCC)		
IRIDIUM (I_R)	2720	2×10^{-7}
RHODIUM (R_H)	2240	~ 1×10^{-4}

TABLE 2

MATERIAL PROBLEMS FOR HIGH-TEMPERATURE, HIGH-POWER

SPACE ENERGY-CONVERSION SYSTEMS

HIGHEST-MELTING, LEAST-VAPORIZING METAL CRYSTALS

    BCC: <u>TUNGSTEN</u>

    HCP: <u>RHENIUM</u>

    FCC: <u>IRIDIUM</u>

DELETERIOUS INTERSTITIAL IMPURITIES

    <u>OXYGEN</u>, <u>CARBON</u>, NITROGEN AND HYDROGEN

EFFECTIVE LOW-VAPOR-PRESSURE GETTERS FOR INTERSTITIALS

    <u>HAFNIUM</u> AND <u>THORIUM</u> (MULTIPLY BENEFICIAL

    DISPERSED REFRACTORY INTERSTITIAL PRODUCTS)

PRIMARY PROBLEMS

    <u>DUCTILITY</u>

    <u>RECRYSTALLIZATION</u> (NUCLEATION OR PRIMARY

    RECRYSTALLIZATION AND GRAIN GROWTH)

7

TABLE 3

MATERIAL PROBLEMS FOR HIGH-TEMPERATURE, HIGH-POWER

SPACE ENERGY-CONVERSION SYSTEMS

DUCTILITY: TRACE-IMPURITY EFFECTS

INTERSTITIALS (ESPECIALLY GRAIN-BOUNDARY-SEGREGATED

INTERSTITIAL PRODUCTS) GREATLY REDUCE

DUCTILITY (IN THE FOLLOWING ORDERS).

VIA GROUP (C_R, M_O, W): CARBON (MOST EMBRITTLING),

OXYGEN, NITROGEN AND HYDROGEN

VA GROUP (V, N_B, T_A): HYDROGEN (MOST EMBRITTLING),

NITROGEN, OXYGEN AND CARBON

RECRYSTALLIZATION GREATLY REDUCES DUCTILITY BY

LOCALIZING BRITTLE INTERSTITIAL PRODUCTS IN GRAIN

BOUNDARIES AND INCREASING THEIR INTERGRANULAR

CONCENTRATIONS THROUGH GRAIN-GROWTH REDUCTION

OF THE TOTAL INTERGRANULAR SURFACE.

(Th) and hafnium (Hf) within the ultralloys (refs. 18 to 23, 31, 35 and 37).
Th is one of the best getters for O yielding high-melting, low-vaporizing
ThO_2 (refs. 18 to 23). And Hf is one of the better getters for C producing
high-melting, low-vaporizing HfC (refs. 21 to 23). As extremely fine
dispersions HfC and ThO_2 produce very positive results in W, Re alloys
(refs. 31, 35, 37 and 46). A few of these advantages appear in Tables 4 and
5 while Table 6 lists some simplified reasons for specific-additive
influences on recrystallization and ductility.

1.3 ADDITIVE EFFECTS ON REFRACTORY-METAL DUCTILITY AND RECRYSTALLIZATION

The preceding considerations of ultimate materials for high-
temperature, high-power space energy-conservation systems enable elemental
and systemic refractory-metal selections for pertinent research. And among
the major material problems for high-temperature, high-power space energy-
conversion systems the related characteristics of ductility and
recrystallization are both important and enigmatic. These and some other
aspects partially listed in Tables 2, 6 and 7 allowed focusing on the
specific materials and phenomena for initial studies in this essential and
engrossing technological area. In particular this work begins with W
because it is the most refractory element with impeding ductility problems.
W also submits to very effective high-temperature, hard-vacuum clean-up
procedures. And substantive scientific information on various high-
temperature W properties exists in the open literature.

Partly because of existing facilities, capabilities and expertise the
research on recrystallization and ductility of W with low-level additives
initially comprises the study areas outlined in Table 8. Zone-refining and
isothermal-annealing processes coupled with hardness and tensile testing as

9

TABLE 4

"MECHANICAL PROPERTIES OF A TUNGSTEN-23.4 PERCENT RHENIUM-0.27 PERCENT HAFNIUM-CARBON ALLOY"

(KLOPP AND WITZKE (NASA LERC): J. LESS-COMMON METALS, 24 (1971), 427 TO 443)

W, 23.4 RE, LOW-LEVEL HFC OFFERS

- CREEP STRENGTHS SIMILAR TO THOSE OF W,26RE AT >1920° C

- AT LOWER TEMPERATURES, CREEP (AND ULTIMATE) STRENGTHS CONSIDERABLY GREATER THAN THOSE OF W,26RE

- MICROSTRUCTURAL RECRYSTALLIZATION AT >1700° C

- DUCTILITY (4T) BEND AS-ROLLED TO - 30° C

- DUCTILITY TO <0° C AFTER >1980° C ANNEALING

TABLE 5

"THORIATED RHENIUM, TUNGSTEN ALLOYS FOR ELECTRON-TUBE APPLICATIONS"

(FRED FOYLE (RE DIV., CHASE BRASS & COPPER; PRES., RHENIUM ALLOYS, INC.):

(7TH NATIONAL CONFERENCE ON TUBE TECHNIQUES, SEPTEMBER 1964)

W, 15 RE, 2 TH O_2 IS

- STRONGER AT $>1500^0$ C THAN W, 2THO_2 WHICH IS STRONGER THAN W (MANY TIMES STRONGER THAN MO, RE ALLOYS).

- QUITE DUCTILE EVEN AFTER 2450^0 C SERVICE:
  A 0.020" D WIRE BENDS A FEW TURNS AROUND A
  0.040" D MANDREL (A CONTINUOUS 1T BEND TEST
  RATHER THAN THE STANDARD 4T VERSION).

- "READILY BENT AFTER WELDING."

  ("A 74W, 24RE, 2THO_2 ALLOY HAS MAXIMUM DUCTILITY....")

TABLE 6

MATERIAL PROBLEMS FOR HIGH-TEMPERATURE, HIGH-POWER
SPACE ENERGY-CONVERSION SYSTEMS

RECRYSTALLIZATION: TRACE-ADDITIVE EFFECTS

UNIFORMLY DISPERSED TRACE ADDITIVES PROMOTE
HOMOGENEOUS IMPERFECTION AND NUCLEATION.

"IMPURITY DRAG" AND "PINNING" INHIBIT LARGE-GRAIN GROWTH.

HIGHER RECRYSTALLIZATION TEMPERATURES WITH
SMALLER, MORE-UNIFORM CRYSTALS RESULT.

INTERGRANULAR-IMPURITY CONCENTRATIONS REMAIN MUCH LOWER.

TRACE ADDITIVES ARE GENERALLY MOST EFFECTIVE IN
SOLID SOLUTION, NEXT PRECIPITATION, THEN DISPERSION.

TRACE-ADDITIVE CHEMISTRY CAN HAVE A PROFOUND EFFECT.

12

TABLE 7

MATERIAL PROBLEMS FOR HIGH-TEMPERATURE, HIGH-POWER

SPACE ENERGY-CONVERSION SYSTEMS

DUCTILITY AND RECRYSTALLIZATION OF HIGH-PURITY REFRACTORY METALS

o W(BCC), R_E(HCP) AND I_R(FCC) WERE SELECTED AS HIGHEST-MELTING, LEAST-
   VAPORIZING EXAMPLES OF THEIR CRYSTAL SPECIES.

o W (VIA), R_E (VIIA) AND I_R (VIII) REPRESENT DIFFERENT CHEMICAL GROUPS.

o FEW RECRYSTALLIZATION RESULTS EXIST FOR HIGH-PURITY W, R_E AND I_R.

o ZONE REFINING PURIFIES W, R_E AND I_R BY IMPURITY VAPORIZATION AS WELL
   AS SEGREGATION.

o LOW VAPORIZATION OF W, R_E AND I_R ENABLES VERY-HIGH-TEMPERATURE
   OBSERVATION OF RECRYSTALLIZATION BY THERMIONIC-EMISSION MICROSCOPY.

o W, R_E AND I_R ARE EXCELLENT C_S-DIODE ELECTRODES: W, 25 R_E SERVES WELL
   IN HIGH-TEMPERATURE HEAT PIPES ("HIGH-TEMPERATURE, HIGH-POWER SPACE
   ENERGY-CONVERSION SYSTEMS").

o R_E AND I_R BOTH IMPROVE DUCTILITY AND RECRYSTALLIZATION RESISTANCE IN
   HIGH-STRENGTH, LOW-CREEP W ALLOYS.

o W, R_E AND I_R COULD BE MAJOR COMPONENTS IN ULTIMATE SPACE ALLOYS.

13

TABLE 8

MATERIAL PROBLEMS FOR HIGH-TEMPERATURE, HIGH-POWER

SPACE ENERGY-CONVERSION SYSTEMS

<u>RECRYSTALLIZATION AND DUCTILITY STUDIES</u>

(POLY-, BI- AND SINGLE-CRYSTAL SAMPLES)

HIGH-TEMPERATURE STUDIES

ZONE REFINING

ISOTHERNAL ANNEALING

THERMIONIC-EMISSION MICROSCOPY

MASS SPECTROMETRY AND SPECTROPHOTOMETRY

HOT HARDNESS AND ELECTRICAL RESISTIVITY

ROOM-TEMPERATURE STUDIES

STANDARD METALLOGRAPHY

ELECTRON TRANSMISSION MICROSCOPY

CHEMICAL ANALYSES (AUGER, ELECTRON PROBE....)

TENSILE, BENDING, HARDNESS, RESISTIVITY....

THEORETIC AND CORRELATIVE ANALYSES

well as other high-temperature and room-temperature sensing and examination promise enlightening results. For example W with minor Re percentages as well as additions of ThO_2 and HfC in the order of one percent should produce ultimate space alloys. And isolating the individual as well as compound contributions for the additives will illuminate salient mechanistic and phenomenal effects.

1.4 RECRYSTALLIZATION

Because recrystallization implications pervade material problems for high-temperature, high-power space energy-conversion systems, further amplification of its signals seems apropos: The technological jargon for recrystallization has evolved through several levels of understanding to the point where misinterpretation is not only possible but also probable. Primary recrystallization includes nucleation and primary growth which smears into normal grain growth which can occur with discontinuous or secondary recrystallization which sometimes continues as tertiary recrystallization when mean size attains bulk dimensions. Thus "formation and migration of large-angle boundaries" seems a more appropriate definition because "some recrystallization processes occur without nucleation" (ref. 43). However convenience and consensus push steadily toward the use of "recrystallization" to cover the gamut. For greater specificity the numbered descriptions of Table 9 offer reasonable alternatives for differentiating levels of recrystallization.

In any event crystalline equilibrium obtains practically at the center of a huge pure flawless single crystal. In contrast common thermodynamically unstable lattice states derive from chemical impurities and physical imperfections such as point defects, dislocations, grain

TABLE 9

RECRYSTALLIZATION

REARRANGEMENT AND REDUCTION OF LATTICE IMPERFECTIONS

BELOW THE MATERIAL MELTING POINT LOWERS FREE ENERGY:

1. AGGLOMERATION, REACTION, ULTIMATELY ANNIHILATION OF POINT DEFECTS:

2. SHRINKAGE OF DISLOCATION LOOPS AND DISLOCATION ANNIHILATION:

3. DISLOCATION REARRANGEMENT IN LOW-FREE-ENERGY CONFIGURATIONS:

4. IMPERFECTION REACTIONS PRODUCING LATTICE REGIONS CAPABLE OF GROWTH;

5. GRAIN-BOUNDARY ABSORPTION OF POINT DEFECTS AND DISLOCATIONS:

6. DIMINUTION OF THE TOTAL INTERGRANULAR SURFACE.

1 AND 2 ARE "RECOVERY." 3 CAN BE EITHER "POLYGONIZATION" YIELDING
SUBGRAINS WITH LOW-ANGLE BOUNDARIES OR "NUCLEATION." 4 IS "NUCLEATION,"
ALSO TERMED "PRIMARY RECRYSTALLIZATION." 5 AND 6 ARE "GRAIN GROWTH."

boundaries and external surfaces. Diminishing, ultimately eliminating these instabilities reduces total free energy -- driving recrystallization and its "zone-refining" proclivities toward the huge pure flawless single crystal.

Grain-growth velocity equals the product of the boundary mobility and the resultant driving force. In the usual example cold work produces a driving force equivalent to the free-energy-density difference across the intergranular region which is proportional to the imperfection-density difference across the migrating boundary. A variety of driving forces appears in Table 10 (A and B).

As Table 6 implies dragging forces, which oppose grain-boundary migration, arise from solute atoms, precipitants, dispersed particles, surface grooves.... Concentration of such drag configurations often produces grain-boundary pinning. An inverse drag coefficient can be considered a specific mobility which characterizes boundary migration for each driving force. Mobilities are simple in concept but complicated in evaluation -- often occurring as complex functions grain-boundary velocity. In actuality appropriate mobility summations correspond to resultants for driving and dragging forces.

Reference 47 describes grain-boundary migration as an evolution of the reaction-rate theory, presented for a rather pertinent model in Table 11. On this theoretic basis references 43, 47 and many others contributed to the development of exemplary boundary-migration expressions given in Tables 12 through 15 and illustrated by Figure 1. These equations differ only in the initial factor which oversimplifies the definition and separability of grain-boundary-migration mechanisms. But their heuristic value is undebatable.

17

TABLE 10A
RECRYSTALLIZATION

DRIVING FORCES FOR GRAIN-BOUNDARY MIGRATION

ORIGIN	EQUATION	ESTIMATED MAGNITUDE (N/m^2)
STORED ENERGY	$\Delta\rho\Gamma$	10^7
REVERSED-CAPILLARY	$2\gamma f/r$	10^6
ELECTRIC	λE	10^5
CAPILLARY	$2\gamma/r$	10^4
SURFACE ENERGY	$2\Delta\gamma/d$	10^4
MAGNETIC	$(\frac{1}{2})\Delta\mu H^2$	10^3
MECHANICAL	0σ	10^3
TEMPERATURE GRADIENT	$\delta S\nabla T$	10^2
ELASTIC ENERGY	$(\frac{1}{2})\Delta s\sigma^2$	10^2
ELECTROMIGRATION	$2nq\rho Z^*J$	10^2

MASTELLER AND BAUER: RECRYSTALLIZATION OF METALLIC MATERIALS

18

TABLE 10B

RECRYSTALLIZATION

DRIVING-FORCE SYMBOLS

$\Delta\rho \equiv$ DIFFERENCE BETWEEN DISLOCATION DENSITY (M^{-2}) IN TWO ADJACENT GRAINS DEFINING THE BOUNDARY, $\Gamma \equiv$ DISLOCATION LINE ENERGY (J/m), $\gamma \equiv$ INTERFACIAL (GRAIN BOUNDARY) ENERGY (J/m^2), $f \equiv$ GENERALIZED AMPLIFICATION FACTOR (DIMENSIONLESS), $r \equiv$ RADIUS OF CURVATURE OF BOUNDARY (m), $\lambda \equiv$ NET ELECTRIC CHARGE PER UNIT BOUNDARY AREA (C/m^2), $E \equiv$ ELECTRIC FIELD (V/m), $\Delta\gamma \equiv$ DIFFERENCE BETWEEN SURFACE ENERGY OF TWO ADJACENT GRAINS DEFINING THE BOUNDARY (J/m^2), $d \equiv$ SPECIMEN THICKNESS (m), $\Delta\mu$ DIFFERENCE BETWEEN MAGNETIC PERMEABILITY IN TWO ADJACENT GRAINS DEFINING THE BOUNDARY (H/m), $H \equiv$ MAGNETIC FIELD (A/m), $\Theta \equiv$ MISORIENTATION BETWEEN GRAINS DEFINING A (LOW-ANGLE) BOUNDARY (RADIANS), $\sigma \equiv$ STRESS FIELD (Pa), $n \equiv$ NUMBER OF ATOMS PER GRAIN BOUNDARY AREA (m^{-2}), $S \equiv$ ENTROPY $(J/^{\circ}Cm^3)$, $\nabla T \equiv$ TEMPERATURE GRADIENT $(^{\circ}C/m)$, $\Delta s \equiv$ DIFFERENCE BETWEEN ELASTIC COMPLIANCE CONSTANTS IN TWO ADJACENT GRAINS DEFINING THE BOUNDARY (m^2/N), $q \equiv$ ELECTRIC CHARGES (C), $\rho \equiv$ ELECTRICAL RESISTIVITY (Ωm), $Z^* \equiv$ (NORMALIZED) DIFFERENCE BETWEEN (ELECTRON) SCATTERING CROSS SECTIONS IN THE ACTIVATED AND GROUND STATES (DIMENSIONLESS), $J \equiv$ CURRENT DENSITY (A/m^2), and $\delta \equiv$ GRAIN BOUNDARY THICKNESS.

19

TABLE 11

SIMPLIFIED REACTION-RATE THEORY

FOR PURE-METAL OXIDATION CONTROLLED BY IDEAL-SOLUTION MIGRATION (AFTER EVANS FROM HURLEN) THE ABSOLUTE REACTION-RATE THEORY (EYRING, LAIDLER AND GLASSTONE) YIELDS AN EXPRESSION FOR ONE-DIMENSIONAL NET TRANSPORT OF A SPECIES:

$$v = (\lambda kT/h)exp\left(-\Delta G_o^{\ddagger}/RT\right)[c \; exp(-\alpha\lambda zFd\phi/RTdx) - (c + \lambda \; dc/dx)exp((1 - \alpha)\lambda zFd\phi/RTdx)]$$

THE PRE-BRACKET FACTOR, SPECIFIC RATE FOR A UNIT CONCENTRATION WITHOUT FIELDS, INVOLVES NO NET TRANSPORT. THE FIRST TERM IN THE BRACKETED FACTOR REPRESENTS ACCELERATION BY THE FIELD. THE SECOND TERM IN THE BRACKETS COVERS RETARDATION. THEN v IS THE NET TRANSPORT RATE; λ, THE EQUILIBRIUM DISTANCE BETWEEN MIGRATING CHARGED PARTICLES; k, BOLTZMANN CONSTANT; T, DEGREES KELVIN; h, PLANCK CONSTANT; $\Delta G_o^{\ddagger}$, STANDARD CHEMICAL ACTIVATION ENERGY; R, GAS CONSTANT; c, CONCENTRATION OF MIGRATING SPECIES; α, SYMMETRY FACTOR; z, MIGRATING-PARTICLE CHARGE; F, FARADAY EQUIVALENT; ϕ, INNER POTENTIAL; AND x, DISTANCE IN THE TRANSPORT DIRECTION.
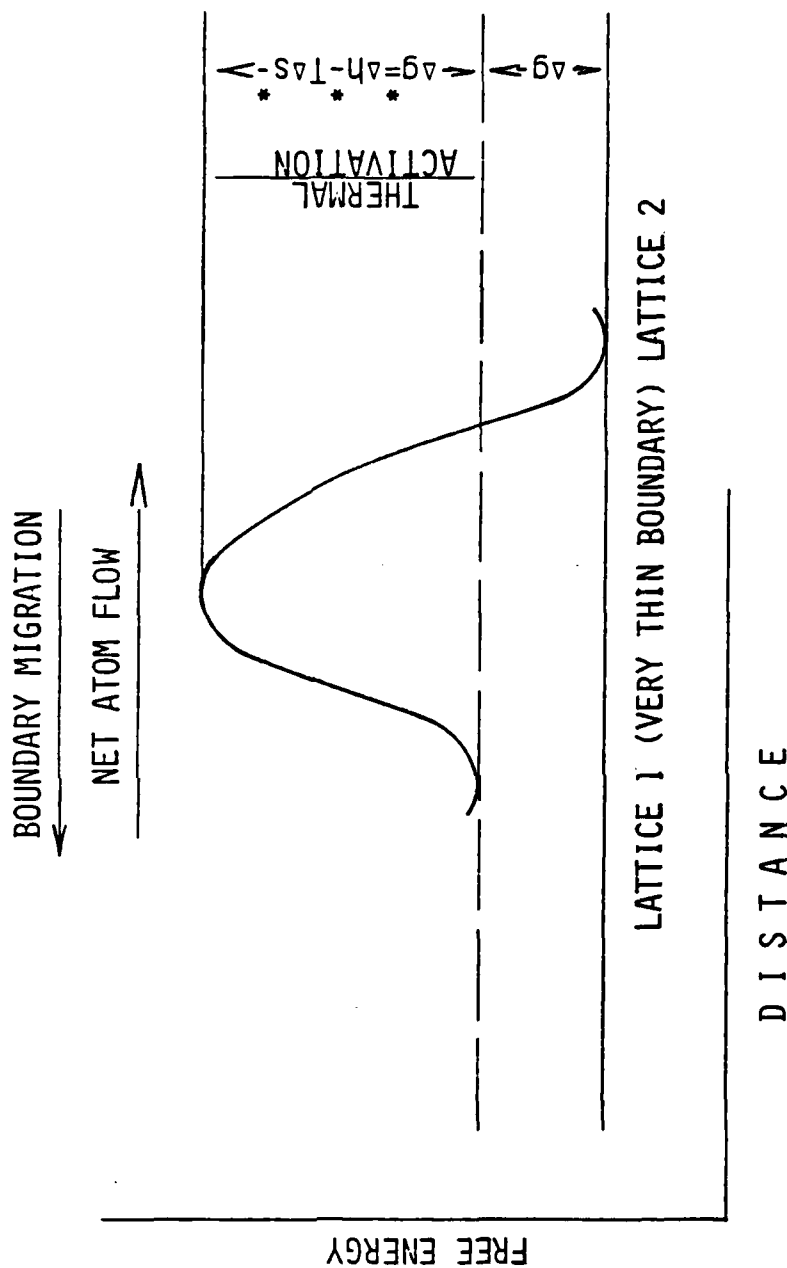
20

FIGURE 1
RECRYSTALLIZATION

BOUNDARY MIGRATION

NET ATOM FLOW

THERMAL ACTIVATION

$\Delta g = \Delta h - T \Delta s$

Δg

LATTICE 1 (VERY THIN BOUNDARY) LATTICE 2

FREE ENERGY

D I S T A N C E

TABLE 12
RECRYSTALLIZATION

1-TO-2 ATOM FLOW
→

ν_1 exp $(- g^*/kT)$

$\nu_1 \approx \nu_2 \approx \nu$ = LATTICE-ATOM OSCILLATORY FREQUENCY

NET BOUNDARY -

MIGRATION RATE = $v \approx v \approx \nu \lambda [1 - \exp(-\frac{\Delta g}{kT})] \exp(-\frac{\Delta g^*}{kT})$

λ = EFFECTIVE ATOM DISPLACEMENT THROUGH THE BOUNDARY

$\Delta g/kT << 1$ FOR PURE-METAL RECRYSTALLIZATION

BOUNDARY-MIGRATION RATE = $v \approx v \approx \nu \lambda (\frac{\Delta g}{kT}) \exp(-\frac{\Delta g^*}{kT})$

2-TO-1 ATOM FLOW
→

ν_2 exp $[-(\Delta g^* + \Delta g)/kT]$

22

TABLE 13

RECRYSTALLIZATION

CRYSTAL-STEP MODEL FOR GRAIN BOUNDARY MIGRATION

ASSUMPTIONS: CLOSELY PACKED (FCC) PLANES END AT BOUNDARIES IN PERIODIC STEPS HAVING KINKS WHICH CAN RELEASE OR RECEIVE ATOMS THAT DIFFUSE THROUGH INTERGRANULAR REGIONS. Δg^* IS THE SUM OF FREE ENERGIES FOR TRANSITIONS OF SUCH ATOMS; δ IS THE GRAIN-BOUNDARY WIDTH, GREATER THAN SINGLE-JUMP λ; f_1 AND f_2 ARE POSITIVE FUNCTIONS OF STEP DENSITIES ON OPPOSING BOUNDARY SURFACES AND OF VACANCY EFFECTS. THEN -

$$\psi = \frac{\lambda}{\delta} \left[1 + \frac{\lambda}{\delta} \left(\frac{1}{f_1} + \frac{1}{f_2} \right) \right]^{-1} < 1$$

AND -

GRAIN-BOUNDARY
MIGRATION RATE $\quad = V = \psi \, \nu \, \lambda \left(\frac{\Delta g}{kT} \right) \exp \left(- \frac{\Delta g^*}{kT} \right)$

GLEITER: ACTA MET. 17, 853, 1969

23

TABLE 14

RECRYSTALLIZATION

VACANCY MODELS FOR GRAIN-BOUNDARY MIGRATION

ASSUMPTIONS: MIGRATION VELOCITY INCREASES WITH RISING BOUNDARY VACANCY FRACTION C_m - AS INDICATED BY NUMEROUS EXPERIMENTS: DIFFUSION JUMPS ACROSS BOUNDARIES OCCUR THROUGH VACANCY-SITE CHANGING PROCESSES. BECAUSE INSTANTANEOUS C_m's DEPEND ON VACANCY INJECTION, COLLECTION AND EJECTION MECHANISMS, THEY ARE COMPLEX FUNCTIONS OF BOUNDARY VELOCITIES AND TEMPERATURES AS WELL AS VACANCY SOURCE AND SINK EFFECTS. THEN –

GRAIN-BOUNDARY
MIGRATION RATE $= V \approx C_m \nu \lambda \left(\frac{\Delta g}{kT}\right) \exp\left(-\frac{\Delta g^*}{kT}\right)$

24

TABLE 15

RECRYSTALLIZATION

SATURATION MODEL FOR GRAIN-BOUNDARY MIGRATION

ASSUMPTIONS: DISLOCATION PROCESSES PROPOSED BY
LI (1961) AND MODIFIED BY GRABSKI (1969) RESULT
IN ALLOWED MATERIAL TRANSPORT ONLY ACROSS AN
"ACTIVE CROSS SECTION" FRACTION σ OF THE GRAIN-
BOUNDARY SURFACE. THUS SATURATION LIMITS THE
MIGRATION VELOCITY:

GRAIN-BOUNDARY
MIGRATION RATE $= V \approx \sigma \nu \lambda \left(\frac{\Delta g}{kT}\right) \exp\left(-\frac{\Delta g^*}{kT}\right)$

Still further simplifications for grain growth in much more complex two-phase systems appear as radius, time relationships with effective coefficients for various diffusion types in Tables 16 and 17. Effects of dispersed particles on grain-growth control through pinning manifest quite simply in the equation of Table 17.

Many of the recrystallization mechanisms touched only as tops of the complex scientific topography of this important technology submit to description by thermal rules of thumb. Such a mechanistic listing comprises the temperature resolution given in Table 18. Most of these approximate thermal boundaries have been encountered by those who work with high-temperature alloys. Recognition of these transitions emphasizes that direct and side effects of recrystallization exert abstruse influences on strength, creep, compatibility...and ductility of refractory alloys. And those properties are major considerations in ultrathermal alloy applications.

But ductility and recrystallization are often critical parameters in the capability of ultralloys to adapt themselves and ceramics to fabrication and service requirements. Thus a better understanding of refractory-alloy recrystallization is a crucially essential part of overcoming the material problems for high-temperature, high-power space energy-conversion systems.

26

TABLE 16
RECRYSTALLIZATION

GRAIN GROWTH OF TWO-PHASE ALLOYS

(HORNBOGEN: METALL 29, 247, 1975)

ELEVATED TEMPERATURES ACCENTUATE RECRYSTALLIZATION OF TWO-PHASE MICROSTRUCTURES DRIVEN BY INTERFACIAL ENERGY DENSITIES WHICH ARE FUNCTIONS OF GRAIN SIZE $r_{\alpha\alpha}$. THEN FOR BOUNDARY ($D_{\alpha\alpha}$ OR $D_{\alpha\beta}$), DISLOCATION-CORE PIPE (D_p) OR VOLUME (D_V) DIFFUSION SIMPLE GROWTH, TIME LAWS OBTAIN:

$r_{\alpha\alpha} \propto (D_{\alpha\alpha}t)^1$ PRIMARY OR SECONDARY RECRYSTALLIZATION

$r_{\alpha\alpha} \propto (D_{\alpha\alpha}t)^{\frac{1}{2}}$ GRAIN GROWTH (RARELY OBSERVED)

$r_p \propto (D_V t)^{1/3}$ DISPERSED-PARTICLE GROWTH (OFTEN SEEN)

$r_{\alpha\beta} \propto (D_{\alpha\beta}t)^{\frac{1}{4}}$ DUPLEX-STRUCTURE GROWTH (GRAIN-SIZE DIFFUSION DISTANCES FOR DUPLEX MICROSTRUCTURES RESULT IN RELATIVELY STABLE FINE-GRAINED ALLOYS.)

TABLE 17

RECRYSTALLIZATION

THERMAL STABILITY OF DUPLEX ALLOYS

(HORNBOGEN: METALL 29, 247, 1975)

NORMAL-GRAIN AND DUPLEX-STRUCTURE GROWTHS

SUCCUMB TO DISPERSED-PARTICLE CONTROL WHEN

DRIVING AND PINNING FORCES ARE EQUAL. THEN –

$$r_{\alpha\alpha}^{crit.}(t) = A \frac{r_p(t)}{f} = A^* \frac{(D_v t)^{1/3}}{f}$$

WHERE A's ARE GEOMETRIC FACTORS DEPENDENT ON

LOCAL-PARTICLE SHAPE AND SIZE DISTRIBUTIONS.

THE DISPERSED-PARTICLE VOLUME FRACTION f THAT

STABILIZES GROWTH DECREASES CONSIDERABLY WITH

PREDOMINANT GRAIN-BOUNDARY PARTICULATE LOCATION.

TABLE 18

RECRYSTALLIZATION

APPROXIMATE THERMAL BOUNDARIES FOR ALLOYS

HALF THE ABSOLUTE MELTING POINT ($0.5T_M$) OFTEN INDICATES IMPORTANT INCIPIENCE OF THERMALLY ACTIVATED PROCESSES.

BELOW $0.3T_M$ TO $0.4T_M$ SHORT-RANGE (ELECTRONIC, STACKING-FAULT, LOCAL-ORDER) INTERACTIONS GENERALLY DOMINATE.

LONGER-RANGE SOLUTE, DISLOCATION INTERACTIONS CONTINUE THEIR INFLUENCES TO $0.5T_M$ OR HIGHER.

ABOVE $0.75T_M$ TO $0.8T_M$ INCREASED MOBILITY OF SOLUTE ATOMS GREATLY REDUCES THEIR HINDRANCE OF DISLOCATION MOVEMENT.

ARRHENIUS RELATIONS FOR GRAIN-BOUNDARY MIGRATION VELOCITIES OFTEN BREAK AT $\sim 0.8T_M$ AND EXHIBIT MUCH LOWER ACTIVATION ENERGIES IN THE HIGHER-TEMPERATURE RANGE.

REFRACTORY-DISPERSION STRENGTHENING GENERALLY EXCELS FOR APPLICATIONS OF ALLOYS NEAR THEIR MELTING POINTS.

29

1.5 REFERENCES

1. A. Hyder and P. Turchi: Preface; Proceedings of the AFOSR Special Conference on Prime Power for High Energy Space Systems; Norfolk, Virginia; February 1982.

2. M. Cohen: High Power Requirements, p. I-3, ref. 1 proceedings.

3. T. Mahefkey: "Thermionic Application for Future Air Force Space Power Systems"; 16th IECEC (Intersociety Energy Conversion Engineering Conference), Atlanta, Georgia; August 1981.

4. S. Mullin, L. Randolph, W. Hudson and J. Ambrus: Advances in Space Power Research and Technology at the National Aeronautics and Space Administration, ibidem.

5. D. Buden: "The Acceptability of Reactors in Space," ibidem.

6. V. Kuznetsov et alii: "The State and Directions of Thermionic Converters Research in the USSR, 11th IECEC, September 1976; foreign-paper presentation.

7. V. Kuznetsov: Operation of Thermionic Reactor-converters TOPAZ-1 and TOPAZ-2, proceedings of the 3rd International conference on Thermionic Electrical Power Generation-Volume I, Juelich, Germany, June 1972.

8. I. Morohkov (Soviet Union), G. Newby (United States), M. Pecqueur (France). W-J. Schmidt-Juster (Federal Republic of Germany) and K. Beckurts (moderator, FRG): Panel discussion of future thermionic power generation and its applications, 3rd International Conference on Thermionic electrical Power Generation, Juelich, FRG, June 1972.

9. V. Kuznetsov: Development and construction of the Thermionic Nuclear Installation TOPAZ, Atomnaya Energiva, volume 36, June 1974.

10. V. Bel'giy: The On-Board Computer for Diagnosis of Satellite Power Units, IAF-79-F-168 Preprint, XXX Congress of the International Astronautical Federation, Munich, September 1979.

11. J. Grey and M. Gerard: A Critical Review of the State of Foreign Space Technology, AIAA Report to NASA, NASA Contract NAS W-3098, February 1978.

12. E. Knorre: Nuclear Energy for Space Exploration, New Times (translation), Number 7, Moscow, February 1978.

13. E. Galloway: United National Consideration of Nuclear Power for Satellites, IAF-79-IISL-19, XXX Congress of the International Astronautical Federation, Munich, September 1979.

14. J. P. Layton, J. Grey and F. C. Schwenk: A Survey of High-Temperature, Compact Nuclear Fission Reactors, T-SAC Report 82-001 prepared for Committee on Advanced Nuclear Systems, Energy Engineering Board, Commission on Engineering and Technical Systems National Research Council, July 1982.

15. J. Morris: Space-Nuclear-Reactor Questions, 18th IECEC, August 1983.

16. J. Morris: Thermionic Energy conversion (TEC) Topping Thermoelectrics, IEEE Conference on Plasma Science (COPS), May 1981, DOE/NASA/1062-8 (sic), NASA TM-81677.

17. J. Morris: The Space Nuclear Reactor, Air Force AFWAL TM- , Arizona State University ERC-R-82004 (transmitted September 1981), to be published.

18. J. Morris: Tungsten, Rhenium alloys in space Nuclear Reactors, Air Force AFWAL TM- , Arizona State University ERC-R-82005 (transmitted October 1981), to be published.

19. J. Morris: Direct-Energy-Conversion Implications of Space Nuclear Reactors, Proceedings of the 17th IECEC, August 1982.

20. J. Morris: SP-100 Evolutions from SPAR Concepts, Air Force AFWAL TM- , Arizona State University ERC-R-82040 (transmitted September 1982), to be published.

21. J. Morris: Ultralloys for Nuclear Thermionic Conversion, 18th IECEC, August 1983.

22. J. Morris: Ultralloys for Current and Future Space Power, Air Force AFWAL TM- , Arizona State University ERC-R-83025 (transmitted June 1983), to be published.

23. J. Morris: Pre-1973 Refractory-Alloy Technology to Improve and Simplify In-Core Thermionic Energy Conversion, Air Force AFWAL-TM- (transmitted November 1983) to be published.

24. NASA Conference: Future Orbital Power Systems Technology Requirements, NASA CP-2058, September 1978.

25. J. Morris: Optimize Out-of-Core Thermionic Energy Conversion for Nuclear Electric Propulsion, IEEE Conference on Plasma Science (COPS), May 1978, also NASA TM-73892.

26. J. Morris: High-Thermal-Power-Density Heat Transfer with Electrical Isolation at High Temperatures, LeRC disclosure LEW-12950-1, July 1977 (cited and discussed in refs. 21).

27. E. Savitskii, M. Tylkina and K. Pavarova: Rhenium Alloys, Izdatel'stvo "Nauk", Moscow, 1965.

28. M. Pridantsev: Structures and Properties of Heat-Resistant Metals and Alloys, Izdatel'stvo "Nauk", Moscow, 1967.

29. R. Yoda, T. Itagaki and T. Hamada: Some Properties of Tungsten-Rhenium Alloys, Japan Institute of Metals Journal, Volume 34, November 1970.

30. M. Majdic and G. Wirth: Uber das Rekristallisationsverhalten Einer mit Thorium-Oxid Dispersionsgeharteten Wolfram-Rhenium-Legierung in

Vergleich zu Reinem Wolfram, Journal of Less-common Metals, Volume 24, 1971.

31. W. Klopp and W. Witzke: Mechanical Properties of a Tungsten -23.4 Percent Rehenium -0.27 Percent Hafnium-Carbon Alloy, Journal of Less-Common Metals, Volume 24, 1971, also NASA TN D-6328.

32. S. Golovanenko, A. Natapova, B. Klypin and T. Kesazv: Recrystallization of Tungsten Alloys, Metallovedenie i Termicheskaya Obrabotka Metallov Number 9, September 1976.

33. G. Hoppin: Investigation of Joining the Refractory Metals Tungsten and Niobium, GE Contract with WADD, Materials Central, USAF, 1960 to 1962.

34. H. Ogden: Development of a Ductile Tungsten Sheet Alloy, BMI contract with Bu Weps, Navy, 1960 to 1962.

35. P. Raffo and W. Klopp: Mechanical Properties of Solid-Solution and Carbide-Strengthened Arc-Melted Tungsten Alloys, NASA TN D-3248, February 1966.

36. W. Klopp: Review of Ductilizing of Group VIa Elements by Rhenium and Other Solutes, NASA TN D-4955, 1968.

37. W. Witzke: Effects of Composition on Mechanical Properties of W-4 Re-Hf-C Alloys, Metallurgical Transactions, Volume 5, February 1974 (also NASA TN D-7210).

38. M. Gavrilyuk: The Nature of Cold Brittleness in Refractory Metals of Group VIa, Metallovedenie i Termicheskaya Obrabotka Metallov, Number 1, January 1972.

39. Ye. Savitskiy, V. Checkhovskoy, K. Povarova, V. Zaychenko, P. Makrov and V. Petukhov: Study and Applications of Rhenium Alloys, ISS1edovaniye i Primeneniye Splavov Reniya, "Nauka" Press, 1975.

40. Ye. Savitskiy, V. Bykov, K. Povarova, L. Alekseyeva, S. Budagovskiy, P. Makarov and I. Kondakhchan: Effect of Alloying with Niobium, Rhenium and Osmium on the Physical Properties of Cast Tungsten Alloys of Rare Metals with Special Physiocochemical Properties, "Nauka" Press, 1975.

41. L. Murr: Interfacial Phenomena in Metals and Alloys, Adison-Wesley, London, 1975.

42. J. Tien and G. Ansell: Alloy and Microstructural Design, Academic Press, New York, 1976.

43. F. Haessner: Recrystallization of Metallic Materials, Dr. Riederer Verlag GmbH, Stuttgart, 1978.

44. M. Garfinkle: Effect of Rhenium Alloying on Lattice Dilation of Group VI-A Refractory Metals, Metallurgical Transactions, Volume 1, April 1970.

45. D. Novick: A Field Ion Microscope Investigation of the Tungsten-Rhenium-Oxygen System, Columbia University Rh.D. dissertation, University Microfilms, Ann Arbor, 1968.

46. F. Foyle: Thoriated Rhenium-Tungsten Alloys for Electron Tube Applications, 7th National Conference on Tube Techniques, National Advisory Group on Electron Devices, September 1964.

47. J. Christian: The Theory of Transformations in Metals and Alloys, Pergamon Press, Oxford, 1975.

2. ZONE REFINING OF TUNGSTEN

I.] <u>Zone Refining</u>:

   i) Introduction

  ii) Zone Melting

 iii) Zone Refining

  iv) Distribution Coefficient

   v) Floating-Zone Technique

  vi) Shapes and Sizes of Floating Zones

 vii) Electron-Beam Heating

II.] <u>Literature Survey on Purifying Materials Using Electron-Beam Floating Zone (EBFZ) Refining.</u>

III.] <u>High Vacuum Set-Up for Zone Refining Tungsten:</u>

   i) Initial Conceptual Design

  ii) Modified Configuration

 iii) Stepper-Motor-Operated UHV Linear-Motion Drive

  iv) The Vacuum System

IV.] <u>Theoretical Analysis of Zone Refining</u>

   i) An Introduction

  ii) Literature Survey on the Theory of Zone Refining.

 iii) Proposed Analytical Work for Zone Refining of Tungsten

     Nomenclature

     Reference

2. ZONE-REFINING

Introduction

The first important application of zone melting was purifying germanium for use in transistors. The method was soon widely adopted by transistor and diode manufacturers throughout the world. However zone melting can be applied to many other substances, in fact to any substance that can safely be melted and that exhibits a difference in impurity concentration between liquid and freezing solid. Consequently the method has found widespread use: in research and manufacture for purification and crystal growth of metals, semiconductors and organic or inorganic chemicals. Quite a few zone-refined metals are available in small quantities, and commercial use in the field of chemicals is steadily increasing.

However in the context of studying material problems for high-temperature, high-power space energy-conversion systems we use zone refining not only for purifying materials but also to distribute a desired impurity very uniformly throughout a single crystal. This proved to be a major contribution by zone refining as the problem of distributing impurity very uniformly remained an unsolved problem for a considerable period of time. Besides manipulation of impurities, zone melting is finding increased use as a method of growing single crystals particularly by the floating-zone technique.

Zone Melting

This is a general term for controlling the distribution of soluble impurities or solutes in crystalline materials. Here a short molten zone travels slowly through a relatively long solid charge and while traveling redistributes the solutes in the charge.

A molten zone traversing an ingot has two liquid, solid interfaces: a melting interface and a freezing interface. At the melting interface, solid material is merely melted and mixed with the contents of the zone. At the freezing interface the solute concentration in the just-freezing solid generally differs from that in the liquid. If the solute lowers the melting point of the solvent its concentration in the freezing solid will be lower than in the liquid. If the solute raises the melting point of the solvent its concentration in the freezing solid will be greater than in the liquid and the liquid will be depleted of solute. Thus a freezing interface can reject certain solutes and attract others.

Zone Refining

If the object of a zone-melting process is to purify a material then the resulting process is termed a zone-refining process. In zone refining a series of molten-zone passes through the charge in one direction. Impurities travel with or opposite to the zones depending on whether they lower or raise the melting point of the charge substance respectively. They become concentrated in one or the other end of the charge thereby purifying the remainder. The degree of separation increases with the number of passes. The number of passes is defined as the number of single zones which pass through the charge. The degree of separation approaches a limit as the number of passes becomes infinite. Zone refining can be used to concentrate desired impurities as well as to remove undesired ones. It can also be used in special circumstances as an analytical tool for detecting impurities unobservable by conventional techniques.

36

The Distribution Coefficient "k"

There are two parameters that can be used to mathematically express the results of zone-melting operations. They are

a) a parameter of the apparatus such as zone length, ingot length, number of passes and

b) a parameter of the material, namely the distribution coefficient "k." It is defined as the ratio of solute concentration in the freezing solid to that in the main body of the liquid. The value of "k" will be greater than or less than unity depending on whether the solute raises or lowers respectively the melting point of the solvent. The magnitude of "k" may vary from less than 10^{-3} to greater than 10 and will depend on the conditions of freezing such as rate of zone travel and degree of mixing in the liquid. It may also depend on the direction of certain crystal planes with respect to the liquid, solid interface.

Floating-Zone Technique[1]

Certain materials when melted are so reactive or so effective as solvents that they cannot be zone refined to high purity in a container. Techniques of zone melting without a container have been used to produce materials of very high purity. Most widely used is the floating-zone technique in which a molten zone is held in place by its own surface tension between two vertical colinear solid rods as shown in Figure 1.
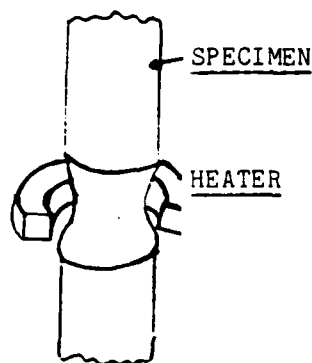
SPECIMEN

HEATER

Figure 1.

Float zoning has been one of the most useful techniques of zone melting. It is widely used in the manufacture of silicon, and has been applied in the laboratory to many refractory metals, semiconducting components and other inorganic compounds.

Shapes and Sizes of Floating Zones

The stability of molten zones has been analyzed mathematically and the results have received ample experimental verification. Heywang and Ziegler[2] showed, for round rods that the maximum length (height) of zone that can be supported by its own surface tension increases linearly with rod radius for small radii and approaches a limit at large radii. The fundamental equation governing the shape of the surface of a liquid under the influence of surface tension γ and gravity is

$$P = \gamma \left[\frac{1}{R_1} + \frac{1}{R_2} \right] \tag{1}$$

At all points, P must be equal and opposite to the pressure exerted by the gravitational head of the liquid. By applying appropriate boundary conditions the limiting maximum height was found to be

$$\ell_m \cong 2.8 \sqrt{\frac{\gamma}{\rho g}} \tag{2}$$

Figure 2 shows a plot of the maximum height ℓ of the floating zone versus radius r for round rods of equal diameters.

33

$$\ell/\sqrt{\gamma/\delta g}$$ (y-axis)

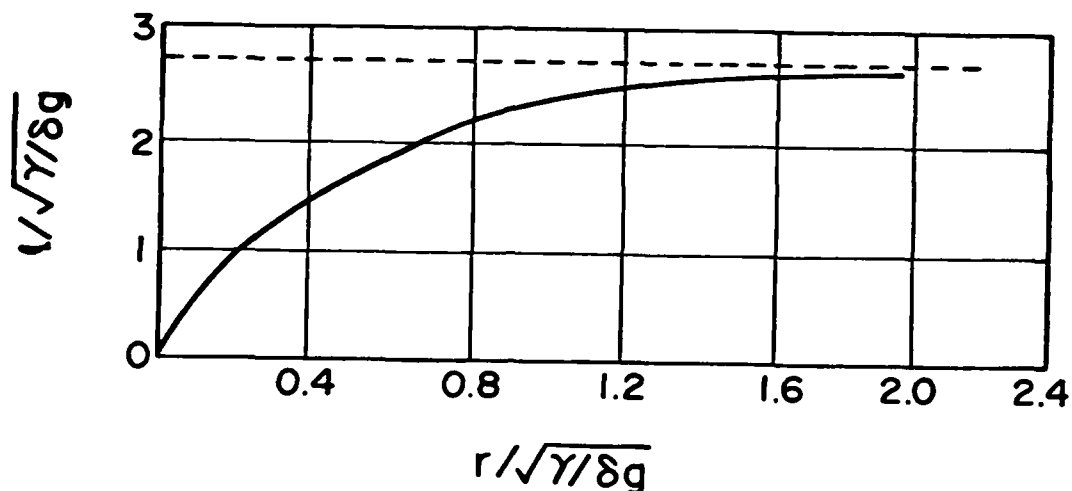$$r/\sqrt{\gamma/\delta g}$$ (x-axis)

Figure 2 Maximum height ℓ_m of floating zone versus radius r for round rods of equal diameter.

The analysis indicates no upper limit on diameter; the main practical difficulty in using large diameters is to melt the entire cross-section without having the zone length exceed ℓ_m.

Considering materials in general, we note that Equation (2) shows that the maximum stable zone height ℓ_m increases as the square root of the surface tension γ of the liquid. Although for a given liquid the surface tension generally decreases as the temperature increases, for materials in general, the surface tension is higher the higher the melting point is. Thus the very materials which are most troublesome to zone melt in a container (because of their high melting points) are the most likely candidates for floating-zone techniques. A rough rule of thumb for metals is that the melting point should exceed about 1000°C.

Electron-Beam Heating

Since its introduction in 1956[3] Electron-Beam Zone Melting (EBZM) has grown rapidly. In essence the electron-beam furnace is a high-vacuum diode

in which as shown in Figure 3 the anode is a rod containing a floating zone, and the cathode is a single turn of (usually) tungsten wire or strip with a pair of focussing plates to confine the beam. For high-melting metals powers are of the order of hundreds of watts furnished at potential differences of the order of kilovolts and currents of the order of tenths of an ampere.

A major problem in EBZM arises from outgassing of the heated charge which causes fluctuating electrical breakdowns due to the formation of glow discharges between anode and cathode. However suitable control circuits can be developed to overcome this problem.

Because of the very high melting temperatures and the vacuum ambient, purification is often as much by volatilization as by zone refining. Contamination of the charge by volatilization of impurities in the filament or the filament itself is a limitation in the design shown in Figure 3. But this problem has been lessened by a focussing arrangement of Cole[4] et alii in which the filament cannot see the molten zone. The electrons are deflected in a curved path by a water-cooled copper cage and focussed about 3 cm below the filament.

A Literature Survey on Purifying Materials Using Electron Beam Floating Zone Refining Techniques

R. G. Carlson[5] was one of the first persons to zone refine tungsten by electron bombardment. He describes an apparatus for refining tungsten in vacuum by the floating-zone method. It consists of 4 components: vacuum system, power supply, anode support and traversing cathode. Spectrographic analysis along the length of a purified tungsten rod indicated that molybdenum may not be removed by zone refining but rather by volatilization. Further, x-ray diffraction studies show that tungsten rods purified in this

1. Specimen

2. Reflector Plate

3. Shield

4. Molybdenum Block
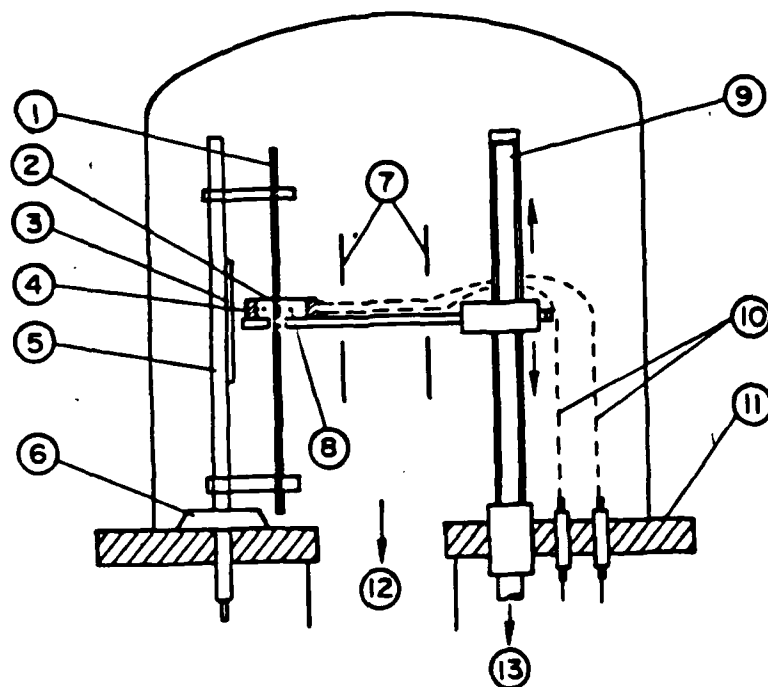
5. Holder Frame

6. High-Voltage Lead

7. Radiation Shields

8. Filament

9. Drive Shaft

10. Flexible Filament Leads

11. Base Plate

12. To Diffuser Pump

13. To Variable-Speed Motor

FIGURE. 3: A Typical Electron-Beam Floating-Zone Unit.

41

manner are single crystals, and these crystals as grown from the melt do not exhibit preferential growth. It is demonstrated by bending one of the single crystals that the purified tungsten rods have high ductility.

A. S. Yue and J. B. Clark[6] used the zone-melting technique for the determination of the eutectic composition in complex metal systems. The application of this method is demonstrated in a simple eutectic system Mg, Al in which the eutectic composition is known and in a complex ternary system Mg,Al,Zn in which the literature is uncertain as to the composition of the ternary eutectic. The result was that zone melting could be used for determining the eutectic composition if

a) maximum segregation during freezing is promoted by a slow speed of zone travel and agitation of the molten zone to promote the maintenance of a uniform composition throughout the liquid zone and

b) the alloy composition is selected to freeze predominantly by the eutectic reaction to form a eutectic plateau at the end of the bar.

The zone-melting method for determining the eutectic composition works best in phase systems in which the slope of the liquid toward the eutectic composition is high.

In Mg,Al,Zn alloys zone melting produced a eutectic structure with alternating regions of fine and coarse eutectic. The origin of these bands were not known.

E. Buehler and J. E. Kungler[7] studied the physical and chemical changes that were produced by processes such as heat treating, melting and zone refining on high-purity molybdenum. These studies were conducted using resistance ratio $(R_{273°K}/R_{4.2°K})$ measurements. Pronounced effects were observed that were associated with recrystallization at about 1200°C and with melting. Melting alone was found to result in a substantial

42

purification by the evaporation of impurities such as iron. Zone refining was found to be reasonably effective with four passes producing a three-fold decrease in resistance ratio and a minimum ratio of 0.0003. With the aid of low-temperature measurements it was also shown that the buildup of a deposit of the material being zone refined, on the radio frequency coil used for heating, could lead to contamination of the sample.

John R. Gould[8] presented a mathematical treatment of multiple-pass floating-zone refining of semiconductors including the evaporation of solutes from the melt at reduced pressure. Vapour pressures and evaporation rate constants for phosphorus, arsenic and antimony in germanium have been determined from floating-zone experiments conducted at 10^{-5} mm Hg. Rate sensitivity of arsenic in germanium has been examined over the growth-rate range of 1 to 10 inches per hour. The equilibrium value of the segregation coefficient of arsenic in germanium, as determined by an extrapolation of these data, was found to be 0.09.

R. R. Soden[9] et alii prepared rhenium single crystals by electron-beam float-zone melting with resistance ratios ($R_{273°K}/R_{4.2°K}$) exceeding 30,000. In one crystal a ratio in excess of 55,000 was obtained. They found that purification occurs both by selective vaporization as well as zone refining.

R. E. Reed[10] used EBFZ to vacuum purify vanadium. Here EBFZ melting vanadium three passes at 3.9 in./hr. in 4×10^{-10} torr vacuum resulted in resistance ratios of about 700 and a total impurity content of 50 wt. ppm. The zoning reduced both carbon and oxygen content. However while carbon removal was always accompanied by a lowering of oxygen content the reverse was not true. The removal of oxygen was probably accomplished by the formation and volatilization of VO. The mechanism for carbon removal was not clearly resolved. Nitrogen was not appreciably affected by EBFZ

melting. All metallic impurities with the exception of Ta and W were effectively volatilized. No evidence was found for zone-refining action on any impurity. Vacuum outgassing further reduced the carbon and oxygen level. However the oxygen level was far more effective than the carbon. The nitrogen content increased particularly on the specimens that lost about 40% in weight due to vanadium evaporation. However the effect of vacuum outgassing was less on the highest purity as-zoned specimens.

Shuichi Otake[11] and Maoshi Matsuno purified bismuth by float-zone refining. Here the floating zone-refining method in addition to horizontal zone refining was adopted to obtain extremely pure bismuth. Thereafter single crystals of the desired orientations were grown by using seed crystals. The value of residual resistance ratio $R_{293°K}/R_{4.2°K}$ which was measured along the binary axis was obtained at 738 at the largest. This was the highest value of purity when compared to other published values.

D. Fischer[12] studied solid-phase impurity diffusion and the influence of separating the impure end in zone refining. They found that owing to the great density of high-diffusivity paths solid-state diffusion could not be neglected. Its influence on the concentration profile was described by experiment and theory. Since the concentration gradient and the curvature became very large at the end of the bar (k<1) diffusion rates were especially high in this region. A successive separation of this enriched region may lead to a considerable improvement of zone refining. Theoretical and experimental results obtained with this method were described.

M. Takahashi[13] and colleagues used a floating-zone technique for the synthesis of single crystals of new ferro-electric materials. The molten zone of the material was formed by radiant heating using a halogen lamp. The lamp and the ceramic rod of the material were arranged to be adjacent

44

foci of an elliptical reflector. The temperature fluctuations in the molten zone were reduced by using a constant-power supply to the lamp. $Sr_2NO_2O_7$ was synthesized and grown as pale yellow transparent single crystals. The colour faded when annealed at 1000°C for two hours. The composition of one of the crystals obtained was found to be $Sr_{2.00\pm0.03}Mb_{2.05\pm0.02}O_7$. The laue patterns, conoscopic and orthoscopic figures as well as the electrochemical coupling factor k_{33} before and after poling were observed in order to determine the homogeneity in the crystal. No internal stress or twins were found.

M. Oron[14] designed and constructed an electron beam floating zone furnace capable of melting cylindrical specimens up to 10 mm. in diameter. A circular thermionic tungsten-filament emitter enclosed in a lanthanum housing preventing a direct line-of-sight relation between the cathode and the concentrical specimen rod was used to minimize mutual contamination of the emitter and specimen materials. Since the furnace was designed for melting reactive materials it originally employed an ion-pump vacuum system capable of obtaining lower than 10^{-8} torr levels. For high-outgassing materials the throughput of this pumping system was not sufficient and a replacement by a liquid-nitrogen-2 trapped diffusion-pump system was introduced. This interchangeable vacuum system would cope with problems of high gas loads during melting and still maintain vacuum levels of 10^{-7}-torr range.

R. E. Reed[15] EBFZ melted niobium powder produced by electro-deposition from molten salts, for purification and growth of single crystals. It was necessary to EBFZM with a high oxygen partial pressure to reduce the carbon level. A high resistance ratio ($R_{300°K}/R_{4.2°K}$ = 6500) and a low flow stress (τ = 460 gm/mm²) was obtained after a high-temperature anneal (2350°) in

45

high vacuum (2×10^{-10} torr). Extensive material characterization results were reported for the niobium at various stages in the purification process. The impurity content determined by chemical analyses did not correlate with the resistance ratio. These results imply that interstitial impurity in solid solution is the impurity distribution most affecting dislocation motion.

T. G. Digges Jr.[16] and C. L. Yaws developed a vacuum float-zone process for the preparation of ultrahigh-sensitivity polysilicon crystals. The high-resistivity polysilicon crystals were then converted to dislocation-free single crystals in an inert atmosphere by the dash-float technique. The vacuum float-zone process was based on a semiquantitative purification technique for prediction of silicon bar resistivity after each float-zone pass. Purification was attained by multiple vacuum float zoning on lightly complemented silicon. Impurity removal was achieved by a combination of zone refining and evaporation. Equations were derived to quantitatively determine vacuum float zone-speeds for resistivity targetting.

J. Bressers[17] et alii used the EBFZM technique to prepare single crystals of vanadium with sensitivity ratios in the range of 1000 to 2000. Compression tests on oxygen-doped pure vanadium were carried out at room temperature in order to establish a relationship between resolved shear stress at 0.2% plastic strain and the oxygen concentration. The extrapolated value for $\tau(0.2)$ at room temperature for high-purity, oxygen-free vanadium was found to be 0.42 kg/mm².

S. Takaki[18] and H. Komura prepared high-purity iron by electron-beam floating-zone melting under ultrahigh vacuum. They succeeded in preparing irons of RRR_H (residual sensitivity ratio) larger than 3000 without serious loss of iron. The best iron obtained had an RRR_H of 6000. The paper

reports the purification procedure of these high-purity irons and some preliminary results of quenching experiments with them.

L. Kuchar[19], B. Wozniakova and J. Drapala used binary diagrams to compute the dilute-concentration limit values of the equilibrium distribution coefficients of the metals W, Ta, Mo, Nb, Hf, Zr and Ti in alloy mixtures. These results were presented together with the periodic dependences of k_o on atomic number. For some alloys of W, Nb and Ti the values of k_o were established experimentally by the frozen-zone method, and the experimental values were in good agreement with the theoretical values.

The most recent work on EBFZM was conducted by A. Eyer[20] and company. Dislocation-free single crystals of silicon were grown by the floating-zone technique using radiation heating in a closed double-ellipsoid-mirror heating facility. The focussed radiation of two halogen lamps served as the energy source. Total power to maintain a molten zone of 10 mm diameter and 15 mm length was 800 W. The influence of the growth parameters on zone stability and on the formation of various microinhomogeneities, such as swirl defects revealed by etching techniques and x-ray topography, was discussed. The experiments served as preparation for growing a Si crystal microgravity aboard Spacelab.

High-Vacuum Setup for Zone Refining Tungsten

Initial Conceptual Design

Figure 4 gives the various components that are essential for the proposed floating zone melting facility. This was a conceptual design that was initiated to serve the dual purpose of purifying the material by zone refining and testing it for hot hardness in an environment of ultrahigh vacuum.
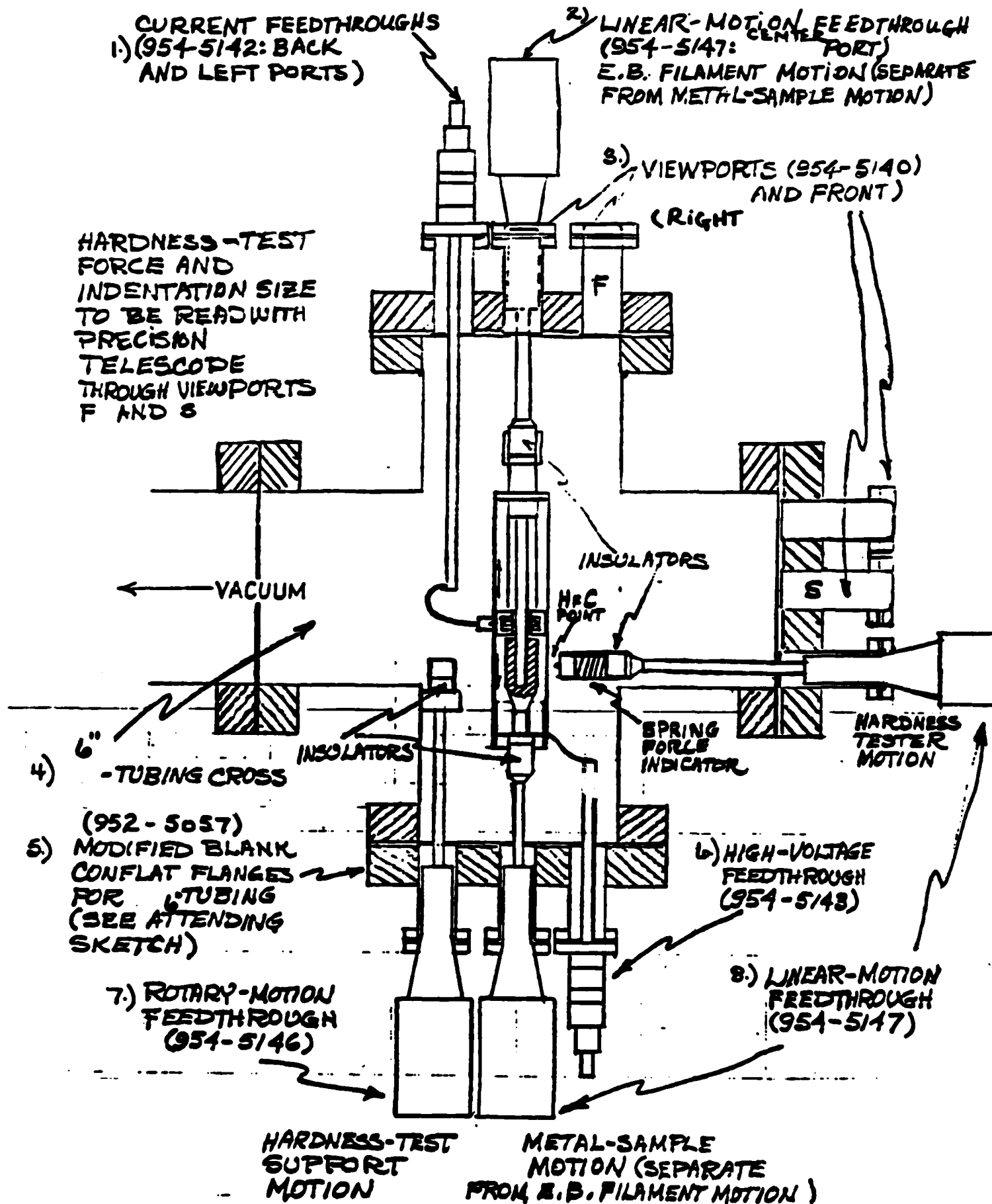
47

CURRENT FEEDTHROUGHS
1.) (954-5142: BACK AND LEFT PORTS)

2.) LINEAR-MOTION FEEDTHROUGH (954-5147: CENTER PORT)
E.B. FILAMENT MOTION (SEPARATE FROM METAL-SAMPLE MOTION)

3.) VIEWPORTS (954-5140) AND FRONT)

(RIGHT

F

HARDNESS-TEST FORCE AND INDENTATION SIZE TO BE READ WITH PRECISION TELESCOPE THROUGH VIEWPORTS F AND S

INSULATORS

H&C POINT

VACUUM

INSULATORS

S

6"
4) -TUBING CROSS

INSULATORS

SPRING FORCE INDICATOR

HARDNESS TESTER MOTION

(952-5057)
5) MODIFIED BLANK CONFLAT FLANGES FOR -TUBING (SEE ATTENDING SKETCH)

6) HIGH-VOLTAGE FEEDTHROUGH (954-5143)

7.) ROTARY-MOTION FEEDTHROUGH (954-5146)

8.) LINEAR-MOTION FEEDTHROUGH (954-5147)

HARDNESS-TEST SUPPORT MOTION

METAL-SAMPLE MOTION (SEPARATE FROM E.B. FILAMENT MOTION)

FIGURE 4: CONCEPTUAL DESIGN FOR COMPACT FLOATING-ZONE-MELTING FACILITY (MOST COMPONENTS ARE SHELF ITEMS AT VARIAN VACUUM DIVISION)

MORRIS

48

In this conceptual design the specimen is held in a vertical position by means of one linear feedthrough, and the electron-beam filament is housed in a chamber which is held by the other linear feedthrough. Since the linear motion provided by the feedthrough is limited the electron-beam filament and specimen were to move in opposite directions to get a maximum length of zone-refined material.

After the necessary number of passes to attain the required concentration distribution the zone-refined specimen would be subjected to a hardness test using the hardness tester shown in Figure 4. A spring-force indicator serves to measure the load exerted, and a precision telescope measures the dimensions of the indentation.

However on closer inspection it was found that there are two factors which do not make this setup as feasible as it appears to be: The first is that of proper alignment of the hardness tester when the indentation is made. This is because of the irregular nature that the surface would assume after zone refining. Thus there is no way to confirm that the load is applied in a direction exactly normal to the surface of the specimen. The second factor is that sufficient room has to be provided inside the four-way cross chamber for the simultaneous opposing motions provided by the feedthroughs. As a result of these difficulties it was decided that the material would be zone refined in one setup and then tested for its properties at elevated temperatures in another setup.

Modified Configuration

The modified configuration shown in Figure 5 has the hardness tester and support eliminated and a linear-motion feedthrough coupled to a stepped-motor drive introduced into the system. Further the linear feedthroughs which support the specimen do not move during the zone-refining process.
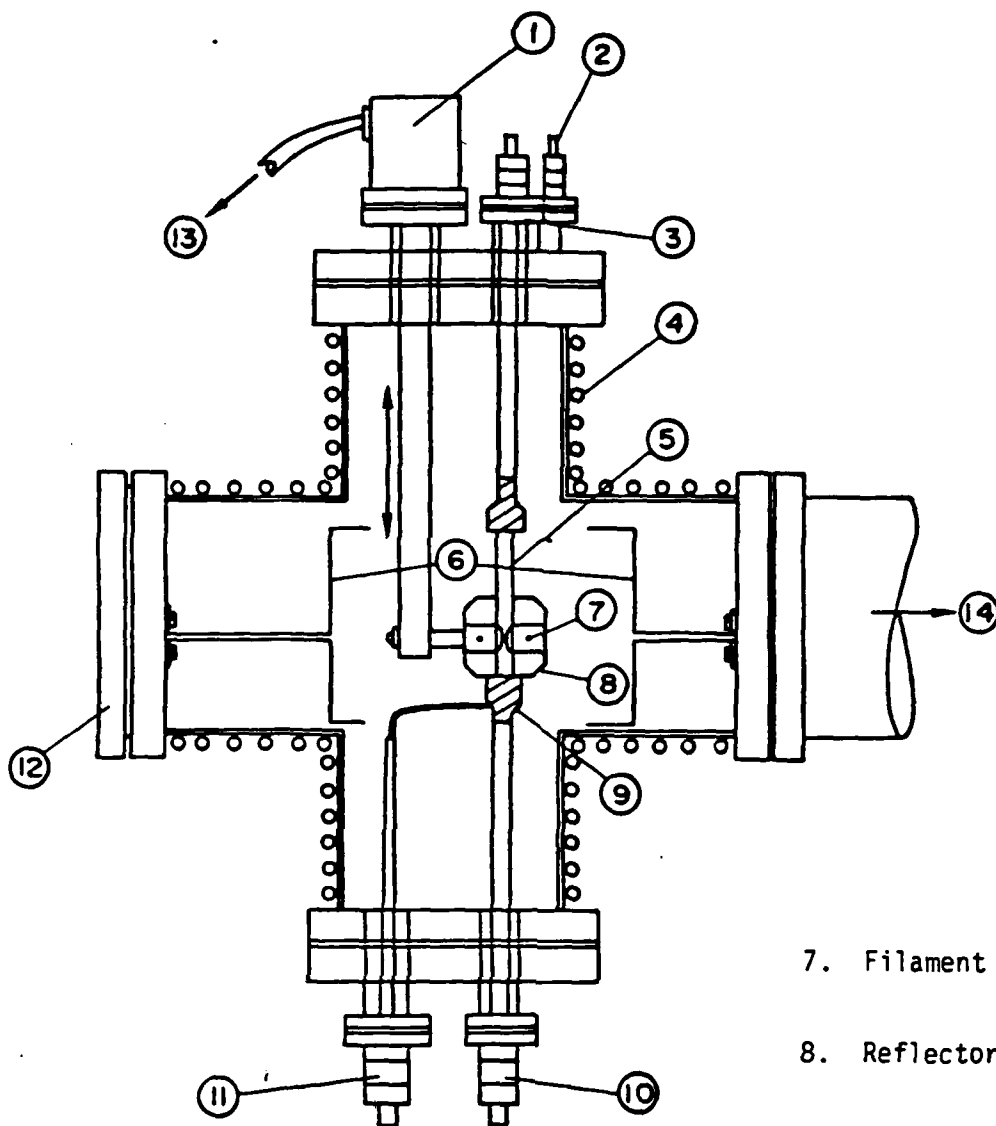
49

7. Filament

8. Reflector plate

9. Insulator

1. Stepper motor drive   10. Linear motion feedthrough

2. Current feedthroughs   11. High voltage feedthrough

3. Linear motion feedthrough 12. View port

4. Water cooling tubes   13. Radiation Shields

5. Specimen   14. To Control unit

6. Radiation shields   15. To vacuum system

FIGURE. 5: Modified configuration

All the motion is executed by the EB source which is coupled to a linear feedthrough that gives a total displacement of four inches.

Radiation shields will be provided around the electron-beam source with the exact location indicated in a final diagram. The figure shows copper tubes which will be brazed on the external surfaces of the four limbs of the chamber to provide water circulation for cooling the chamber during the zone-refining operation.
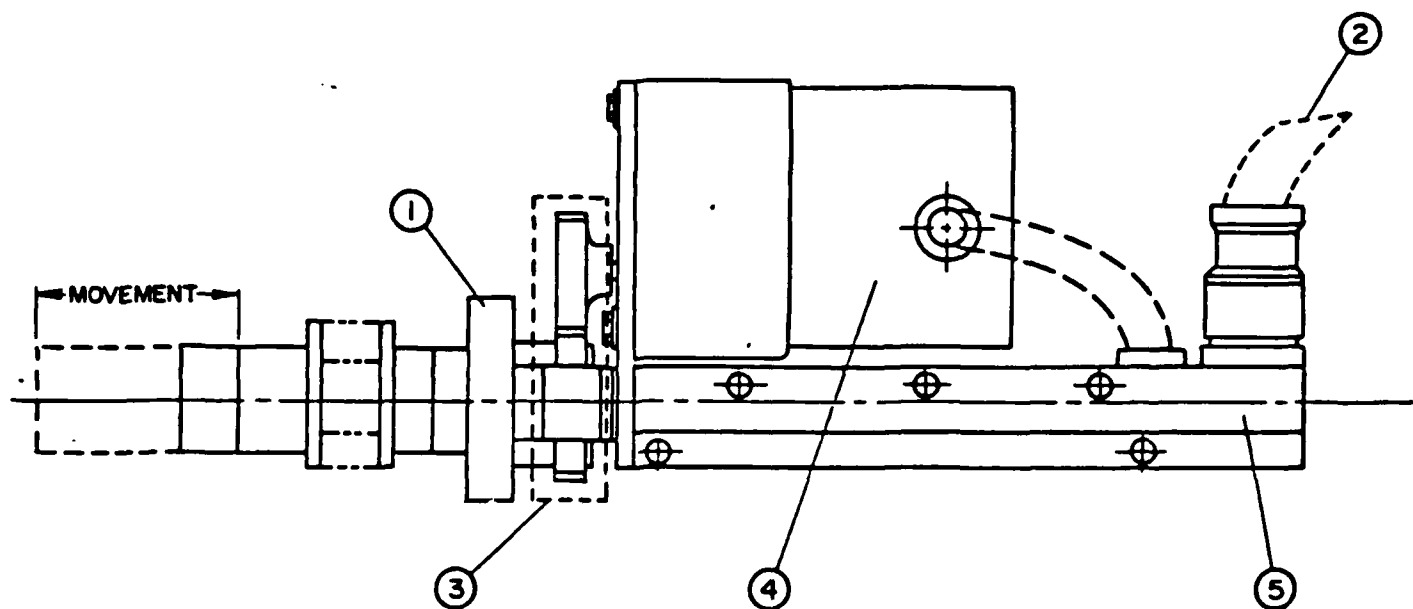
Stepper-Motor-Operated UHV Linear-Motion Drive

This component consists of two parts, the drive itself and the unit that controls the drive and feed rate.

The linear-motion drive shown in Figure 6 has a four-inch movement and is mounted on a 2 3/4-inch OD copper gasket-style flange which in turn is mounted on the top flange of the four-way chamber (indicated in Figure 5).

The stepper-motor control unit is mounted in two standard 19-in.-wide rack-mounting units suitable for operation with the linear-motion drive mentioned earlier. The control unit has the following features

a) Free run

b) Jog (single-1/2-step control)

c) Six-digit thumb-wheel movement indexing

d) Direction control

e) Six-digit up/down counter-display step input to motor in either direction

f) Microswitch-override limit input to the control system

g) Necessary power supply

h) Connection cables to connect the linear-motion drive

i) 110-V (60Hz) operation

1. 70 mm. O.D. Flange

2. To control box

3. Metal guard over gears

4. Motor: Available as a stepper or synchronous motor

5. Cover for travel-limit switches. Two switches fitted as standard.

FIG. 6: Stepped-motor-operated UHV linear-motion drive.

The Vacuum System

Figure 7 shows a special clean turbomolecular-pumped ultrahigh-vacuum system with the zone-refining chamber connected to it. As shown the system consists of a turbomolecular pump (to increase efficiency of pumping and reduce pumping time) along with its numerous accessories such as gauges, isolation valves et cetera. A roughing pump is also shown: The purpose of this is to initiate the evacuation process to about 10^{-4} torr from where the turbomolecular pump evacuates the chamber to a vacuum of 10^{-10} torr.

This kind of arrangement offers two major benefits:

a) The experimental area can be isolated when the system is unattended. And should there be any failure the pumping system would vent only as far as the gate valve, protecting the experiment.

b) It is intended that the equipment be operated in the 10^{-10}-torr range. To be able to accomplish this routinely the turbo pump should not be continually vented back to atmosphere as this could result in water vapour building up on the blades, limiting the ultimate pressure.

Theoretical Analysis of Zone-Refining

Introduction

The theory of zone refining has been well described by Pfann[1] in his textbook. Here we consider the solute distribution after one pass, after successive passes and after an indefinitely large number of passes through an initially uniform ingot. Although the ultimate distribution is seldom reached analyzing it is worthwhile because it is the maximum purification attainable for a given zone length.
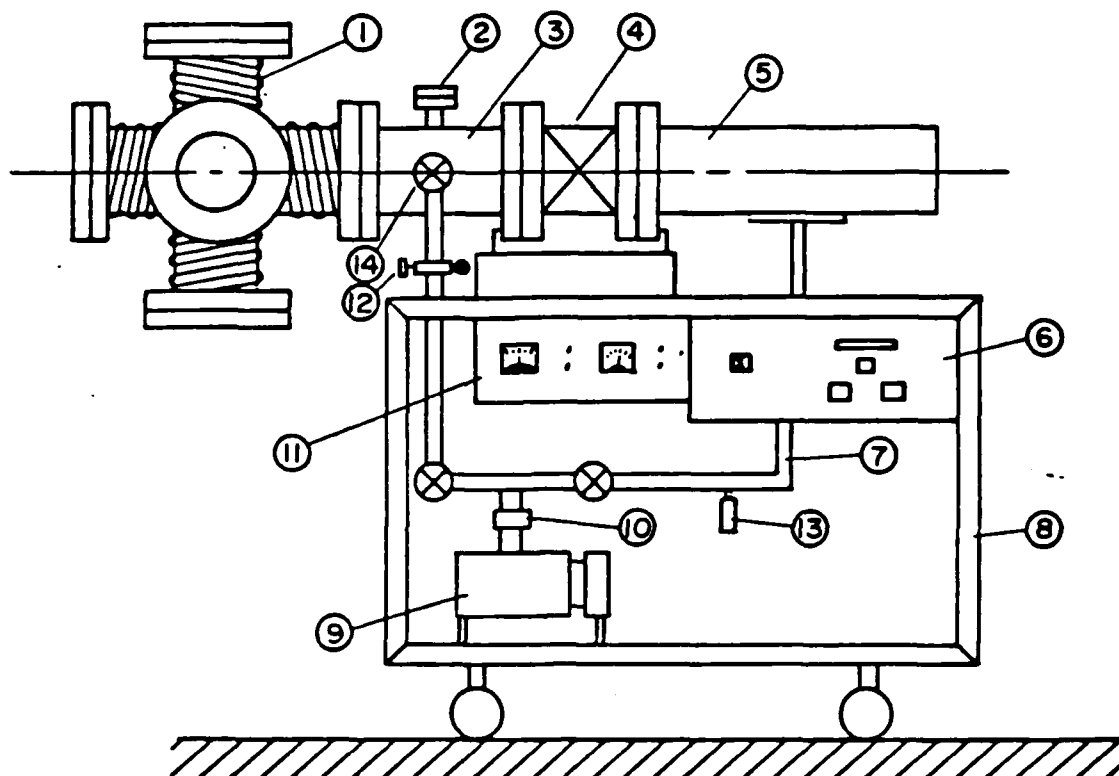
1. Experimental vessel with water cooling tubes
2. Ionization gauge
3. Roughing adaptor
4. Isolation valve
5. TPU - turbo pump unit
6. Pump control
7. Roughing, backing lines
8. Mobile bench
9. Rotary pump
10. Foreline trap
11. Ion, T.C. gauge control
12. Thermocouple, back-to-air facility
13. Thermocouple (backing)
14. All-metal roughing-isolation valve

FIG. 7: The vacuum system

Starting with a single-pass distribution, consider a cylindrical charge comprising two components that can form a solid solution. Let its composition be invariant with distance x along the ingot shown in Figure 8. Cause a molten zone of length ℓ to traverse the charge slowly. Assume the
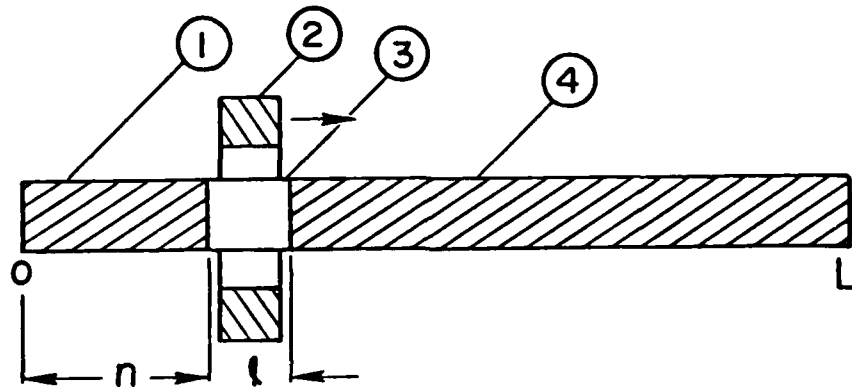

Fig. 8. Molten zone traversing a cylindrical ingot.

distribution coefficient to be less than 1. Passing the zone through the ingot distributes the solute approximately as shown in Figure 9. As the zone advances a short distance the ingot freezes out at $x = 0$ a layer of solute concentration K_{C_o}, and it takes in at $x = \ell$ by melting a layer of concentration C_o. As a result the zone is enriched and subsequently freezes out higher concentrations. As the zone progresses,
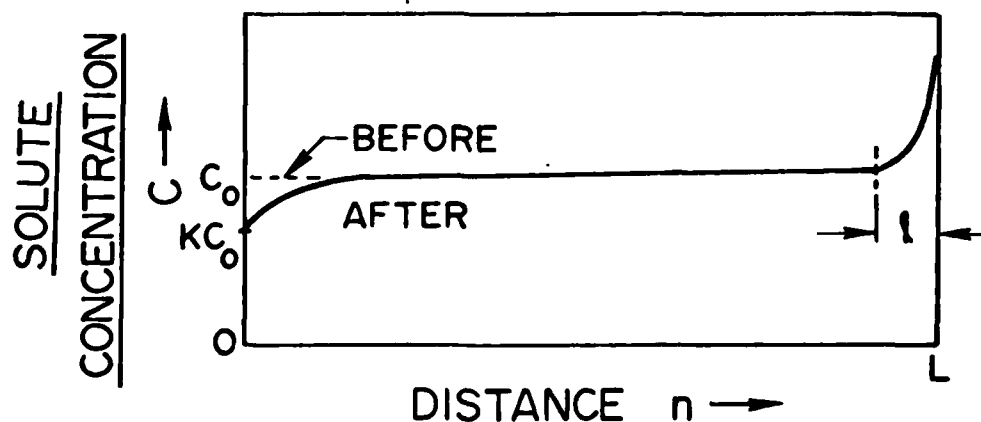

Fig. 9. Approximate concentration of solute after one pass.

55

enrichment continues at a decreasing rate until its concentration attains the value C_o/k. The equation for the process of Figure 9, which may be described as zone melting of a uniform charge, is

$$C/C_o = 1 - (1 - k)e^{-kx/\ell} \tag{3}$$

This equation is valid in all but the last zone length and where the densities of the solid and liquid are equal. If the densities of the solid and liquid are unequal then Equation (3) is modified to

$$C/C_o = 1 - (1 - \frac{k \cdot \rho_L}{\rho_S}) \exp(-\frac{k\rho_L x}{\rho_S \ell}) \tag{4}$$

Curves of C versus x/ℓ, the distance expressed in zone lengths, have been plotted for different values of the distribution coefficient, k.

For multipass distributions it would be most helpful to have a single general equation that expresses solute concentration as a function of distance. But to get such an equation an accurate means of describing multipass operations mathematically must first be available. However suitable approximations have been developed and computed results have been published.

The basic differential equation used was derived independently by Reiss[21] and Lord[22]. It relates the change in solute concentration in the moving zone to the difference between the fluxes of solute entering and leaving the zone. If $C_n(x)$ is the solute concentration freezing out of the zone at distance x in the nth pass the resulting differential equation would take the form,

$$\frac{\ell}{k} d [C_n(x)] = [C_{n-1}(x + 1) - C_n(x)] dx \tag{5}$$

56

After the front of the zone reaches the end of the ingot at $x = L - \ell$ where L denotes the ingot length the zone length is no longer constant, being $L - x$. And the solute is no longer taken in. The Equation (5) then becomes

$$d \; [C_n(x)] = \frac{(1 - k)}{(L - x)} \; C_n(x) \; dx \qquad (6)$$

The solution of this equation is

$$C_n(x) = C_n \; (L - \ell) \left[\frac{L - x}{\ell} \right]^{k-1} \qquad (7)$$

which is a slightly modified version of the normal freezing equation.

A number of investigators have used this form of the solution to generate plots of concentration versus distance for different values of the distribution coefficient k.

Finally at the ultimate distribution which represents the maximum attainable separation the forward convective flux of solute due to the freezing action of the zone is at all points in the charge opposed by an equal backward flux due to the mixing action of the zone. If a molten zone of length ℓ is to pass through the charge without changing the previous distribution the concentration freezing out of the zone at any point x must be the ultimate distribution $C(x)$. And the concentration $C_L(x)$ in the zone must be $C(x)/k$. But $C_L(x)$ is also given by

$$C_L(x) = \frac{1}{\ell} \int_x^{x+1} C(x) \; dx \qquad (8)$$

Assuming unit cross-section, since $C(x) = k \cdot C_L(x)$

$$C(x) = \frac{k}{\ell} \int_x^{x+1} C(x) \; dx \qquad (9)$$

The solution for this is a simple exponential,

$$C(x) = A e^{Bx} \qquad (10)$$

where A and B are constants obtainable from

$$k = \frac{B\ell}{e^{B\ell} - 1} \qquad (11)$$

and

$$A = \frac{C_o BL}{e^{BL} - 1} \qquad (12)$$

As in the other cases ultimate distributions can be calculated for different values of the distribution coefficient.

Literature Survey on the Theory of Zone Refining

Analysis of zone refining has been carried out as early as 1953 when N. W. Lord[22] analyzed the process of molten-zone refining for long ingots and many zone passages. Formulas were derived which gave the resultant impurity distribution in terms of finite series. A comparison with another approximate procedure by Hamming has also been presented. Curves representing residual impurity concentrations after molten zone passages for different values of k have also been presented.

I. Braun[23] et alii presented a complete solution of the equations governing the redistribution of solutes in zone-melting processes. The effect of normal freezing in the last zone length of a bar is treated rigorously. The solutions hold for all values of the distribution coefficient k. Numerical calculations have been made of the concentration profiles resulting from repeated zone melting, and specimen graphs have been presented.

Howard Reiss[21] considered mathematically the zone-melting process in which redistribution of solute in a solid bar is affected by the passage of a molten zone. Simple approximate techniques were developed for computing the manner in which redistribution occurs as molten zones continue to pass. The introduction of the "zone-melting flux" provided valuable insight into the nature of the phenomenon as well as a central mathematical theme in terms of which the process could be discussed. Curves have been presented for typical and general cases.

Among the persons who developed analytical expressions for ultimate distribution (infinite number of passes) for long ingots was Volchock[24]. He simplified the analysis by assuming a uniform distribution in the last zone length. However the expression developed by Velicky[25] was based on the assumption of a normal freezing distribution. He found that even though the simple exponential form of the governing equation was correct for a long ingot at regions distant from the end the constant A in Equation (12) would be less than that in Equation (10) because the normal freezing distribution piles up impurity more steeply at the ingot end than does the exponential distribution assumed by Pfann.

Helfand and Kornegay have gone a step further by showing that a complete solution of the zone-melting problem can be achieved in a finite ingot not only for the ultimate distribution but also for any number of passes. They reduced the complexity of the problem by using a nonphysical function $C_n(x)$ defined as a solution of the Equation (5) in the region of $-\infty$ to the beginning of the ingot. Further the index n (number of passes) is handled by a generating function:

$$F(x,z) = \sum_{n=1}^{\infty} C_n(x)z^{n-1} \tag{13}$$

An equation for $F(x,z)$ from $-\infty$ to the last zone length is easily solved by Laplace transforms, and this is joined to whatever function one wishes to assume for the last zone, exempli gratia normal freezing.

Analytical Work for Zone Refining of Tungsten

Based on the information available on the theoretical analysis of zone refining it has been proposed to generate curves of concentration of tungsten with rhenium for different distribution coefficients.

These theoretically obtained curves will later be compared with the concentration curves obtained by actually zone refining tungsten. Preliminary work on the analysis has been initiated.

NOMENCLATURE

P =   Inward pressure exerted by the surface of the liquid

γ =   Surface tension

R_1, R_2 = Principal radii of curvature (taken in the vertical plane through the axis for round rods)

ρ = Density

g = Gravitational constant

C = Solute concentration in the solid

x = Distance from the point at which the first solid

C_o = Mean solute concentration

k = Distribution coefficient

ℓ = Length of the molten zone

ρs = Density of the solid

ρ = Density of the liquid

$C_n(x)$ = Solute concentration freezing out of the zone at a distance x in the nth pass.

$C(x)$ = Ultimate distribution after an indefinite number of passes

A = Constant from Equation (11)

B = Constant obtainable from Equations (11) and (12)

61

REFERENCES

1. William G. Pfann, "Zone Melting", John Wiley and Son, 1966.

2. W. Heywang and G. Zeigler, Z. Naturforsch., Vol. 9a, 561 (1956).

3. M. Davis, A. Calverley, and R. F. Lever, J. Appl. Phys., Vol. 27, 195 (1956).

4. M. Cole, C. Fisher, and I. A. Bucklow, Brit. J. Appl. Physics, Vol. 12, 577 (1961).

5. R. C. Carlson, "Tungsten zone melting by electron bombardment," J. of Electrochemical Society, Vol. 106, No. 1, (1959).

6. A. S. Yue and J. B. Clark, "The determination of the eutectic composition by the zone-melting method," Trans. of the Metallurgical Society of ASME, Vol. 221, 383 (1961).

7. E. Buehler and K. E. Kunzler, "Observations concerning zone refining and thermal treatment of molybdenum from low temperature resistance measurements," Trans. of the Metallurgical Society of ASME, Vol. 221, 957 (1961).

8. John R. Gould, "Evaporation of solutes in floating zone refining of semiconductors," Trans. of the Metllurgical Society of ASME, Vol. 221, 1154, (1961).

9. R. R. Soden, G. F. Brennert, E. Buehler, "The preparation of high purity rhenium single crystals," J. of Electrochemical Society, Vol. 112, No. 1 (1965).

10. R. E. Reed, "Electron-beam float zone and vacuum purification of vanadium," J. of Vacuum Science and Technology, Vol. 7, No. 6 (1970).

11. Shuichi Otake, Naoshi Matsumo, "Purification of bismuth by the floating zone refining," Japanese J. of Appl. Physics, Vol. 10, No. 9 (1971).

12. D. Fischer, "A study on zone refining: solid-phase impurity diffusion and the influence of separating the impure end," J. of Appl. Physics, Vol. 44, No. 5 (1973).

13. M. Takahashi, S. Nanamaku, and M. Kimura, "The growth of ferroelectric single crystal $Sr_2Mb_2O_7$ by means of F.Z. technique," J. of Crystal Growth, Vol. 13/14, 681-685 (1972).

14. M. Oron, "Very high vacuum electron beam floating zone furnace," Vacuum, Vol. 24, No. 2.

15. R. E. Reed, "EBFZM and vacuum degassing of niobium single crystals," J. Vac. Sci. Tech., Vol. 9, No. 6 (1972).

16. T. G. Digges Jr. and C. L. Yaws, "Preparation of high sensitivity silicon by vacuum float zoning," J. of the Electrochemical Society, Vol. 121, No. 9 (1974).

17. J. Bressers, R. Creten, G. Van Holsbeke, "Preparation and characterization of high purity vanadium by EBFZM," J. of Less Common Metals, Vol. 39, 7-16 (1975).

18. S. Takai and H. Kimura, "Preparation of high purity iron by electron-beam floating-zone melting under ultra-high vacuum," Scripta Metallurgica, Vol. 10, 1095-1100 (1976).

19. L. Kochar, B. Wozniakova, and J. Drapala, "Segregation behaviour during the zone melting of refractory metals," J. of Crystal Growth, Vol. 52, 359-366 (1981).

20. A. Eyer, B. O. Kolbesen, and R. Mitsche, "Floating zone growth of silicon single crystals in a double-ellipsoid mirror furnace," J. of Crystal Growth, Vol. 57, 145-154 (1982).

21. H. Reiss, Trans. ASME, Vol. 200, 1053 (1954).

22. N. W. Lord, Trans. ASME, Vol. 197, 1531 (1953).

23. I. Braun, S. Marshall, "On the mathematical theory of zone-melting," Brit. J. of Appl. Phys., Vol. 8 (1957).

24. B. A. Volchok, Soviet Physics - Solid State, Vol. 4, 789 (1962).

25. B. Velicky, Phys. Stat. Sol., Vol. 5, 207 (1966).

3. HARDNESS TESTING AT ELEVATED TEMPERATURES

I) Hot-Hardness Testing:

    i) Introduction

    ii) Hot-Hardness-Testing Requirements

   iii) High-Temperature Hot-Hardness Testing

    iv) Effect of Atmosphere on a Hot-Hardness Test

    v) Dynamic Hot-Hardness Testing

    vi) Positioning and Measurement of Impressions

II) Literature Survey on Hot-Hardness Testing:

III) Temperature dependence of Hardness:

    i) Metals and Alloys

    ii) Intermetallic Compounds

   iii) Nonmetallic Materials

    iv) Indentation Fracture

IV) Utility of Hot-Hardness Measurements to Study High-Temperature-Material Problems

3. HARDNESS TESTING AT ELEVATED TEMPERATURES

Introduction

Hardness is a nebulous property which cannot be correlated with any individual mechanical parameter but does certainly have tenuous relations with many properties. Nevertheless it should be remembered that most metallurgical investigations utilize hardness tests while at least in the early stages many are completely dependent on this simple rapid non-destructive procedure. Hardness testing has gained such wide commercial application that in the USA alone more than 75 million hardness tests are performed daily.

Hot-Hardness Testing Requirements

Hardness testing requires measurement of the edges of a surface impression, and consequently the state of this surface is very important. Oxidation or other corrosion introduces imprecision into the results. Thus most elevated-temperature testing must guard against this. Consequently it is seldom possible to use a standard hardness machine for testing a heated sample in air. So hot hardness testing necessitates a vacuum or inert-atmosphere chamber with a seal through which the indenter must slide frictionlessly. However in our case we would like to test the hardness of the tungsten, rhenium alloys at temperatures of the order of 2000°C. And at such elevated temperatures the possibility of using an indenter is reduced to a minimum.

Because of the problems encountered at elevated temperatures this kind of hardness testing has led to limited commercial exploitation[1]: It seems that only the Rockwell instrument is produced with a standard high-temperature sensor.

65

High-Temperature Hot-Hardness Testing

It would be impossible to describe adequately the multitude of hot-hardness techniques reported since Brinell's first crude attempts in 1905^2. Table 1 lists the important characteristics of a wide selection of these methods. However in this context it is important to remember that the atmosphere surrounding the specimen and indenter is of considerable importance at high temperatures. Tests in air are limited to oxidation resistant metals and metals which are not subject to hardening or embrittlement by oxygen or nitrogen absorption. This restricts tests to relatively few materials and to temperatures below 500°C.

Effect of Atmosphere on a Hot-Hardness Test

The purest atmosphere easily obtainable is a vacuum. Therefore much hot-hardness testing has been performed "in vacuo." It does however have two drawbacks:

1) Some samples have relatively high vapor pressures at elevated temperature, and resulting surface losses influence size and clarity of the impression.

2) If the tester employs an external loading device then atmospheric pressure will produce its own variable-load on the indenter system. Of the working atmospheres indicated in Table 1 inert gases are safest and most expensive. To prevent gases from ingressing into the chamber from outside or from insulating materials the best equipment isolates the specimen and indenter atmosphere from the insulation or uses radiation shields.

The influence of the atmosphere on the indenter material is very important at higher temperatures. Diamond, the standard material for Vickers indenters, begins to graphitize in vacuo above 1100°C and may react

66

Table 1) Summary of hot hardness test procedures

Instrument or loading system	Indenter Type	Material	Maximum temperature, °C	Loading time, sec.	Atmosphere	References
Brinell	Ball	Steel	—	30	Air	55, 56
			150	30	Air	57
		Cermet	900	30	Air	58
Spring-loaded	Ball	Steel	200	Various	Air	54
Electromagnetic device	Ball, Vickers and Cone.	Diamond	500	Various	—	59
Vickers	Pyramid	Diamond	950	15	Vacuum	60
			1150	15	Hydrogen	61
			1150	15	Hydrogen	62, 63
Dead load	Pyramid	Sapphire	1600	10	Argon	64
			1000	10	Vacuum	65
		Diamond	1000	10	Vacuum	66
		Diamond	280	6	Salt bath	67
		Diamond	550	6	Salt bath	68
		Diamond	1000	Various	Argon	69
		Sapphire	500	75	He + 2% H	70–72
		Sapphire	800	—	Salt bath	73
Vickers	Pyramid	WC	900	8	Vacuum	74
		Corundum	1300	3600	Vacuum	75
		Earthenware	1480	20	—	76
Pneumatic loading	Pyramid	Diamond	700	15	Vacuum	77
Lever loading	Cone	Corundum	1900	Various	Nitrogen	78, 79
Rockwell	Brale	Diamond	900	10	Nitrogen	80
Cowdrey Mutual Indentation	Parallel cylinders	High speed steels	800	30	Air	81
Dead load Microhardness	Pyramid	Diamond	800	—	Hydrogen	82
		Various	1500	Various	Vacuum	83
Hydraulic Microhardness	Pyramid	Various	1500	15	Vacuum	84
Rebound dynamic	Ball	WC	600	—	Air	73
Rebound dynamic	Ball	WC	2000	—	Vacuum	85
Dynamic impression	Ball	Steel	900	—	Air	86
Dynamic spring punch	Brale	High speed steel	600	—	Salt bath	87

67

with carbide forming elements below 1000°C. For these reasons artificial sapphire or corundum indenters are often preferred although they are three or four times softer.

Dynamic Hot-Hardness Testing

Dynamic tests obviate problems of the indenter, which may be unheated, so that even hardened steel balls have been used. The interpretation of dynamic hot-hardness test results is difficult as it introduces the effects of loading rate and duration. At temperatures in the creep region (above $0.5\ T_m$) deformation is strongly time dependent, and this may be used to advantage in indentation creep studies. The simplest type of loading is the dead-load type. They only source of inaccuracy here is likely to be friction in the guide mechanism and the bushing for entering the furnace chamber. The bushing has to be gas tight and heat conducted along the cylindrical extension rod may cause thermal expansion problems. Intelligent use of water cooling, lubricants and low-expansion materials will reduce the risks. It is in the realm of hot-microhardness testing that these problems become acute. Special precautions are necessary to avoid loading errors and to produce constant loading rates.

Positioning and Measurement of the Impressions

The incorporation of a viewing window into the chamber is fairly simple, but a built-in microscope to measure the impressions at temperature seems unnecessary. Feeler rods or electrical devices can be installed to indicate contact of the specimen by the indenter while impressions can be measured on the cold specimen after the test. This procedure involves negligible thermal contraction of the impression. Traversing mechanisms may be of the screw, push-rod type or a rotating eccentric anvil type.

Literature Survey on Hot-Hardness Testing

Frederick Bens[3] was one of the initial investigators of elevated-temperature hardness testing of metals and alloys. He devised an apparatus for determining the hardness of metals at temperatures up to 1700°F. The apparatus was designed to rest on the stage of a standard Vickers hardness machine. The values of hardness determined are presented in Table 2 and the test setup in Figure 1a.

W. Chubb[4] measured hardness of metals at temperatures just above and just below their allotropic change point and established that crystal structure has a real effect on the strength of metals. It was found that bcc structure is always the softer structure when it is involved in an allotropic transformation. The close packed and more-complex structures are inherently harder and may be expected to be better base materials for high-strength alloys.

M. Semchyshen[5] and Torgerson obtained deviated-temperature hardness of iron, molybdenum, tungsten and S-816. They developed an apparatus for determining the hardness of metals from room temperature to 3000°F. Figure 1b gives a schematic representation of this apparatus. The hardness determinations were carried out in a purified argon atmosphere.

In 1960 L. M. Fitzgerald[6] developed a new method of determining hardness of materials having melting points in the region of 3000°C. They used tungsten-carbide balls as indenters and a photomultiplier tube to measure the height of rebound. Figures 2 and 3 give some of the intricate details of the apparatus and principle used in measuring the hardness.

Chubb[7] et alii conducted a complete hardness survey of the zirconium, uranium system from room temperature to 900°C. The composition of maximum hardness increased from 40 atomic percent (a/o) zirconium at room

Table 2)
Hot Hardness of Some Metals and Alloys

	Temperature				Temperature		
	F	C	VPN		F	C	VPN
Chromium, vacuum melted and cast	80	27	135	Stellite No. 21	80	27	314
	932	500	113		932	500	...
	1112	600	119		1112	600	...
	1292	700	97		1292	700	...
	1600	870	61		1472	800	176
Iron	80	27	77	51% Mo, 49% W Alloy	80	27	295
	932	500	45		900	482	228
	1112	600	21		1100	593	202
	1292	700	16		1200	648	196
Molybdenum sintered and swaged bar	80	27	206		1300	704	196
	932	500	116		1400	760	190
	1112	600	105		1500	815	185
	1292	700	102		1600	870	168
	1600	870	87	18-4-1 High Speed Steel, oil quenched from 2400 F (1315 C) and tempered 1 hour at 1050 F (565 C)	80	27	870
Tungsten, sintered and swaged bar	80	27	351		932	500	616
	1000	538	200		1112	600	506
	1100	593	197		1292	700	274
	1200	648	206		1600	870	75
	1300	704	193	6% Mo, 6% W High Speed Steel, oil quenched from 2300 F (1260 C) and tempered 1 hour at 1050 F (565 C)	80	27	894
	1400	760	194		932	500	644
	1500	815	184		1112	600	552
	1600	870	162		1292	700	246
	1700	925	156		1600	870	67
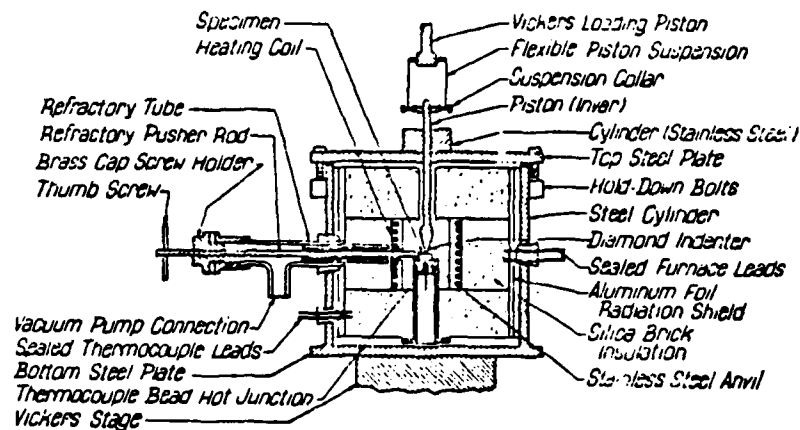
Fig 1a Design of Hot Hardness Tester.

Table 3
Hardness of Zirconium-Uranium Alloys

Nominal Alloy Composition		Hardness (DPH), kg/mm², at Temperature, °C										Type of Uranium and Melting Method a
At % U (Balance Zr)	Wt % U (Balance Zr)	Room	300	500	600	650	700	750	800	850	900	
0	0	113	53	33	22	—	16.6	12.5	9.3	7.2	1.4	D-A
0	0	138	58	39	27	—	14.5	11.1	8.7	8.4	2.6	F-I
4	10	240	195	85	32	—	9.8	6.1	4.4	4.2	2.8	D-A
4	10	197	141	108	51	—	25	16.4	8.2	2.9	2.0	F-I
8.5	20	235	182	102	24	—	6.4	—	3.6	2.7	2.1	D-A
8.5	20	252	188	136	56	—	10	7.3	5.0	4.2	3.7	F-I
14	30	243	185	136	28	—	10.5	7.3	4.3	3.2	—	D-A
14	30	298	249	168	75	—	10	7.4	5.7	4.8	4.1	F-I
20	40	295	255	172	70	—	9.7	6.8	5.4	4.1	—	D-A
20	40	271	227	178	96	13.7	10.0	6.3	5.4	—	3.6	D-I
20	40	302	264	194	100	15.7	11.9	8.2	7.0	—	4.9	F-I
27	50	272	242	183	92	—	10.9	8.5	6.9	5.9	4.5	D-A
27	50	264	262	192	101	18.7	12.8	10.4	8.6	—	5.9	F-I
36	60	279	231	211	96	—	15.7	12	9.9	7.6	7.1	D-A
36	60	364	337	249	81	17.1	18.0	15.2	11.5	—	7.3	D-I
36	60	242	247	224	104	23	16.9	12.5	9.5	—	6.3	F-A
48	70	350	293	210	75	—	19.0	15	12.5	10.8	8.5	D-A
48	70	370	320	245	73	15.4	10.5	14.9	13.7	—	8.4	F-I
60	80	411	341	212	57	—	12.8	18.1	13.6	11.2	8.9	D-A
60	80	391	341	200	90	26	13.1	14.8	15.7	—	8.8	F-I
60	80	386	335	213	77	22	10.3	10.6	11.9	—	8.4	F-A
60	80	421	354	209	80	25	7.6	15.0	12.1	—	7.3	D-I
77	90	359	258	129	26	—	4.6	10.6	8.6	—	5.9	D-A
77	90	363	258	159	68	—	14.0	9.6	7.1	5.2	2.2	F-I
88	95	307	181	106	49	22	7.6	5.4	4.4	—	3.0	D-A
88	95	347	130	118	38	—	6.4	4.7	3.6	2.7	2.3	F-I
95	98	283	155	85	49	35	39	2.3	2.0	—	1.7	D-A
100	100	249	91	29	14.5	—	33	—	—	—	—	D-A
100	100	263	144	49	23	17.5	43	28	1.7	—	0.6	D-A
100	100	200	68	23	13	—	31	—	—	—	—	F-I
100	100	265	117	37	18.7	12.7	33	23	0.79	—	0.72	F-I

(a) D = Derby uranium
F = Fernald uranium
A = Arc-melted alloy
I = Induction-melted alloy

1 Dead Weight
2 Bellows
3 Water-Cooled Bearing
4 Argon Inlet
5 Steel Indenter Shaft
6 O Ring
7 Molybdenum Indenter Shaft
8 Heating Element
9 Sapphire Indenter
10 Test Specimen

11 Molybdenum Stage
12 Thermocouple Tube
13 Furnace Shell
14 Ground Joint
15 Stage Holder
16 Spur Gear
17 Internal Gear
18 Steel Balls
19 Clamp
20 Stage Rotation Knob
21 Rubber Tubing Seal
22 Argon Outlet
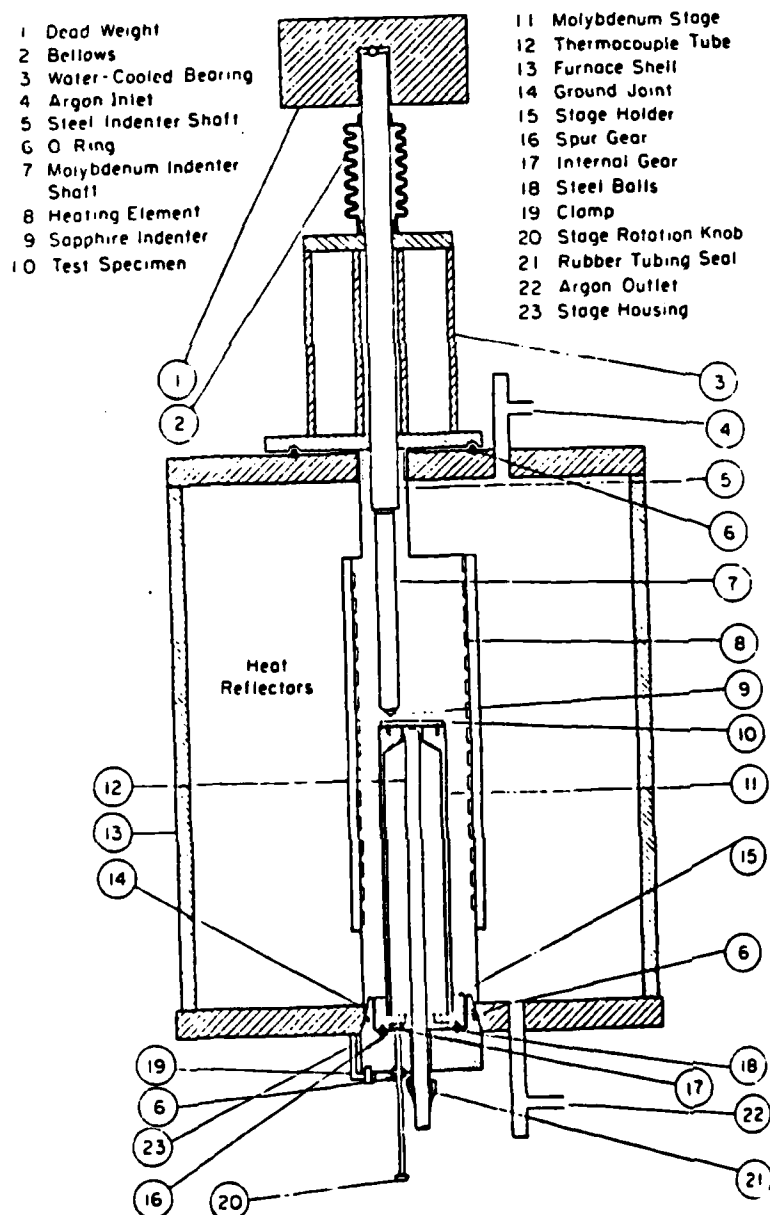23 Stage Housing

Heat Reflectors

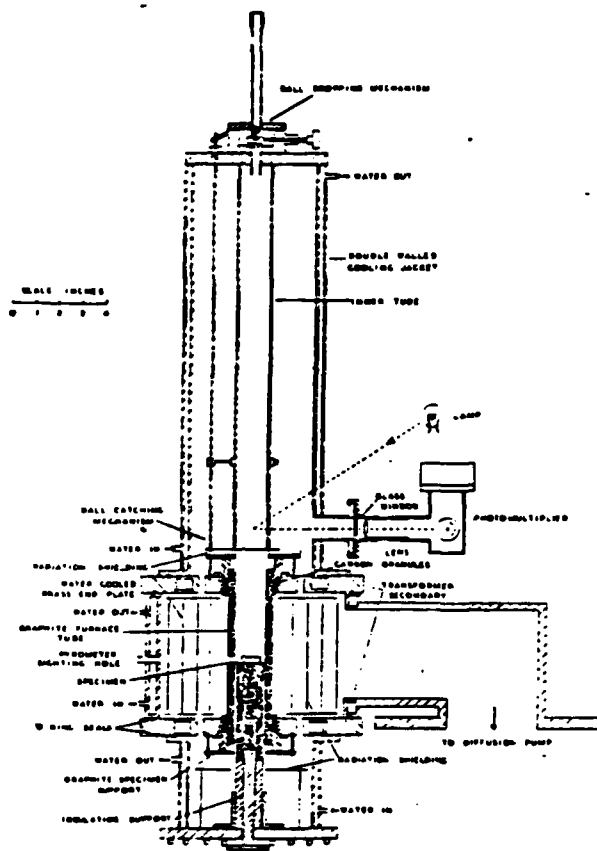Fig 1b. Hot Hardness Tester For Tests To 3000 °F.

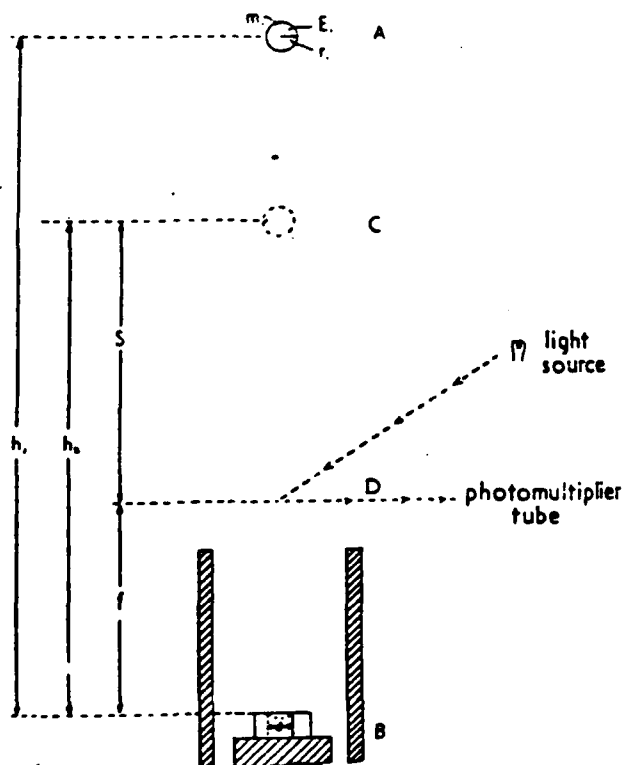Fig. 2 : Schematic sectional view of hot-hardness apparatus
and furnace assembly

Fig. 3, Diagram representing positions of indenter before
and after rebound. Optical arrangement of light source and
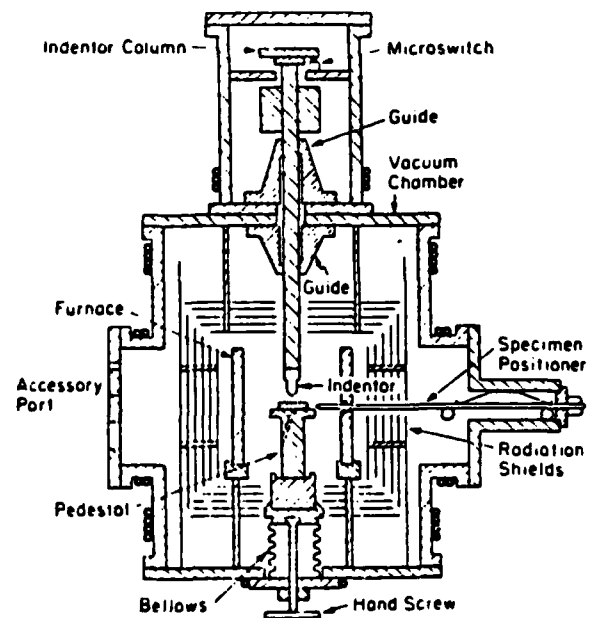photo-multiplier tube also shown

Fig. 4 -Vacuum Hot Hardness Machine.

72

temperature to 60 a/o zirconium at 600°C. At 700°C the hardness data indicated the presence of the beta uranium phase in alloys containing 95 and 100 a/o uranium. The apparatus used is shown in Figure 4, and Table 3 gives the hardness data recorded.

J. W. Croffard[8] and Wheeler used the Larson, Miller parameter to correlate time, temperature and indentation creep of magnesium, aluminum and some of their alloys. Aluminum was found to have 1.5 to 2.5 times more indentation creep resistance than magnesium at 300 and 450°C irrespectively.

R. J. Parker[9] used loading times ranging from 10 to 10,000 seconds and concluded that straight line relationships exist between hot hardness and rupture strengths.

L. M. Fitzgerald[10] found that certain materials, although extremely hard at room temperature, generally lose their hardness at about 1000°C. Boron carbide was found to be an exception. Single crystals of TiC appeared to retain their hardness at high temperatures, but the polycrystalline form lost hardness at relatively low temperatures.

Dugdale[11] and Hoggart obtained tensile stress, strain curves for a wide variety of metals and deduced empirical formulae for obtaining hardness and tensile strength from the curves to show the relationship between the two. Their data are presented in Table 4.

A. G. Atkins[12] and D. Tabor developed an apparatus for measuring hardness at very high temperatures by mutual-indentation techniques. The schematic is shown in Figure 5. They could measure the hardness of the hardest materials up to their melting points.

R. D. Koester and D. P. Moak[13] determined the hot hardness of $Ti\ B_2$, $W_2\ B_5$, $Zr\ B_2$, $Hf\ B_2$, $Zr\ O_2$, $Al_2\ O_3$, $Nb\ C$, $Ti\ C$, $Ta\ C_{1-x}$, $Ta_{0.8}\ Hf_{0.2}\ C_{1+x}$, $W_2\ C$ and $(W_{0.65}\ Cr_{0.14}\ Re_{0.14}\ Ta_{0.07})_2\ C$ of < 95% density at temperatures
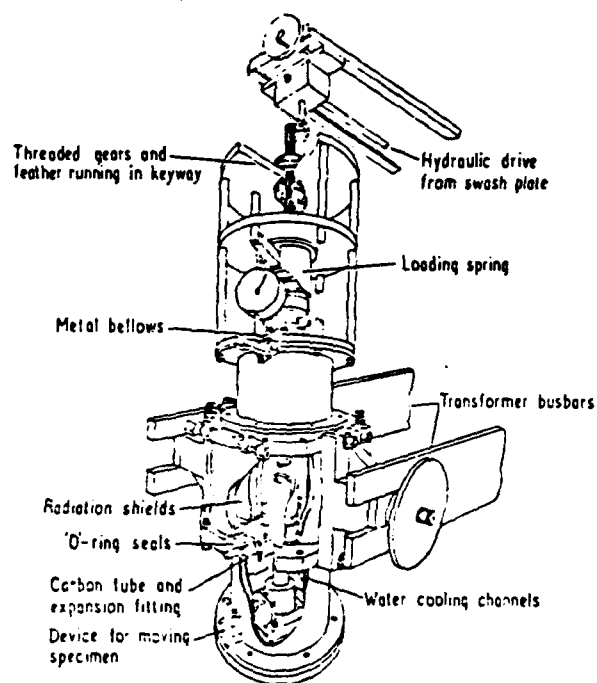
Figure 5 Exploded drawing of hot hardness apparatus.

Fig. 6. (a) Larson-Miller plot of stress rupture and hot hardness data for S-590.
(b) Underwood's method for correlating and extrapolating the results given in (a).

74
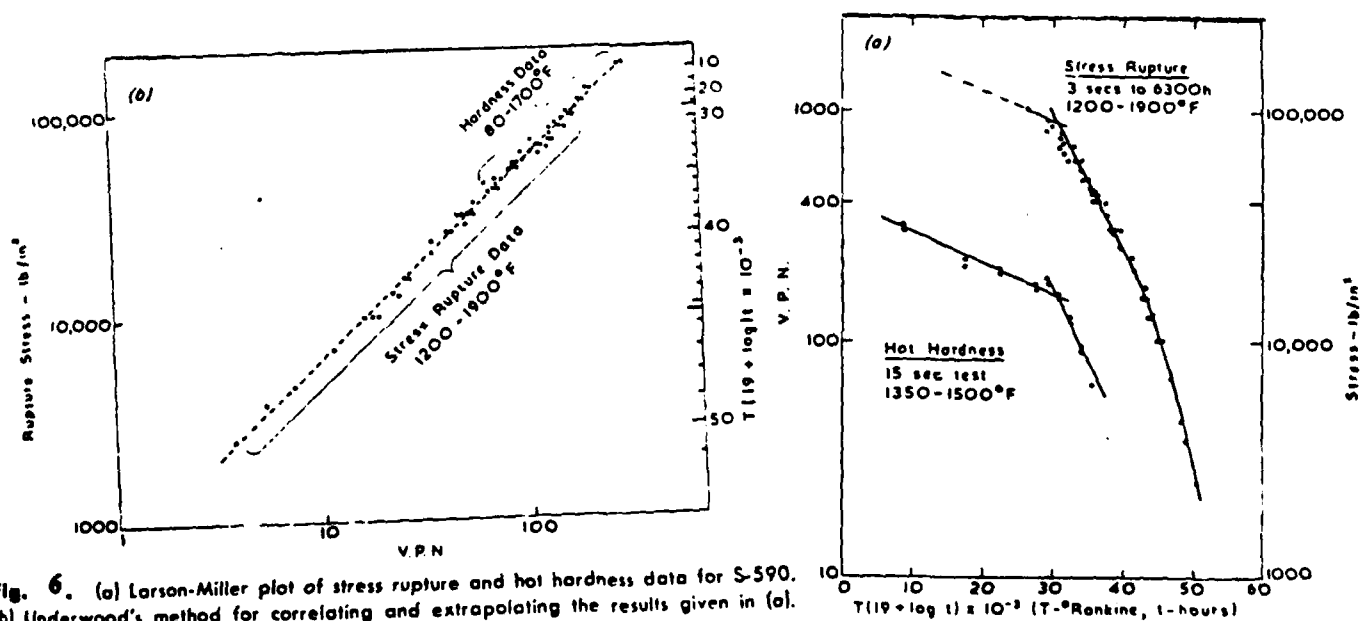
approaching 1900°C. They found that in all cases the hardness decreased rapidly with increasing temperature.

G. A. Geach[14] has published a review of the work done on hot-hardness measurement and the various correlations obtained by different investigators.

Temperature Dependence of Hardness

Metals and Alloys

Perhaps one of the most hopeful engineering uses of hot-hardness testing is the prediction of high-temperature creep properties. Figure 6a shows a standard Larson, Miller plot including 15-sec Vickers hot-hardness results while Figure 6b correlates hardness with rupture stress over a wide range of temperature, time parameter values. These Figures are for S-590 which contains 20% Cr, 20% Ni, 19% Co, 4% Mo, 4% Nb, 0.43% C and the rest Fe.

Westbrook[15] reviewed contributions to the literature on hot hardness and concluded that the results obeyed

$$H = Ae^{-BT} \tag{1}$$

where A and B are constants and T is the temperature. In spite of the variety of testing procedures and metal purities he suggested that A and B are related to the thermal energy of melting and the rate of change of heat content with temperature in a complex manner. Figures 7a and 7b show the variation of hardness with dimensionless temperature ratio for most metals.

Intermetallic Compounds

Mechanical behaviors of secondary phases are important not only through their influence on the properties of alloys containing them but also for

75
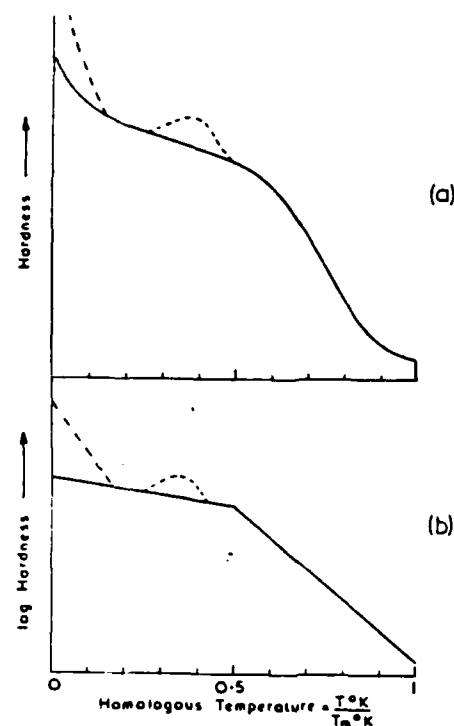
Fig. 7 . Temperature dependence of the hardness of metals. The dotted peak may be present if the sample exhibits strain aging. The rapid increase in hardness at very low temperatures is usually greater in bcc than in fcc structures.
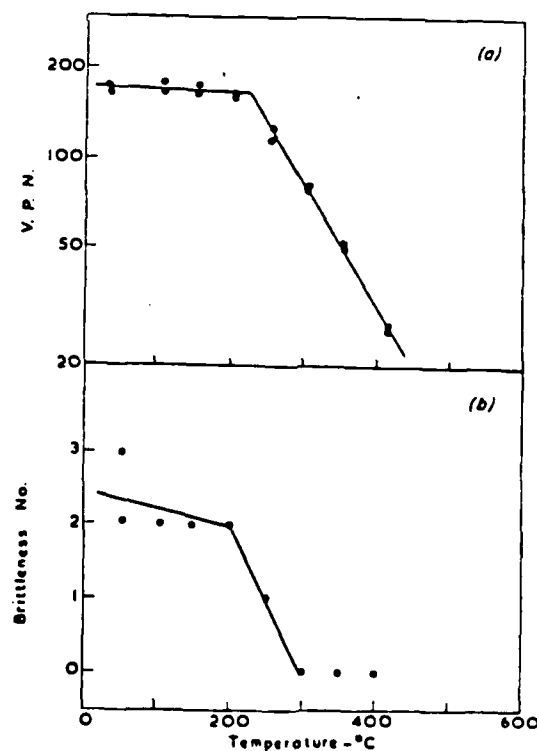
Fig. 8 . Hot Hardness and brittleness of an intermetallic compound (γ-Mg showing that the $0.5T_m$ hardness inflection in (a) is related to increasing plasticity (

76

their own potential as high-temperature materials. It has been shown that compounds with predominantly ionic bonding show a similar softening behavior to those with predominantly metallic bonds, though the former tend to be more brittle and do not soften appreciably below the inflection temperature near $0.5\ T_m$. However above this inflection most materials seem to become softer and more plastic: There deformation of intermetallic phases has been shown to occur in alloys, and extrusions of some intermetallic phases is possible.

Westbrook[16] illustrates the effect of temperature on the hardness of a compound of variable composition. Ag Mg has a wide range of composition on either side of stoichiometry, and at room temperature the hardness is a minimum at the stoichiometric composition. At high temperatures the situation reverses: There the lattice deflects increased diffusion rates so that the Ag Mg composition became the hardest.

Nonmetallic Materials

The Knoop indenter is the most useful in this field although Mohs scratch test has also been widely adopted. Hot-hardness results are available for oxides, carbides, nitrides, silicides and borides. These extremely hard and brittle materials behave similarly to the intermetallic compounds. It has been shown that in many such materials dislocation glide controls low-temperature behavior and climb occurs above about $0.5\ T_m$. Glass is a nonmetallic material with a characteristic noncrystalline structure which exhibits a slow softening up to some specific temperature followed by a rapid fall in hardness accompanied by increased plasticity.

77

Indentation Fracture

In the pyramid hot-hardness test three impressions at any one temperature are adequate to give a consistent hardness value and a semi-quantitative measure of brittleness. This brittleness number increases from zero to ten, as the impression degenerates from a perfect square to a shattered hole. Such a chart has proved satisfactory for illustrating the onset of plasticity in second phases as in Figure 8. This shows that the inflection in the hardness curve coincides with the changeover from the low-temperature brittleness to high-temperature plasticity.

Utility of Hot-hardness Measurements to Study High-Temperature Material Problems

Efforts are being made to accumulate all the information available on hot-hardness tests conducted on tungsten and its alloys. This information will be used along with the results obtained on actual hot-hardness measurements conducted in the laboratory on various tungsten, rhenium alloys to evaluate these alloys with reference to their mechanical, thermionic and thermophysical properties. The proposed activities include the generation of empirical formulae correlating hot hardness and related properties with different amounts of alloying elements in the tungsten, rhenium alloys.

REFERENCES

1. E. R. Petty, "Hardness Testing," Sheffield Polytechnic, Sheffield, England.

2. J. A. Brinell, Iron Steel Mag., Vol. 9, 16 (1905).

3. Frederick P. Bens, "Hardness testing of metals and alloys at elevated temperatures," Transactions of the ASM, Vol. 38, 1946.

4. W. Chubb, "Contribution of crystal structure to the hardness of metals," J. of Metals, p. 189 (Jan. 1955).

5. M. Semchysheu and C. S. Torgerson, "Apparatus for determining the hardness of metals at temperatures up to 3000°F," Trans. ASM, Vol. 50, 831 (1955).

6. L. M. Fitzgerald, "Measurement of hardness at very high temperatures," British J. of Appl. Phys., Vol. 11 (1960).

7. W. Chubb, G. J. Muehlenkamp, and A. D. Schwope, "A hot-hardness survey of the zirconium-uranium system," Trans. of ASM, Vol. 50, 299 (1958).

8. J. W. Goffard and R. G. Wheeler, "Hot indentation testing of magnesium and other selected materials," Trans. ASME, Vol. 215, 902 (1959).

9. R. J. Parker, "Estimation of stress-rupture properties form hot hardness tests," Metallurgica, May 1963.

10. L. M. Fitzgerald, "The hardness at high temperatures of some refractory carbides and borides," J. of Less Common Metals, Vol. 5, 356-366 (1963).

11. D. S. Dugdale and J. S. Hoggart, "Relation between Vicker's hardness and tensile strength," Metalurgica, Vol. 69 (1964).

12. A. G. Atkins and D. Tabor, "Mutual indentation hardness apparatus for use at very high temperatures," Brit. J. Appl. Phys., Vol. 16 (1965).

13. R. D. Koester and D. P. Moak, "Hot hardness of selected borides, oxides and carbides at 1900 °C," J. of the American Ceramic Society, Vol. 50, No. 6 (1967).

14. G. A. Geach, "Hardness and temperature," International Metallurgical Reviews, Vol. 19, (Dec. 1974).

15. J. H. Westbrook, Trans. Am. Soc. Metals, Vol. 45, 221 (1953).

16. J. H. Westbrook, J. Electrochem. Soc., Vol. 103, 54 (1956).

4. PROPERTIES OF TUNGSTEN

I] A Literature survey on the general properties of Tungsten

II] A Literature survey on the properties of zone-refined tungsten

4. PROPERTIES OF TUNGSTEN

Literature Survey on the General Properties of Tungsten

C. H. Schramm[1] and others determined the constitutions of the uranium, tungsten and uranium, tantalum alloys systems and constructed the resulting phase diagrams. The relationship between lattice parameter and composition for tantalum, tungsten solid solutions was delineated. They discovered two phases of the uranium, tantalum, carbon ternary system and described each phase.

S. J. Noesen[2] and J. R. Hughes arc melted several four-inch diameter tungsten ingots in vacuum or hydrogen atmospheres. Melting pressures, melt-off rates, effects of atmospheres and other pertinent factors were examined. Two of the ingots were extruded at 1650°C. They found that a 60% area reduction by rolling (at lower temperatures) resulted in a one-hour recrystallization temperature of 1250°C.

L. A. Niemark[3] et alii studied the kinetics of the "low temperature" recovery of electrical resistivity of both pure and specially doped cold-worked tungsten wire in the temperature range of 250°C to 450°C. A two-stage recovery process was found in both materials with a process change occurring at about 325°C in the undoped tungsten and at about 375°C in the doped tungsten. The calculated activation energies for the first or low temperature stage were 1.5 eV and 1.2 eV for the undoped and doped tungsten respectively. The second stage had activation energies of 1.7 eV and 2.3 eV for the undoped and doped tungsten respectively. The results are presented in Figures 1 and 2.

Sam Leber[4] and J. W. Pugh made single crystals of tungsten and deformed them in tension at 3000°C. The slip traces so formed on these crystals were
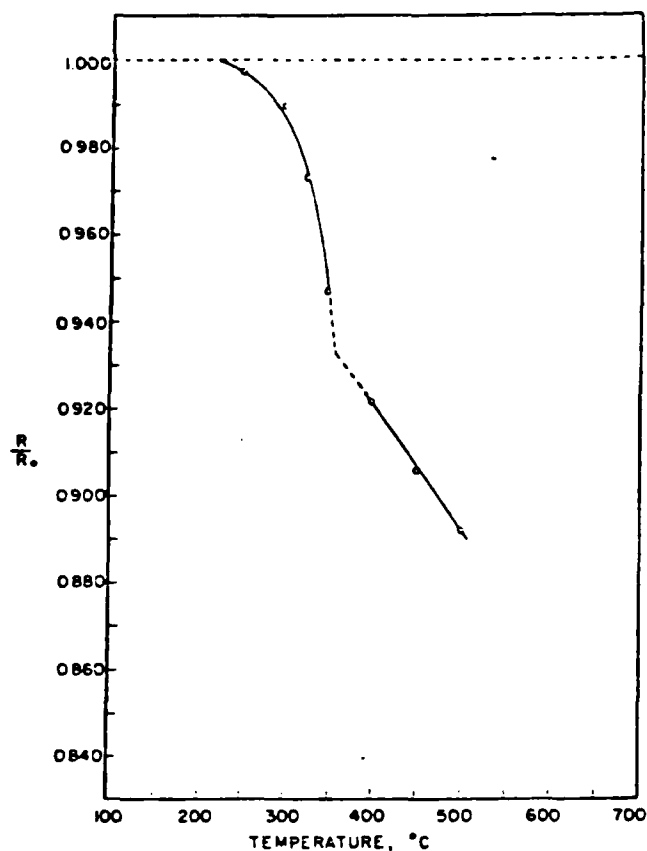
Fig. 1 Isochronal plot of resistivity ratio vs temperature; undoped tungsten (time = 120 min).
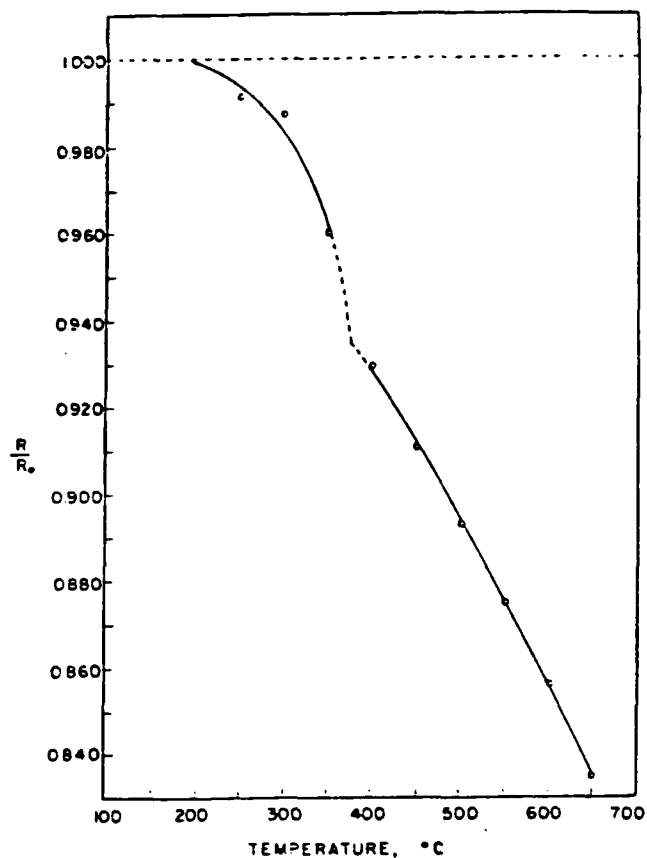
Fig. 2 -Isochronal plot of resistivity ratio vs temperature; doped tungsten (time = 120 min).

Table I. Effective Work Function of Tungsten Alloy Electrodes from Vacuum Emission Vehicle-Generated Schottky Plots

T, K	ϕ_{eff}, eV[*]									
	5 Pct Re	15 Pct Re	25 Pct Re	5 Pct Ta	10 Pct Ta	26 Pct Ta	1 Pct Ir	2 Pct Ir	2.5 Pct Os	5 Pct Os
2153	–	4.89	4.82	–	–	–	5.05	5.08	4.95	4.97
2103	4.95	4.89	4.82	4.95	4.84	4.88	5.08	5.10	4.97	4.98
2053	4.92	4.90	4.81	5.04	4.85	4.89	5.10	5.10	4.97	4.96
2003	4.91	4.89	4.81	5.09	4.84	4.92	5.10	5.10	4.99	4.99
1953	4.92	4.93	4.80	5.15	4.84	4.88	5.30	5.09	5.01	5.01
1903	4.91	–	4.76	5.18	4.85	4.91	5.30	–	–	–
1853	–	–	–	–	4.85	–	5.34	–	–	–
1801	–	–	–	–	–	–	5.37	–	–	–

[*]Experimental error: ±0.04 eV

TABLE 2 Impurity analyses in weight p.p.m. of tungsten single crystal specimens. Metallics—spectrographic analyses; O_2, N_2, and H_2—vacuum fusion analyses; C in specimens F—conductimetric analyses; C in specimens I and J.—low pressure analy-- Estimated precision of all analyses is ±3 p.p.m.

Specimen No.	No. of zone-melting passes	Al	Fe	Si	Mg	Ni	Cu	O_2	H_2	N_2	C
B-1-2	1	2	8	5	50	4	1	20	5	1	–
B-1-4	1	5	2	12	13	4	1	3	4	0.5	–
F-1-1	1	1	1	13	18	3	1	3	2	0.3	–
B-5-3	5	4	8	5	28	4	1	24	3	3	–
H-5-1	5	2	2	9	16	3	1	4	6	0.3	–
F-5-3	5	2	2	10	25	4	1	3	1	0.7	–
F-1-3	1	–	–	–	–	–	–	–	–	–	1*
F-5-5	5	–	–	–	–	–	–	–	–	–	.*
I	5	–	–	–	–	–	–	–	–	–	23*
J	1	–	–	–	–	–	–	–	–	–	1*

* Average of six determinations

82

analysed to determine the apparent slip system. Results indicated that deformation occurs in the (111) direction on planes of maximum shear stress.

L. Jacobson[5] measured the effective work functions of nine tungsten-base alloys. The second constituents in these alloys were 1) 5% Re, 2) 15% Re, 3) 2.5% Os, 4) 5% Os, 5) 1% Ir, 6) 2% Ir, 7) 5% Ta, 8) 10% Ta and 9) 26% Ta. Work functions were determined from vacuum-emission-vehicle and thermionic-emission-microscope measurements. Mosaics of each surface were produced from the microscope, and these mosaics showed the grain structure of the alloys and some anomalous emission areas. Table 1 gives the various work functions and Figures 3a and 3b show some of the microscope mosaics.

R. E. Taylor[6] found that sintered tungsten used by various researchers during a previous international program which included arc-cast and sintered tungsten was unsuitable for use as a standard material due to inhomogeneity and high-temperature instability. He gives results at high temperatures for thermal conductivity, electrical resistivity, specific heat, thermal diffusivity and Wiedemann, Franz, Lorenz ratio for a sample of the NBS sintered tungsten using the Properties Research Laboratory's multiproperty apparatus.

Frits J. A. den Broder[7] studied the surface diffusion of pure tungsten; W, 5% Re; and W, 10% Re alloys at 2500°C and 2650°C in a nitrogen, hydrogen atmosphere by the "scratching-smoothing" method. Scratch profiles were measured by light interferometry. Surface-diffusion constraints were evaluated using the increase in crack width with annealing time by applying the King and Mullins theory. The results showed that surface diffusion depended markedly on surface orientation and increases with rising rhenium content. Typical scratch interferograms are shown in Figure 4.

TABLE 3. Smoothed electrical resistivity values from this study.

Temperature (K)	Electrical resistivity ($\mu\Omega$ cm)	Temperature (K)	Electrical resistivity ($\mu\Omega$ cm)
295.15	5.388	1750	49.04
1050	26.17	1800	50.73
1100	27.76	1850	52.43
1150	29.35	1900	54.15
1200	30.94	1950	55.88
1250	32.55	2000	57.62
1300	34.16	2050	59.38
1350	35.79	2100	61.16
1400	37.44	2150	62.94
1450	39.08	2200	64.74
1500	40.73	2250	66.54
1550	42.38	2300	68.37
1600	44.03	2350	70.19
1650	45.70	2400	72.04
1700	47.37	2450	73.89
		2500	75.77

(a)

(b)

Fig. 3—Thermionic emission microscope mosaics. (a) W-5 pct Re (T_E = 1953 K); (b) W-15 pct Re (T_E = 2063 K).

(a)

(b)

(c)

(d)
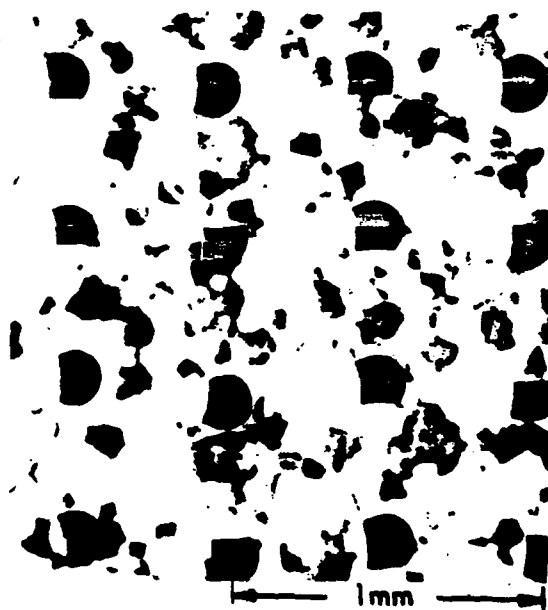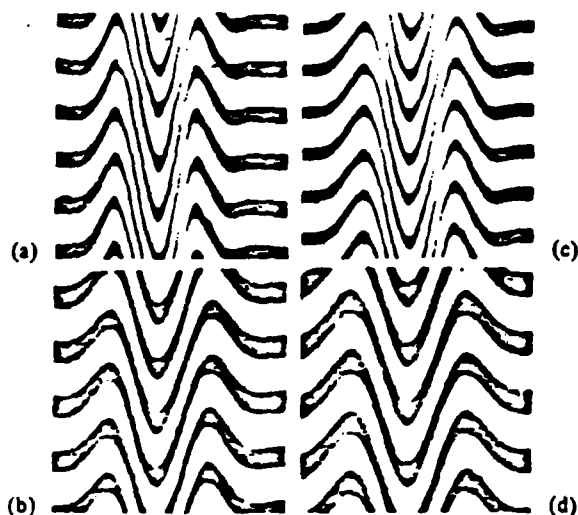
Figure 4 Scratch interferograms on tungsten (a and b) and W-10% Re (c and d) after annealing for 2 5 and 10 h at 2650 °C.

Kazuo Ishikawa[8] and Yasushi Tomida compared the dEN(E)/dE mode spectra A (C and O atoms on tungsten between the widely used peak-to-peak height measurements) and the EN(E) mode spectra H and S (rarely used Auger peak heights and areas) as measures of the signal in Auger electron spectroscopy. They found that such comparisons provided a more sensitive means of detecting chemical change than by observing Auger peak shapes.

A. Modinos[9] presented a semiempirical theory of the electronic work function of the different faces of tungsten. The calculated values of work function were in reasonably good agreement with available experimental data for practically all of the crystallographic planes except the (100) plane. They attributed the discrepancy to the negative contribution to the surface dipole potential from surface state that exists on this plane.

A Literature Survey on Properties of Zone-Refined Tungsten

H. W. Schadler[10] grew single crystals of tungsten by electron-bombardment floating-zone refining and strained them, two percent in tension and bending at 298°K, 77°K and 20°K to determine the modes and crystallography of the plastic deformation at these temperatures. He found that at 77° and 20°K plastic deformation occurred by slip on systems of the type (011) [11$\bar{1}$] and by twinning on (112) planes. For crystals strained at 298°K, deformation occurred by slip in [11$\bar{1}$] directions on either (011) or (112) planes. Figure 5 shows the schematic illustration of the technique for determining the pole of plane from its trace which was used intensively in this work.

H. B. Probst[11] produced mechanical twins in zone-refined tungsten single crystals by explosive working at room temperature. These twins were parallel to [112] planes and have irregular boundaries rather than the classically plane twin boundaries. These boundaries were grooved surfaces

85
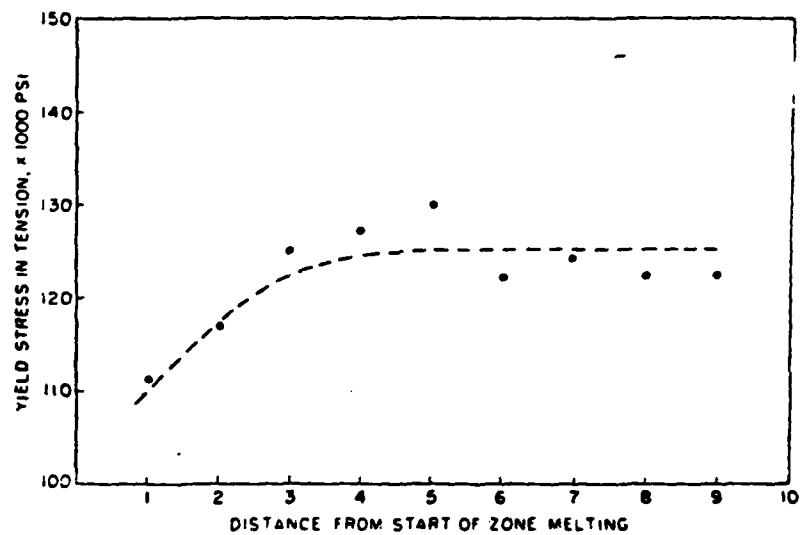
FIG. 7 Yield stress in tension at −196°C vs. the distance from the starting end of zone melting of crystal C.
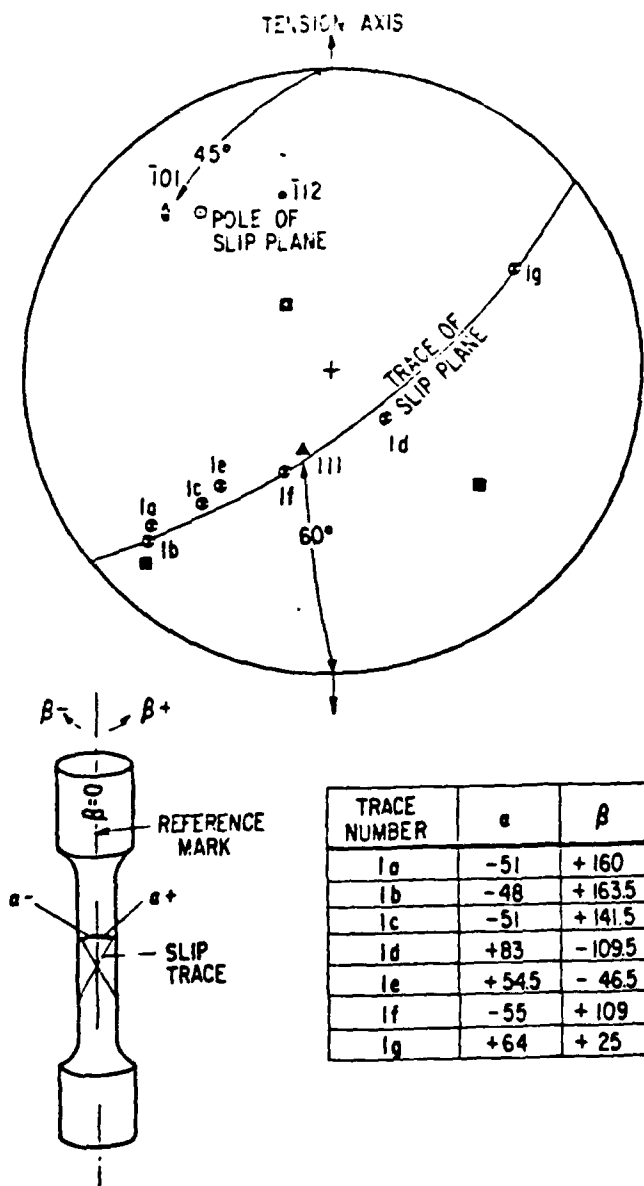
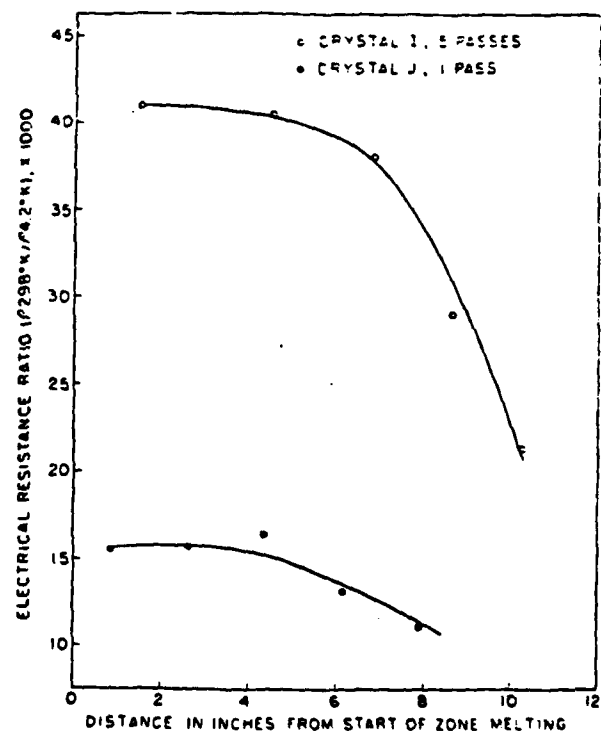Fig. 5 -Schematic illustration of technique for determining the pole of a plane from its trace.

TRACE NUMBER	α	β
I a	−51	+ 160
I b	−48	+ 163.5
I c	−51	+ 141.5
I d	+83	− 109.5
I e	+ 54.5	− 46.5
I f	− 55	+ 109
I g	+64	+ 25

FIG. 6 Variation of electrical resistance ratio (ρ 298°K/ ρ 4.2°K) along the length of single crystals.

86

in which the grooves themselves were parallel to a <111> direction and the sides of the grooves appeared to be parallel to [110] planes.

Ursula E. Wolff[12] observed mechanical twins in tungsten single crystals of a variety of axial orientations deformed at room temperature in tension or bending. Twinning at room temperature occurred only after considerable prior slip. Twins usually preceded fracture and nucleated cracks. In the absence of twinning, tensile samples failed by shear; twinned samples failed by cleavage.

J. L. Orehotsky[13] and R. Steinitz made an analysis of the influence of floating molten-zone travel on the purification of tungsten rods and the effect of this purification on the brittle-to-ductile transition temperature. The major impurities detectable in the original rods, id est Mo and O_2, were reduced by zone refining from 30 to 3 ppm. Tensile tests on three-mil wires drawn from these rods and recrystallized to 17,000 grains/mm² showed a transition temperature of 60°C for the zone purified and 115°C for the original material.

R. C. Koo[14] investigated the effect of purity on the tensile properties of tungsten single crystals grown by electron-bombardment zone melting from -196°C to 29°C. He found that an increase in overall purity resulted in a decrease in the critical resolved shear stress as well as an increase in ductility and facilitated deformation twinning. Electrical resistivity measurements indicated that the amounts of interstitial impurities were of the order of a few atoms ppm. Table 2 gives the impurity analysis in weight ppm of tungsten single-crystal specimens. Figures 6 and 7 show the variation of electrical-resistance ratio and yield stress in tension along the length of single crystals.

R. K. Williams[15] determined the electrical resistivity of zone-refined tungsten between 1100 and 2500°K. The error analysis indicated that the data are accurate to about one percent, and comparison of the results with similar data indicated that it could be pessimistic. The effects of thermionic charge transport on the resistivity data and the performance of uninsulated W,3Re; W,25Re thermocouples were also investigated. Table 3 gives the electrical resistivity data at various temperatures.

REFERENCES

1. C. H. Schramm, P. Gordon, A. R. Kaufmann, "The alloy systems, uranium-tungsten, uranium-tantalum and tungsten-tantalum," Transactions AIME, J. of Metals, Vol. 188, (1950).

2. S. J. Noesen, J. R. Hughes, "Arc melting and fabrication of tungsten," Trans. of the Metl. Society of AIME, Vol. 218, (1960).

3. L. A. Neimark, R. A. Swalin, "Annealing of point defects in cold-worked tungsten and the influence of impurities on the kinetics," Trans. of the Met. Soc. of AIME, Vol. 218, (1960).

4. Sam Leber, J. W. Pugh, "High temperature slip in tungsten," Trans. of Met. Soc. of AIME, Vol. 218, 791 (1960).

5. D. L. Jacobson, "Emission characteristics of some dilute tungsten alloys," Metallurgical Transactions, Vol. 3 (1972).

6. R. E. Taylor, "Thermal properties of tungsten SRM's 730 and 799," Trans. of ASME, Vol. 100 (1978).

7. Fritz J. A. den Broeder, "Surface diffusion of tungsten and tungsten-rhenium alloys," High Temperatures-High Pressures, Vol. 10, 131-133 (1978).

8. Kazuo Ishikawa and Yasurhi Tomida, "Comparison of Auger signals measured using differential and integral Auger spectral from C and O adsorbed on W," J. of Vac. Sci. Technology, Vol. 15, No. 3 (1978).

9. A. Modinos, "The electronic work-function of the different faces of tungsten," Surface Science, Vol. 75, 327-341 (1978).

10. H. W. Schadler, "Deformation behavior of zone-melted tungsten single crystals," Trans. of Met. Soc. of AIME, Vol. 218, 649 (1960).

11. H. B. Probst, "Observations on twinning in zone-refined tungsten," Trans. of Met. Soc. of AIME, Vol. 221, 741 (1961).

12. Ursula E. Wolff, "Twinning and fracture in tungsten single crystals at room temperature," Trans. of the Met. Soc. of AIME, Vol. 224, 327 (1962).

13. J. L. Orehotsky, R. Steinitz, "The effect of zone purification on the transition temperature of polycrystalline tungsten," Trans. of the Met. Soc. of AIME, Vol. 224, (1962).

14. R. C. Koo, "Effect of purity on the tensile properties of tungsten single crystals from -196°C to 29°C," Acta Metallurgica, Vol. 11, 1083 (1963).

15. R. K. Williams, "A study of the electrical resistivity of zone-refined tungsten at high temperatures," J. of Applied Physics, Vol. 46, No. 2 (1975).

5. "FACILITIES"

I] Thermionic Emission Microscope

II] Vacuum Emission Measurements

III] Facility for Material Characterization

5. FACILITIES

Characteristics central to the establishment of a firm understanding of alloy mechanisms include composition, recrystallization temperature, grain growth and structure, component activity, enthalpy and free energy of vaporization as well as and thermal and mechanical stability. Strength and grain-surface characteristics are normally evaluated at room temperature. Such evaluations are being made at operating temperatures with a unique thermionic-emission microscope (refs. 1 to 4). In the microscope an image of the surface of the high-temperature emitter is displayed on a phosphor screen through thermionic emission of electrons from that surface. The emitted electrons are also gathered in a Faraday Cage for subsequent calculation of the work function. The thermionic-emission microscope is not at all similar to a conventional electron microscope. Surface changes such as recrystallization are directly observable on the thermionic-emission-microscope screen. Changes in structure, composition and orientation are detectable through the electron emission. Other surface characteristics such as composition will be measured with the Auger spectrometer and scanning emission microscope (SEM).

To facilitate detailed examination the thermionic-emission microscope utilizes the Faraday cage for the measurement of the electron emission from individual grains and the phosphor screen for displaying the fine-grain structure for visual observation and subsequent emission-micrograph documentation.

Figure 1 is an assembly drawing of the emission microscope indicating the location of the basic components which are the emitter sample; its heater; an X, Y, Z traverse mechanism; lenses; screen; Faraday cage and vacuum system. As previously stated the guarded Faraday cage was

END

FILMED

DTIC
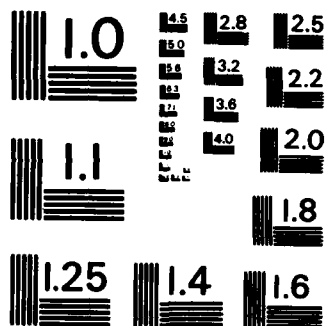
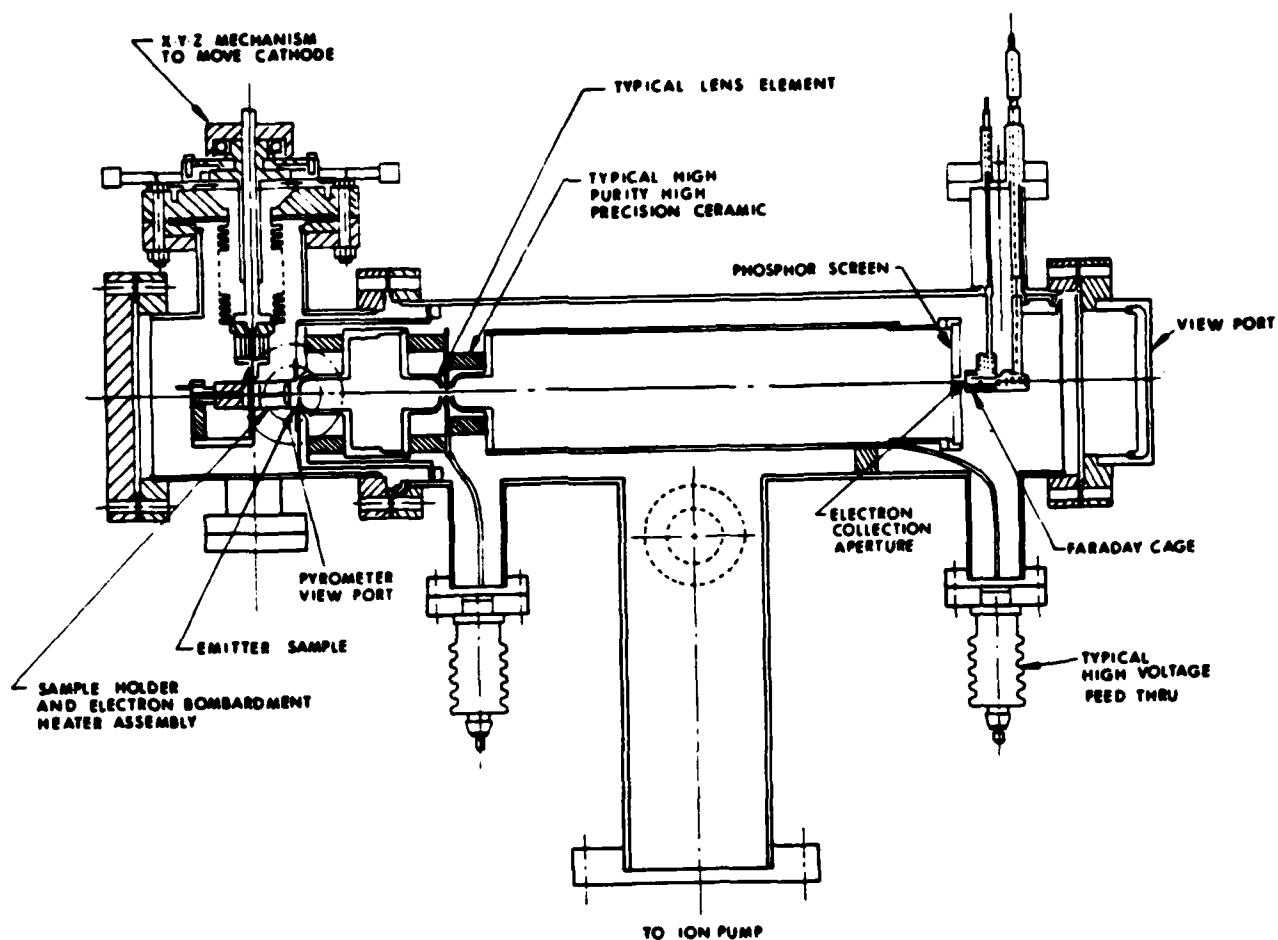MICROCOPY RESOLUTION TEST CHART

NATIONAL BUREAU OF STANDARDS-1963-A

Fig. 1—Thermionic emission microscope assembly and components.

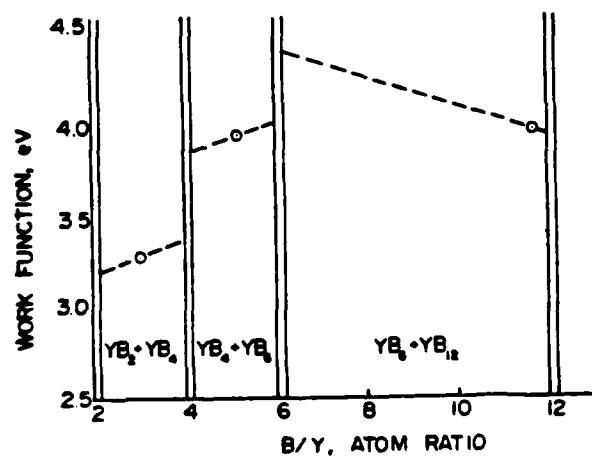Fig. 2 Emissionmicrograph of Mo,LaCrC$_3$

Fig. 3 Work-Function , Composition Relationship

4

THERMIONIC-EMISSION-MICROSCOPE SPECIFICATIONS

- MAGNIFICATION   80 to 1400X

- RESOLUTION $\sim 0.15\mu$

- HIGH TEMPERATURE
  OPERATION   Up to 2300°K

- VACUUM (Vac ion) $< 10^{-8}$ torr at 2300°K

- FARADAY CAGE $\sim 5 \times 10^{-13}$A and above

- x, y, z TRAVERSE   Scan central 3 cm^2 of a 0.75 in.
  MECHANISM   diameter sample. Drive accuracy
                        of $\pm$ 0.0001 in.

QUALITATIVE MEASUREMENTS ON PHOSPHOR SCREEN

CURRENT MEASUREMENTS WITH FARADAY CAGE

$$J_o = \frac{I_c M^2}{A_c}$$

I_c = current collected by Faraday Cage

M = magnification

A_c = current collection cross sectional area

J_o = sample current density

Calculate ϕ effective by substitution of J_o into R.D. eqn.

incorporated into the microscope for the purpose of measuring the effective work function of individual grains on the cathode sample. The guard prevents current leakage across insulators in the measuring circuit, enabling current measurements to be taken below 10^{-11} amp. An electrometer with a noise level of 4×10^{-14} amp was used to measure the current collected by the Faraday cage. The noise level of the entire current-measuring circuit of the microscope is approximately 5×10^{-13} amp. The microscope is operated at vacuum level of 1×10^{-8} torr at emitter temperatures as high as 2300°K.

The Faraday-cage current can be related to the sample electron-current density by the following equation.

$$J_0 = \frac{IM^2}{A_c}$$

where I is the current from the sample as measured in the Faraday cage, M is the magnification at the current collecting plane, A_c is the area of the hole in the center of the screen at the collecting plane, and J_0 is the emitter current density. Details of the thermionic-emission-microscope and Faraday-cage capabilities appear in the following tables.

The effective work function $\emptyset$ is calculated from the Richardson, Dushman equation,

$$J_0 = AT^2 \exp \left[-\frac{\emptyset}{kT}\right]$$

Again J_0 is the emitter current density as measured in the vacuum-emission vehicle or with the microscope. T is the emitter temperature. The parameter A has the value 120 amp per $cm^2 k^2$. k is the Boltzmann constant. And in this case $\emptyset$ is called the effective work function.

94

Figure 2 is a typical emission micrograph at temperature. It is the result of a recent study of low-work-function oxide emitters, in this case molybdenum with vapor deposited $LaCrO_3$. Figure 3 (ref. 2) is the result of a recent study on the YB system which demonstrates the sensitivity of work function to composition. Figure 4 is a plot of work function versus orientation for molybdenum obtained from a polycrystalline sample with the thermionic-emission microscope and Laue-back-reflection orientation determination (ref. 3). Work functions can be determined for selected grains in the polycrystalline sample, and various thermal phenomenon such as grain growth and recrystallization are observable.

A new Faraday Cage has been designed and is being built and fabricated. It is an improved version with external adjustment capability and finer alignment between the various component parts. The drawings are provided in Appendix A.

A vacuum-emission vehicle has been developed especially for measurements taken for the proposed program. The vacuum system consists of sorption roughing pumps, titanium-sublimation intermediate pumping, and 140 liter/sec noble gas vac-ion pumping. Samples are heated by electron bombardment from a high-temperature counter-wound tungsten filament. Sample temperatures are measured with a micro-optical pyrometer viewing a 10-to-1-depth-to-diameter hohlraum. The electron collector shown in Figure 5 (followed by the system specifications) consists of a planar one-half-inch-diameter radiation-cooled molybdenum electrode. The collector is ringed by a large molybdenum guard with a 10-mil spacing between collector and guard ring. These are then balanced through a null meter.

The vacuum-emission experimental facilities and capabilities are shown in Figure 6 and the table that follows it. In operation a potential is set
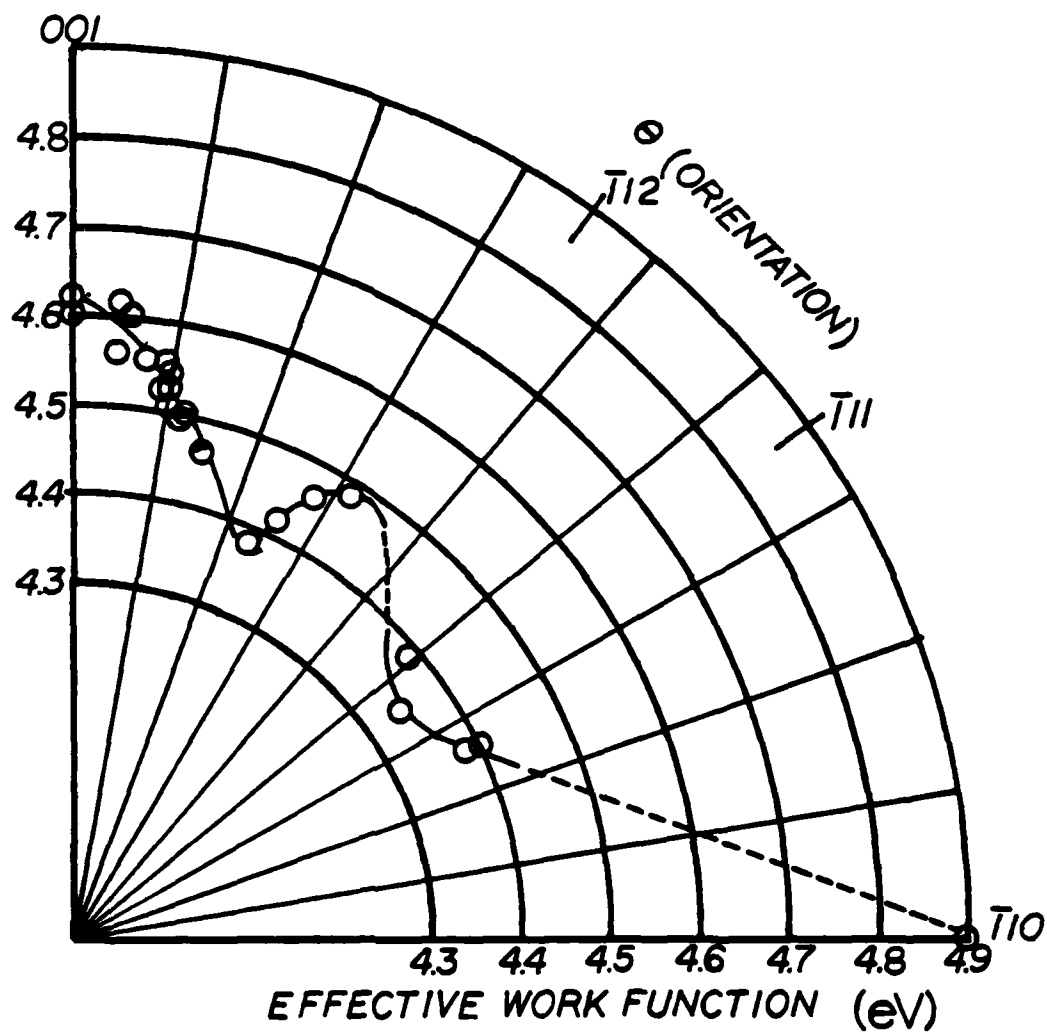
Figure 4 . Polar Plot of ∅ Effective in [110] Zone for Polycrystalline
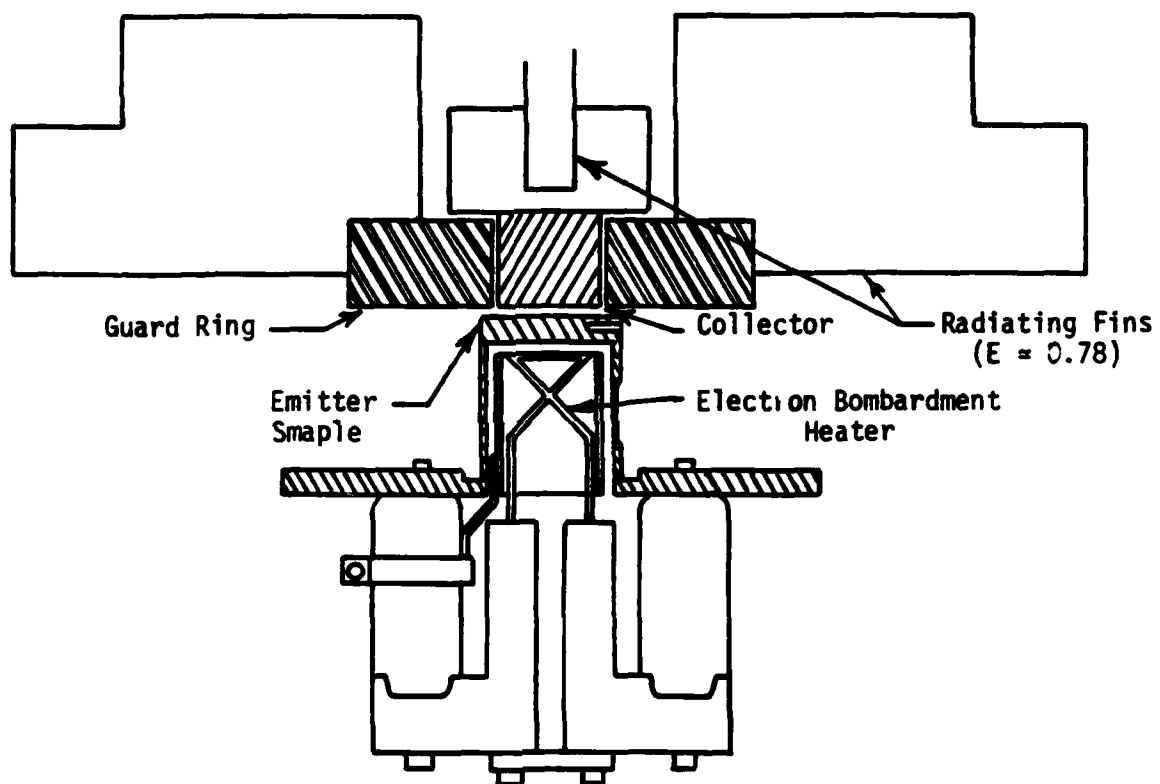Molybdenum Specimen at 1789°K

Guard Ring —
Collector
Radiating Fins
(E ≈ 0.78)

Emitter
Smaple
Electron Bombardment
Heater

Figure 5 .   Schematic of Vacuum Emission Test Vehicle
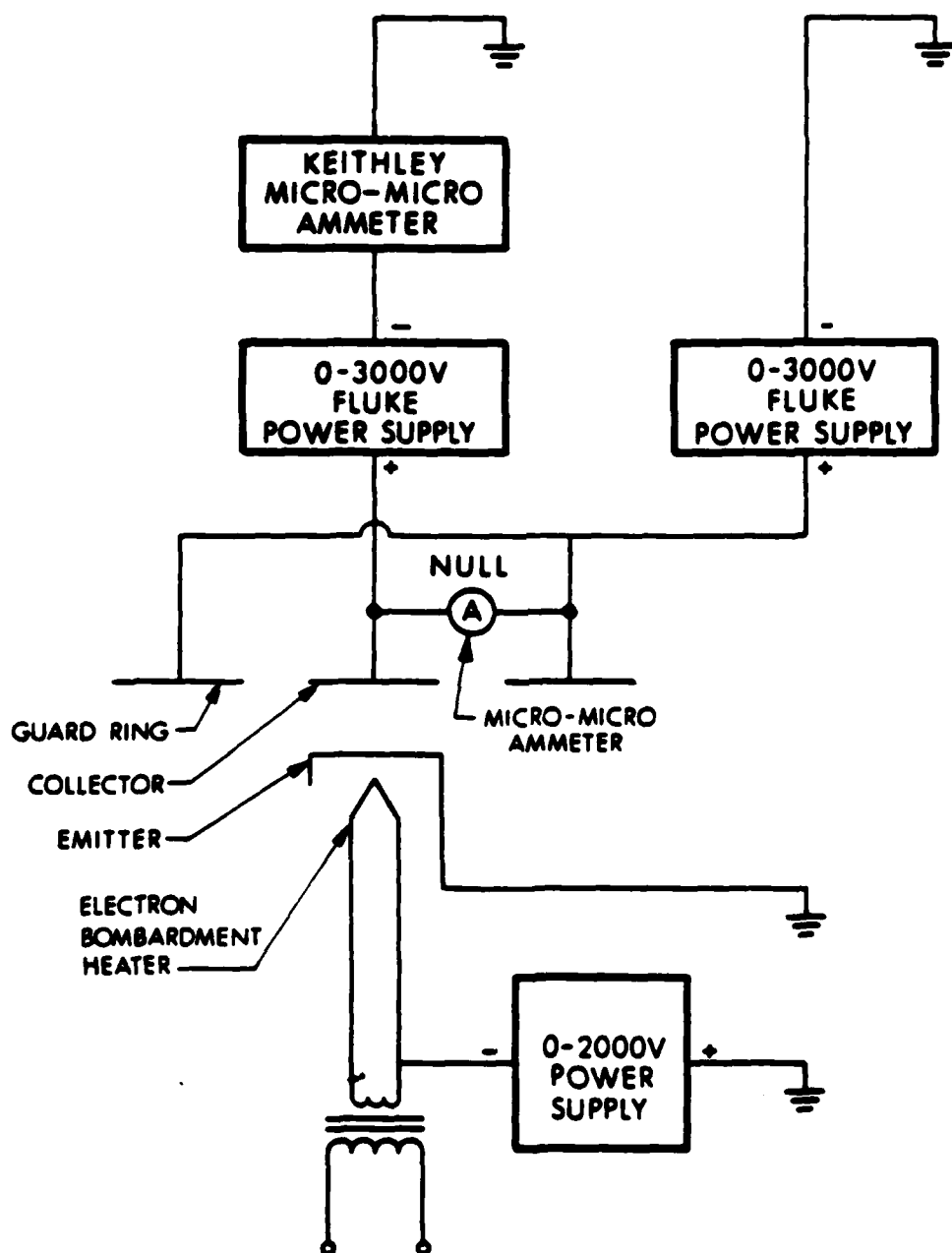
97

Figure 5. Schematic of Electrical Circuit for Vacuum
Emission Measurements

VACUUM-EMISSION SYSTEM

Schottky plots are generated at constant temperature; emission is measured as a function of applied field.

The physical system consists of

* Radiation cooled collector and guard ring

* Electron bombardment heated planar samples

* Vacuum system consists of

  - sorption roughing pump

  - titanium sublimation intermediate

  - 150 l/s Vac ion

  - Vacuum < 10^{-8} Torr

* Temperature measurement by micro-optical pyrometer-sample hohlraum

between the emitter and the collector with a high-precision power supply, and the current is measured with an electrometer. The current leakage is nulled between collector and guard ring by the second power supply connected to the guard ring.

Electron-emission measurements are taken at a number of emitter temperatures for each sample. At each temperature the emission is measured as a function of the applied voltage. With this data as shown in Figure 7 the saturated or zero-field emission from the emitter is determined by generating plots according to the Schottky equation,

$$\log J_{RS} = \log J_R + 1.912/T \sqrt{E} \quad .$$

J_R is the zero-field Richardson current, J_{RS} is the Schottky current, and E is the electric field. The plot of $\ln J_{RS}$ versus $\sqrt{E}$ is extrapolated to determine J_R. J_R is then substituted into the Richardson, Dushman equation $(J_R = J_C)$, and the effective work function is calculated.

Figure 8 is a Richardson plot showing a work-function determination from the zero-field current and temperature. This can be generated with both the thermionic-emission microscope and the vacuum-emission vehicle for comparison.

A quadrupole mass spectrometer with capability from AMV 1 through 350 is used to determine the surface composition at operating temperatures and to determine the evaporation of the alloy elements. Freely vaporizing and Knudsen-cell studies can be made on high-temperature alloys to permit calculation of thermodynamic properties for theoretical modeling. The effects of time and temperature upon the stability induced by interstitial-impurity-gettering alloy additions can be evaluated through these measurements.
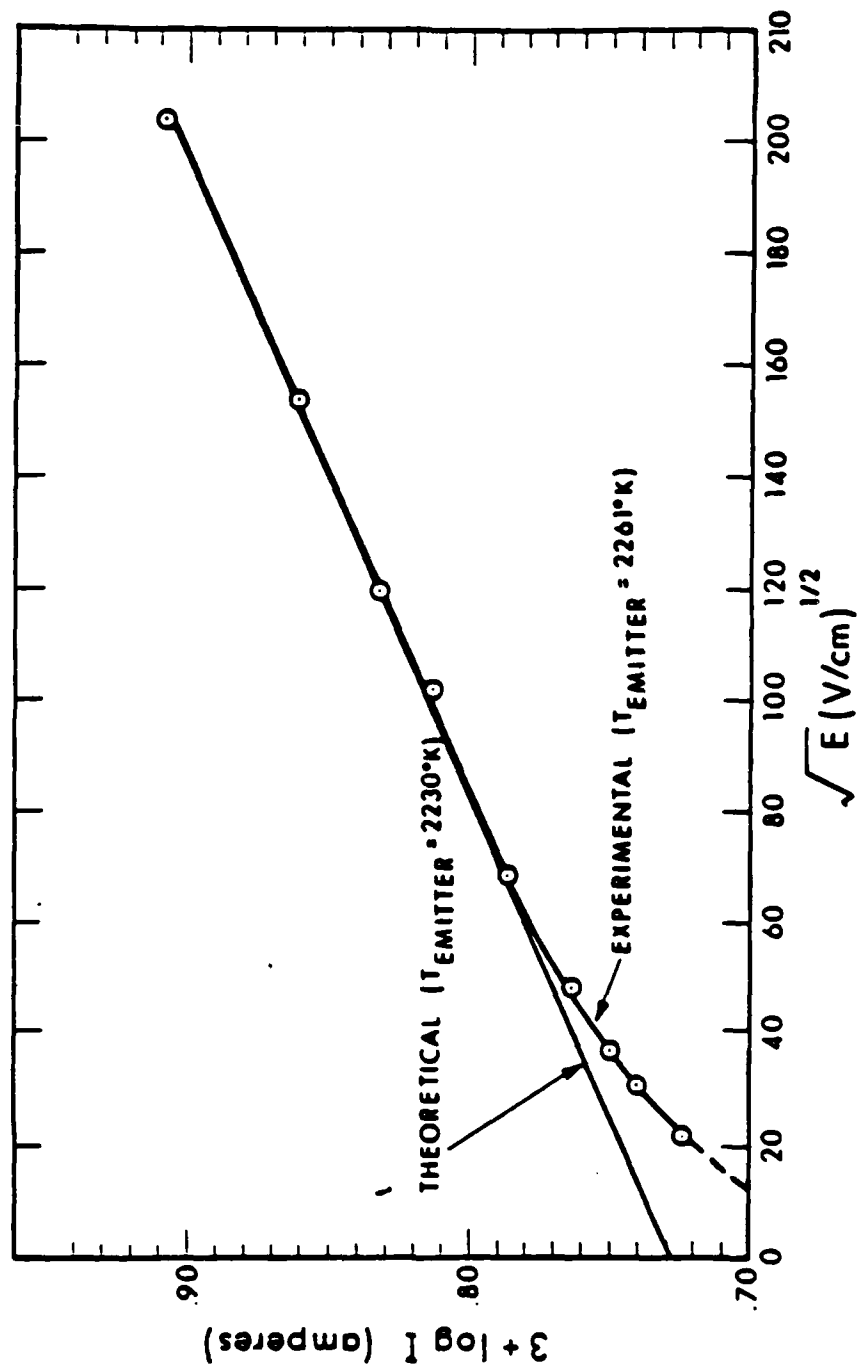
100

Figure 7. Schottky Plot of Emission from Vapor-Deposited Rhenium at an Emitter Temperature of 2261°K
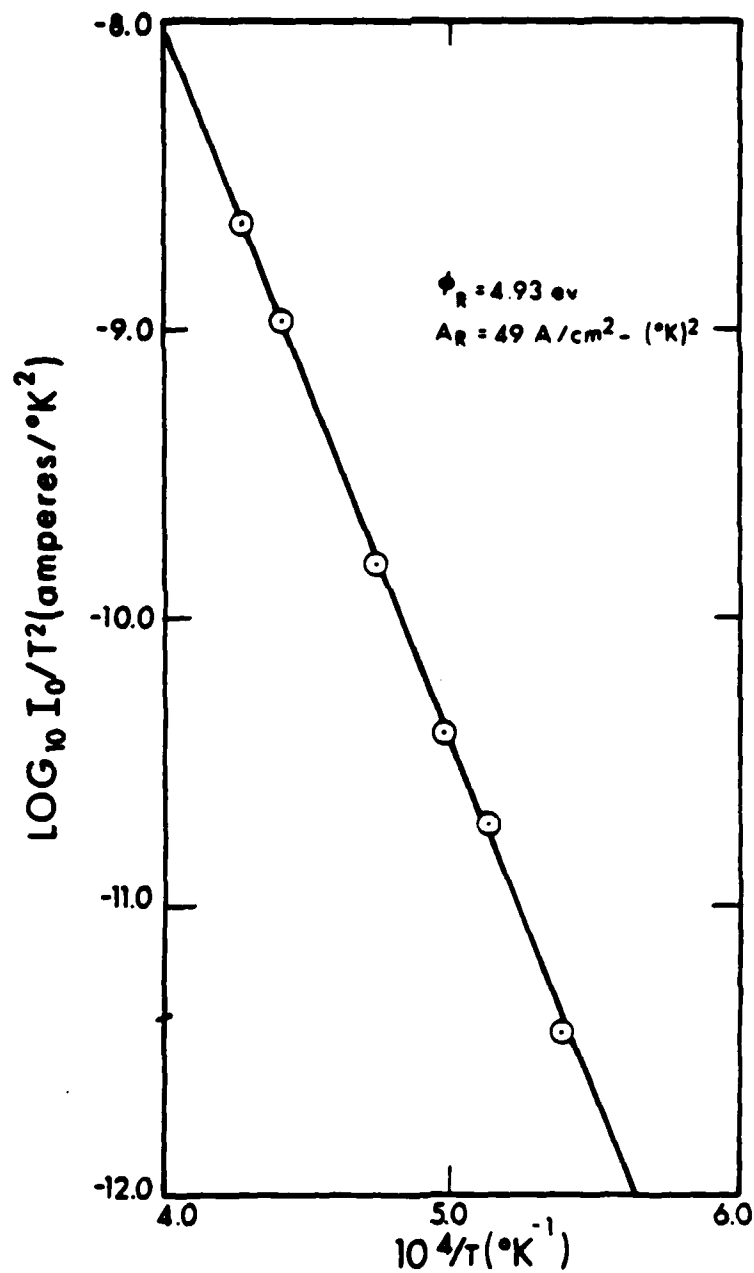
Figure 8. Richardson Plot for Vapor-Deposited Rhenium

Auger spectrometry and microprobe analyses are used for room-temperature surface-composition and surface-distribution characterization. Other x-ray, metallographic-SEM and general materials-testing equipment is available for property measurements which might be desired for completeness. The alloy additions can be studied with Auger spectrometry and the microprobe to determine which interstitial elements are combined with the getters.

Equipment valued then at over a half million dollars was donated to ASU by the NASA Lewis Research Center to pursue high-temperature, high-vacuum materials research. The equipment will be used extensively in the experimental research on this program.

Micro-optical pyrometers are available for high-temperature measurements plus an automatic micro-optical pyrometer system and a unique photon-counting pyrometer.

REFERENCES

1. D. L. Jacobson, "Emission Characteristics of Some Dilute Tungsten Alloys," Metallurgical Transactions, 3, May 1972, p. 1963.

2. J. Jaskie and D. L. Jacobson, "Thermionic Emission and Surface Composition of the Y,B System," Journal of Energy 5, No. 3, May-June 1981, p. 187.

3. D. L. Jacobson and A. E. Campbell, "Molybdenum Work Function Determined by Electron Emission Microscopy," Metallurgical Transactions, 2, Nov. 1971, p. 3063.

4. C. Landrith, "Effective Work Function Determination of Polycrystalline Molybdenum and MoLaCrO$_3$ at Thermionic Emission Microscope," Thesis (Advisor D. Jacobson), May 1982.

SECTION 6. CONCLUDING REMARKS

Theoretical and experimental approaches are underway in this high-temperature materials research. Background literature is continually being reviewed and has been a substantial fraction of the work conducted during the first year. Experimental considerations were extensively reviewed during this time: It was determined that extreme compositional control over samples was a primary requirement. Thus zone refining was determined to be an excellent indeed mandatory method. A zone refiner discussed in Section 2 was designed, and parts were ordered during the first phase of this work.

Material characterizations will involve among other devices the thermionic emission microscope, Auger spectrometer and scanning electron microscope. A high-temperature mass spectrometer will also provide important compositional information. The thermionic microscope is being upgraded for this program and is also reviewed in the preceding section.

Acquisition of high-temperature-strength properties is also important. A proposal was sent to the DOD for university equipment but was not supported. We are seeking funds from various sources to obtain such equipment for this program. By the third year such facilities should be available. Room-temperature testing including hardness and tensile testing with creep and fatigue for later in the program are of primary concern: The ultimate evaluations will involve high-temperature tests. High-temperature hardness is one of the techniques which might be possible in a short time (id est lower cost). Hardness data can be correlated with other important physical properties.

Thus in the present theoretical and experimental approaches, the properties of the initial components typifying advanced systems and the principal methods of investigation are unique. Vaguely competitive research

105

involves molybdenum (Mo) and Mo alloys (LANL), conventional tensile and bending evaluations as well as the usual metallography.

Samples will be fabricated into discs for emission-microscope measurements. Both highly purified and sintered samples are of interest. The latter are pragmatically important because of powder-metallurgy advances and inherent inhibition of recrystallization processes by the particle-surface impurities that resist diffusion and grain growth. The sintered-sample porosity also reduces grain growth. The extensive grain-boundary region of small-grain materials provides an excess sink for distribution of embrittling oxides, nitrides and carbides which otherwise tend to reside in the intergranular boundaries. Some oxides and nitrides may be removable by hydrogen reduction and thermal outgassing. Selected constituents that yield dispersed refractory products will be very effective in enabling high-temperature, hard-vacuum clean-up.

The approach to the research has been to develop the general theories for high-temperature materials characterized by high quality and long life. Recrystallization, ductility, creep strength, vapor pressure, work function, compositional stability and other pertinent phenomena which are crucially important to high-temperature energy converters will continue to be addressed. Techniques for producing and sustaining the desired properties will be investigated from a microscopic, mechanistic viewpoint. Although limited theoretical and experimental information exists for such systems a datum-plane system based on tungsten is indicated and has been selected in the first year for experimental evaluations.

A major consensus indicates that intergrannular segregation of interstitial-impurity products increases brittleness of BCC metals. But a minor consentience raises the possibility that while oxides and nitrides are

106

deleterious carbides improve overall cohesion through grain-boundary effects - and thereby enhance BCC-metal ductility.

Of course recrystallization at high temperatures increases interstitial-impurity transport, hence intergranular precipitation. This mechanism approximates solid-state zone refining. Simultaneously the crystallite surface-to-volume ratio decreases during the recrystallizing process - again raising grain-boundary segregate concentrations. Such mechanisms are important even for very low impurity concentrations.

In order to obtain highly controlled compositions, some samples will be refined by a floating-zone technique. This effort is underway as the first part of the experimental phase of the program.

Central to the property modifications in addition to solution-effect improvements are precipitation and dispersion effects. One such approach involves the addition of very small amounts of excellent getters to the refractory alloy to convert usual intergranular impurities that embrittle into dispersed refractory products that produce high temperature ductility and strength. For example it is known that thoria in small amounts in tungsten improves its strength and ductility considerably. Such improvements are exceptional in tungsten, rhenium alloys through the combined solid-solution and dispersion effects. The proposed alloy getters are designed to tie up the oxygen, carbon and other embrittling impurities to reduce their intergranular effects and increase their microscopically dispersed influences.

This research aims at determining the microscopic processes involved in producing high-quality materials for high-temperature energy converters for space applications. Processes involved in solid-solution alloying modified with stable low-concentration-gettering agents for controlling

107

recrystallization, embrittlement and creep mechanisms in high-quality, high-temperature materials for space-energy conversion systems are proposed.

The acquisition of samples is also being pursued. Some alloys are available commercially while most will need to be tailor made. An agreement with Los Alamos National Labs through Dr. Ed Storms for some sintered samples is pending. In the interim progress on theoretical and experimental facilitation of this critically important project continues.

APPENDIX A

Thermionic Emission Microscope:
Collector and Faraday-Cage Design Drawings

This section includes the various parts of the collector assembly labeled in Figure 1 of Section 4 as the Faraday cage. All parts described in this section are new designs based on the original design of the Faraday cage itself. The electrical feedthrough is identical to the one currently in use except several dimensions. All parts were designed for rigidity and ease of alignment of the collector assembly. Figure 1 shows the seamless decelerator which forms a rigid unit with the guard ring when separated by the ceramic in Figure 2. The decelerator is bolted to the guard ring and electrically insulated from it by parts 3 and 4 (Figures 3 and 4). Figure 5 shows an assembly view of the parts just described. The electrical feedthrough (Figure 6) has slightly different dimensions for added rigidity, such as thicker copper wires and stainless-steel tube. The electrical connections are also longer to account for the added bellows. The copper wires are connected to the Faraday cage assembly by D.B. connector for quick release. The stainless-steel tube (Figure 7) attaches the collector assembly to the electrical feedthrough forming a rigid unit. Figure 8 shows the welded bellows used for ease of alignment of the collector assembly with the rest of the microscope. The two plates such as the one in Figures 9 and 10 are welded to the flanges of the bellows as shown in Figure 8 and are controlled by the two-way screw (Figure 11). The assembly of Figures 8 through 11 enables one to adjust the collector having large motions in the z direction and a limited range in the x and y directions.
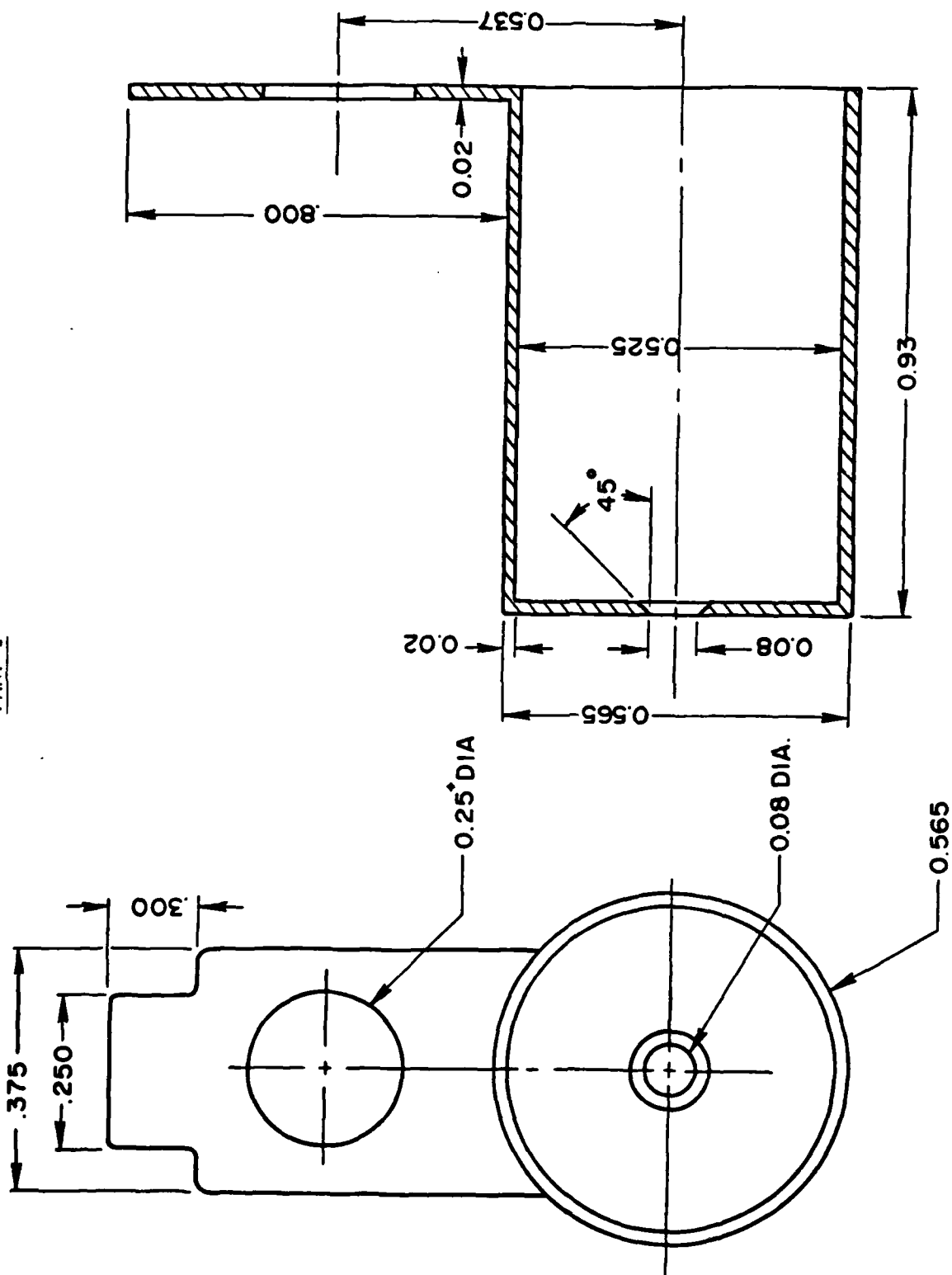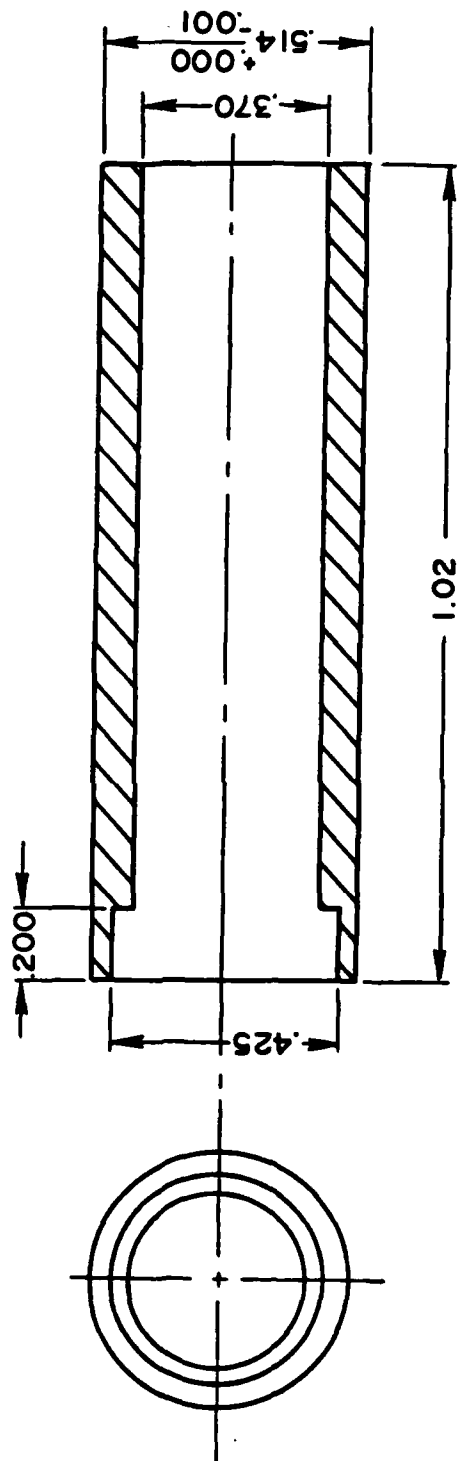
PART 1

FIGURE 1 - SEAMLESS DECELERATOR
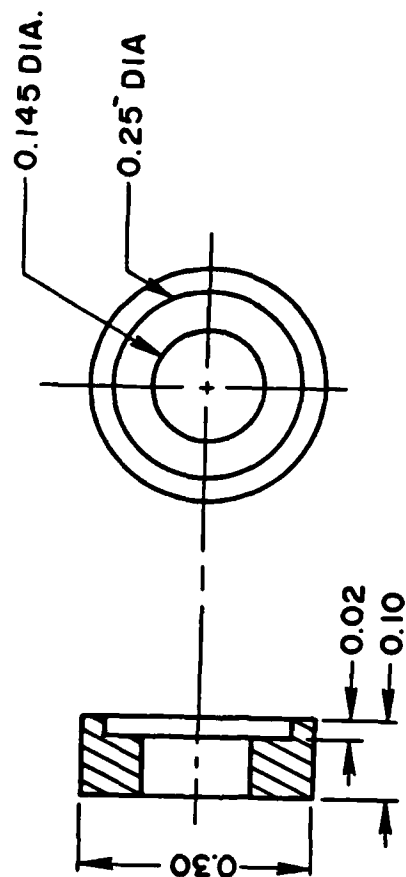
110

PART 2

FIGURE 2 - CERAMIC SPACER

111

PART 3

0.145 DIA.

0.25 DIA

0.02
0.10

0.30

FIGURE 3 - CERAMIC SPACER

112

PART 4

0.3

0.145 DIA.

0.25 DIA.

0.15

0.04

FIGURE 4 - CERAMIC SPACER

113

PART 3

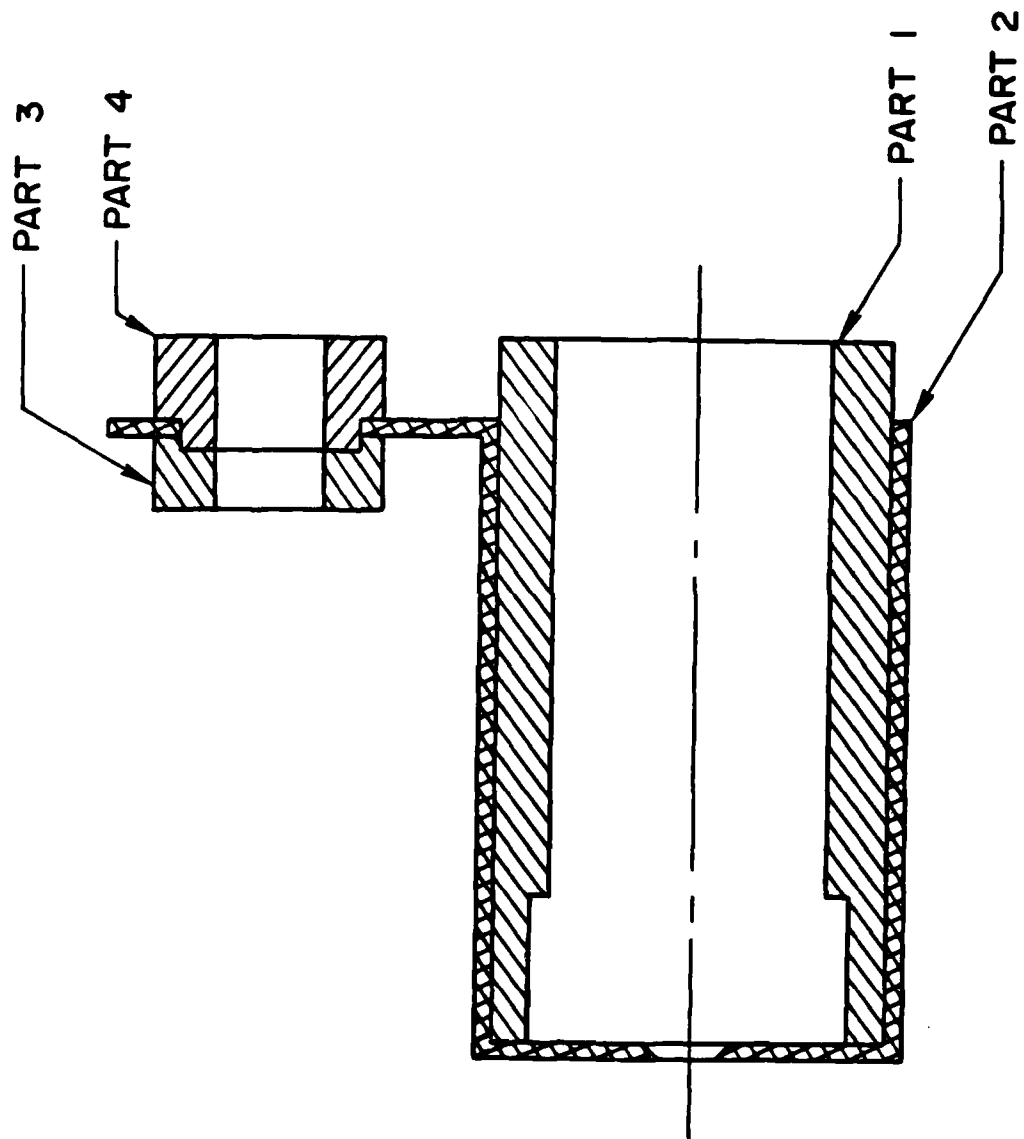PART 4
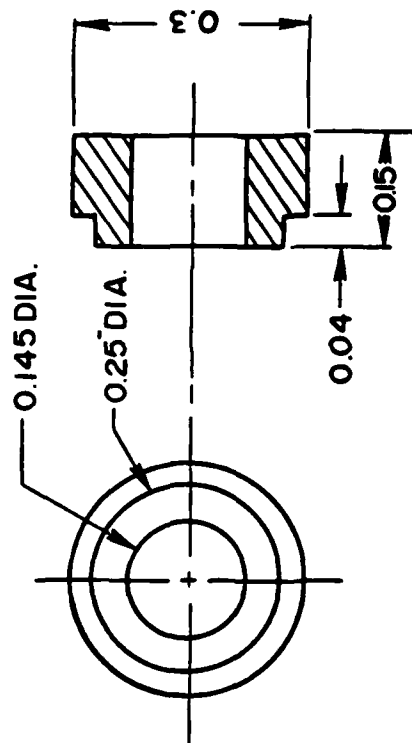
PART 1

PART 2

FIGURE 5 - ASSEMBLY VIEW (COLLECTOR)

114

FIGURE 6 - COLLECTOR FEEDTHROUGH

SPRING

STAINLESS STEEL (304)

CERAMIC

SPRING

0.8

0.180

0.8

COPPER

8.00

4.150

0.020

0.060

0.060

0.250

1.500

115

NOT TO SCALE

38 DRILL-THRU
5-40 UAC-2B-THRU

.25

EXISTING
HOLES
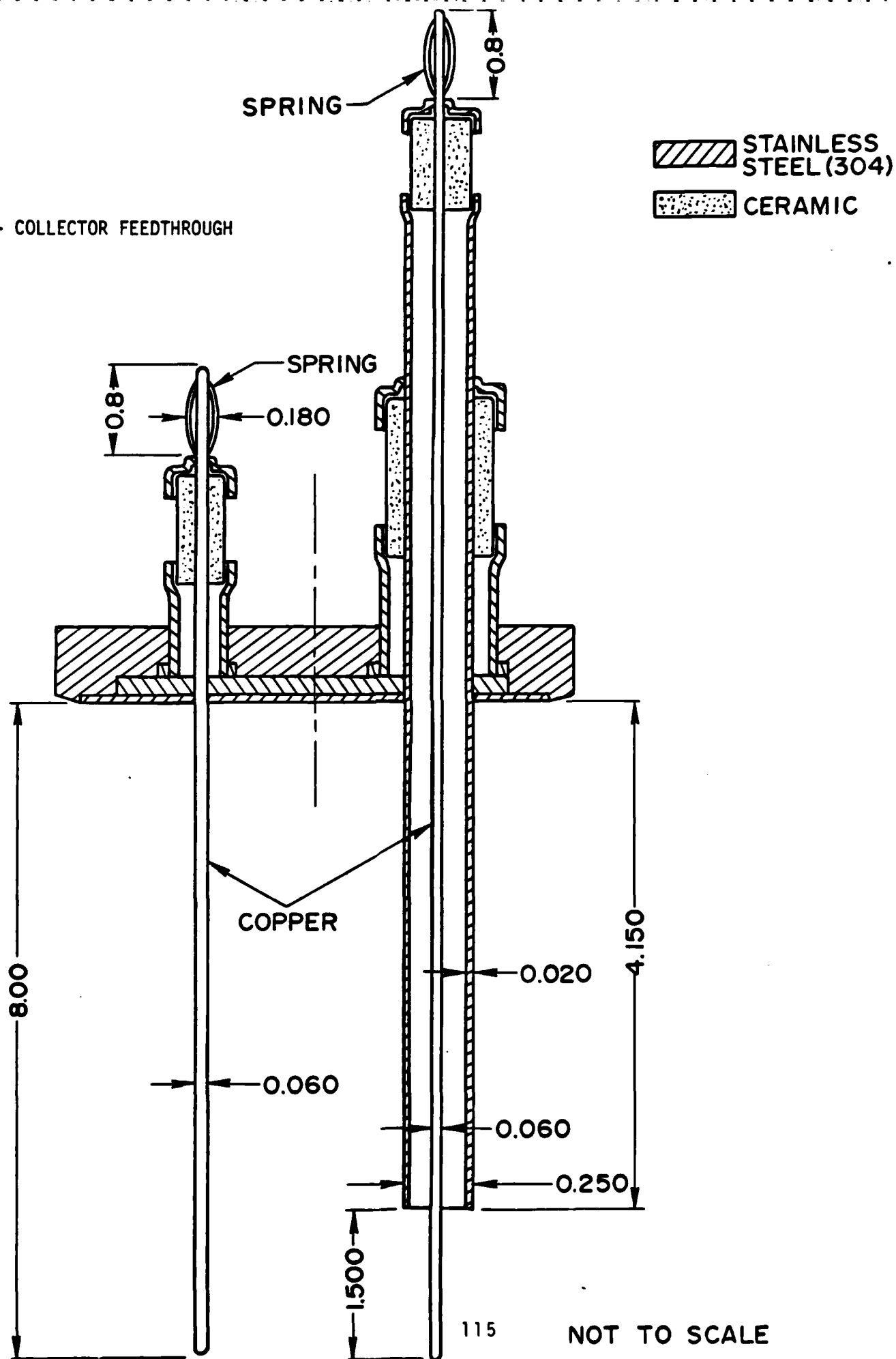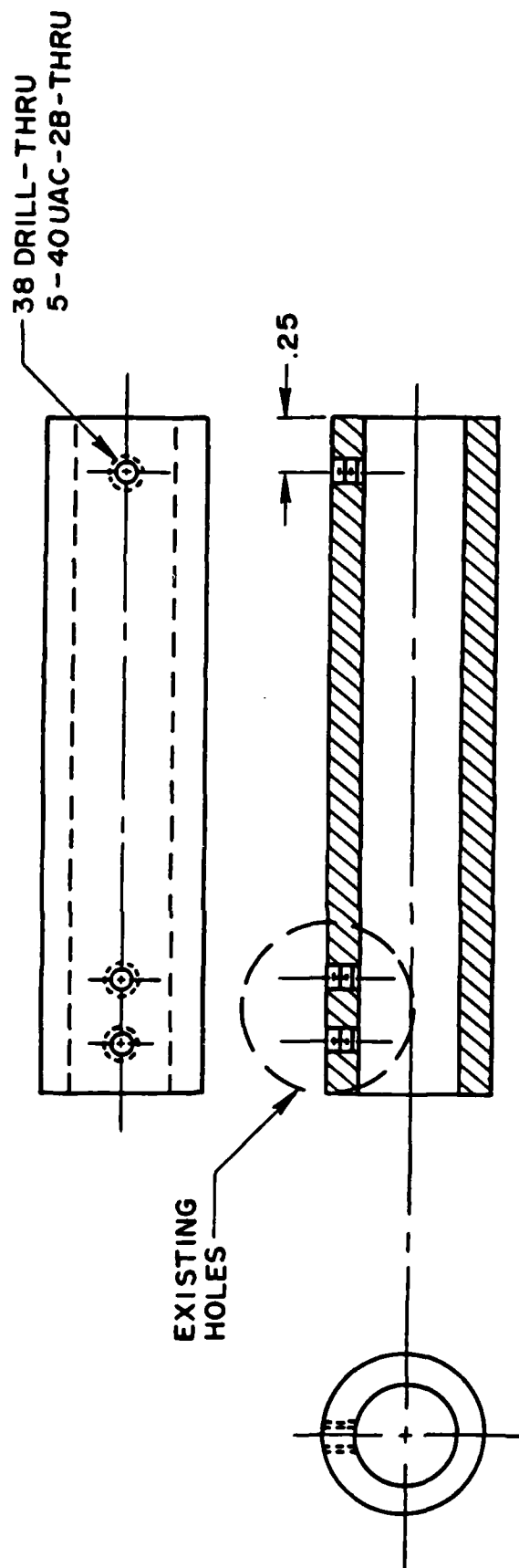
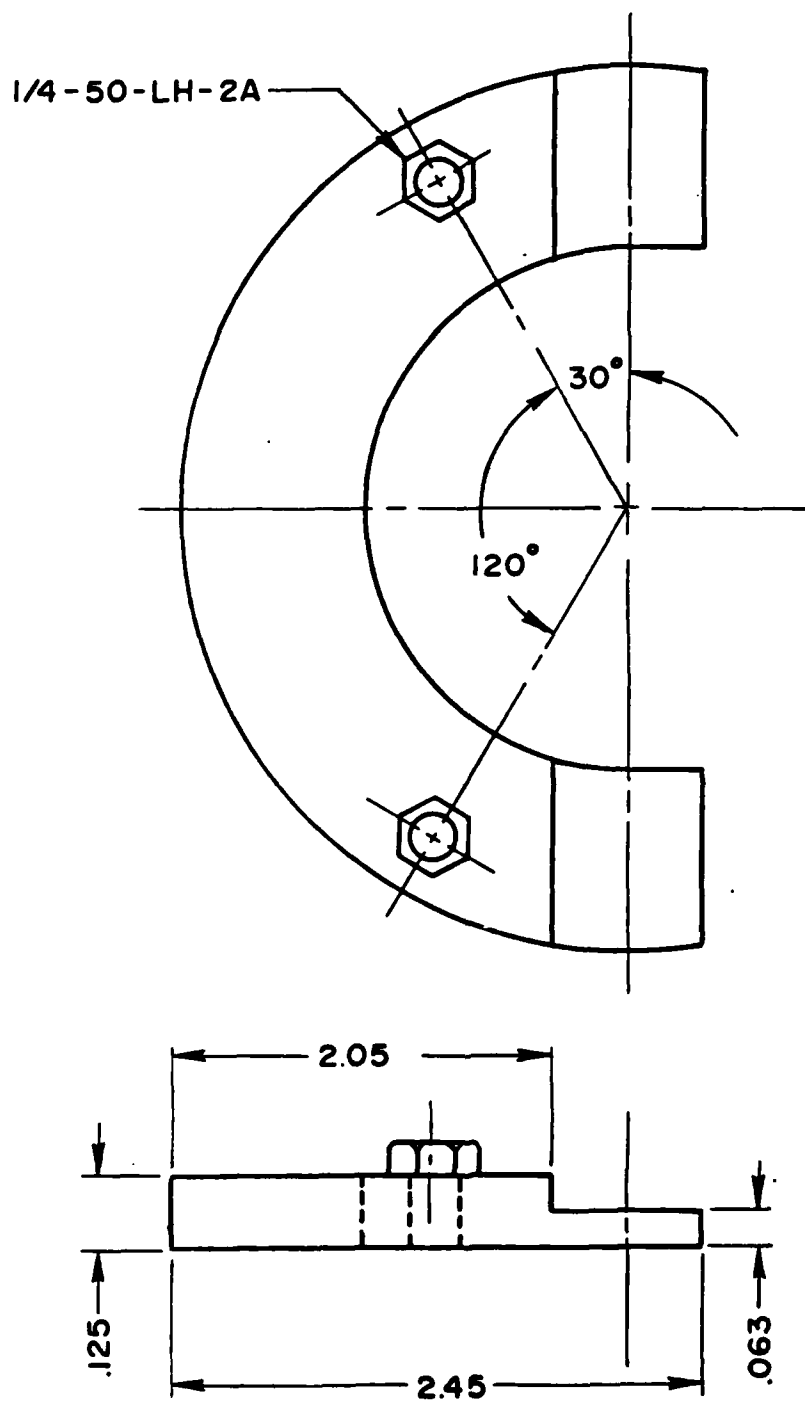FIGURE 7 - STAINLESS STEEL CONNECTOR

116
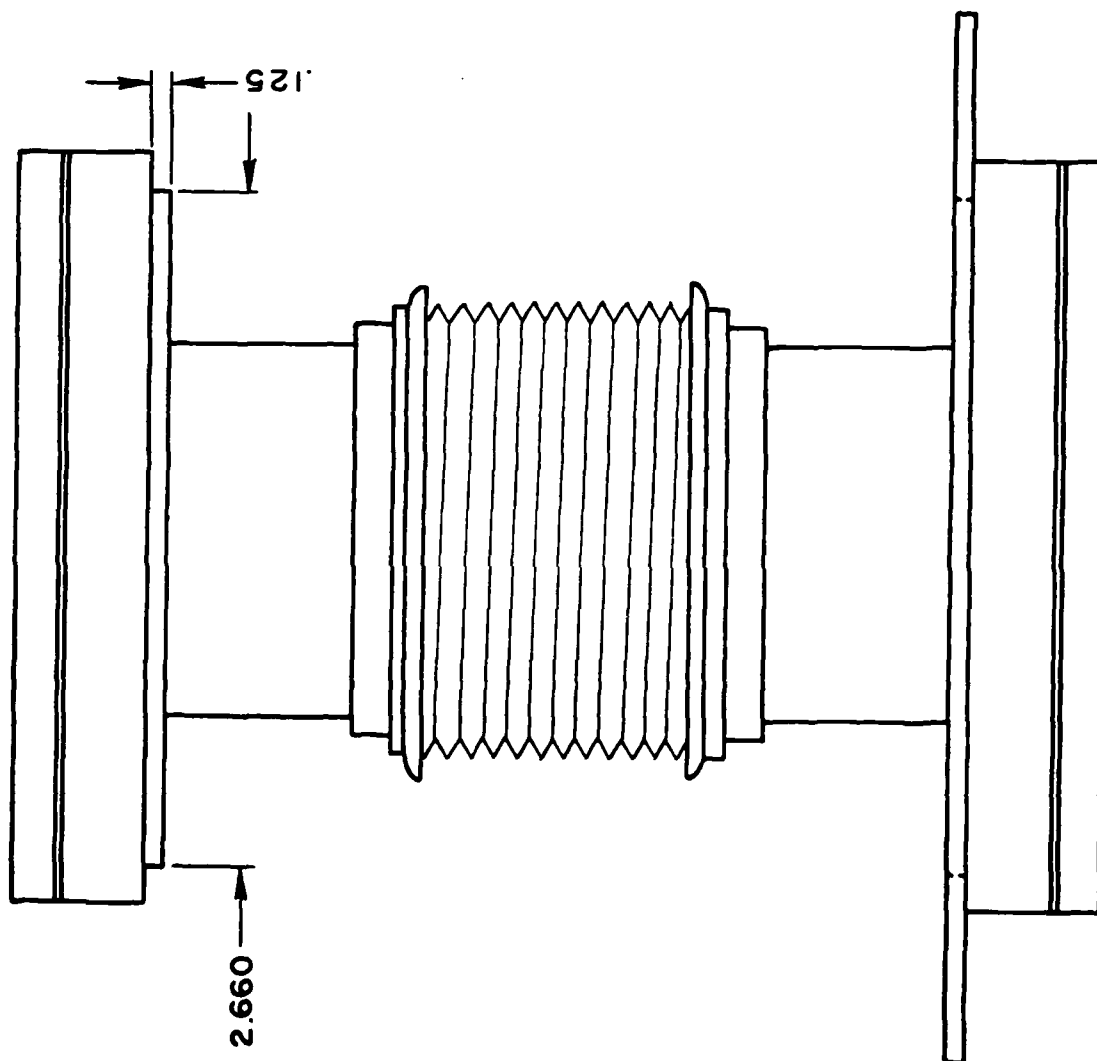
FIGURE 8 - MODIFIED WELDED BELLOWS

.125

2.660

FIGURE 9 - ALIGNMENT PLATE (PART 1)
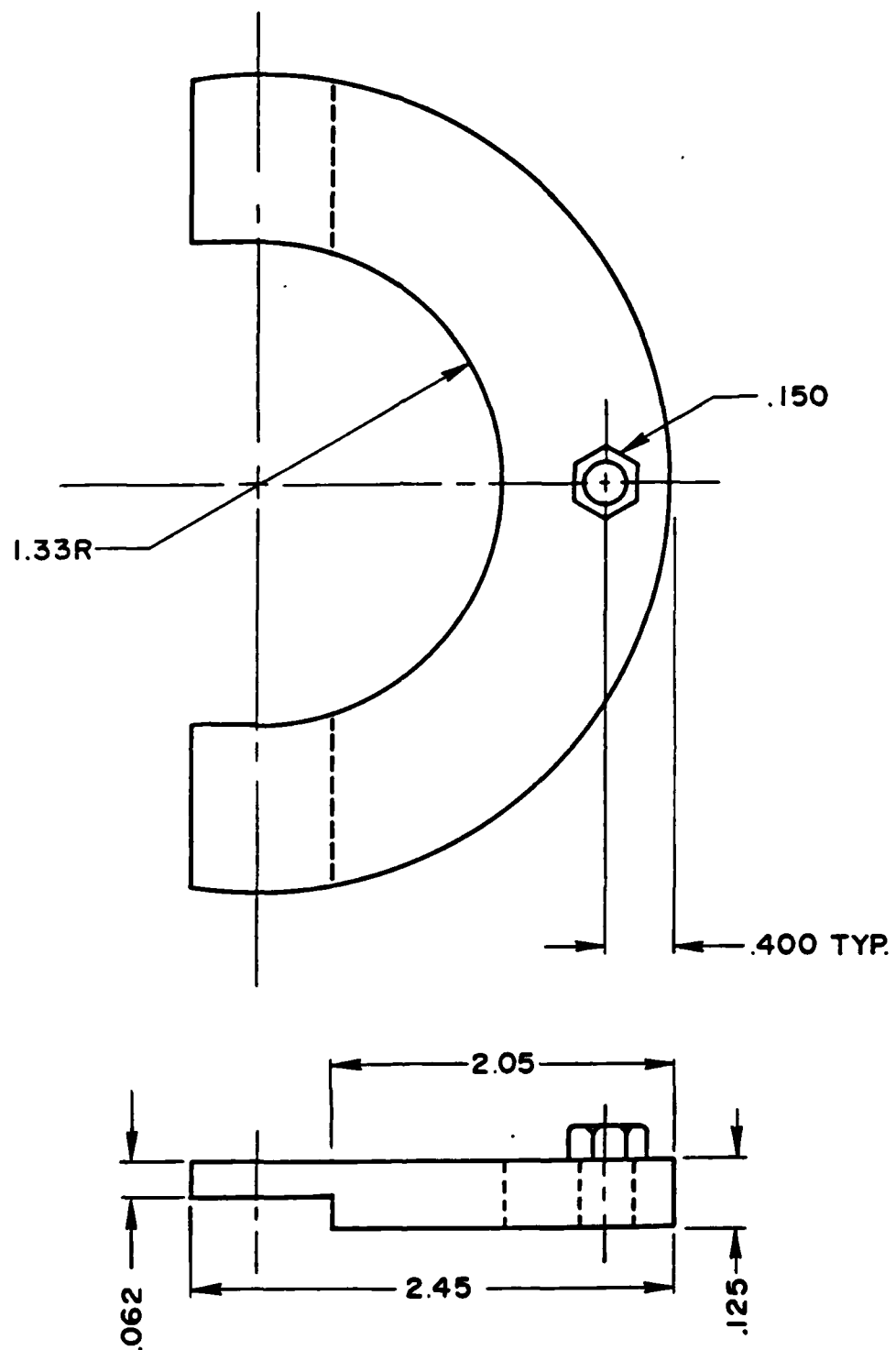
FIGURE 10 - ALIGNMENT PLATE (PART 2)

119

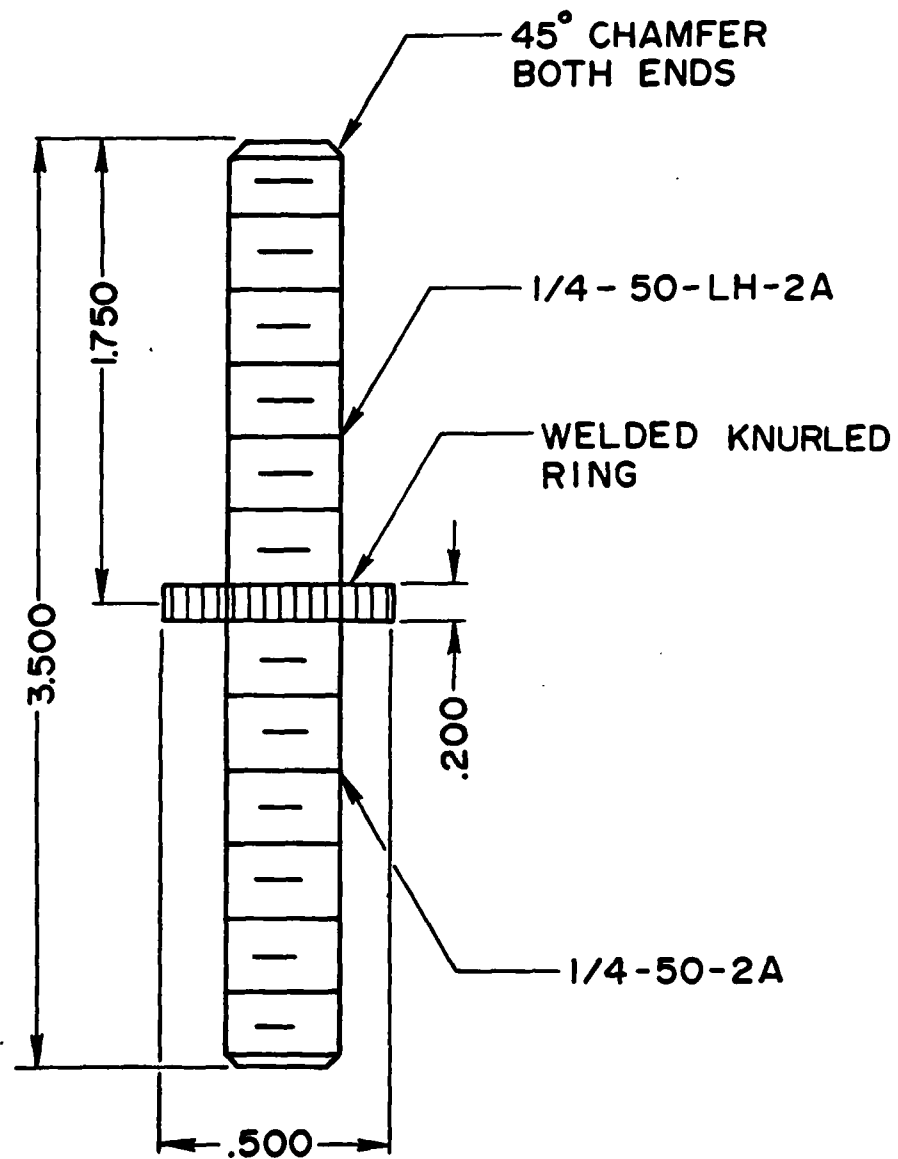45° CHAMFER
BOTH ENDS

1/4 – 50 – LH – 2A

WELDED KNURLED
RING

1.750

3.500

.200

1/4 – 50 – 2A

.500

FIGURE 11 - TWO-WAY SCREW